In Vitro and *In Vivo* Characterization of Tunable Fibrous Scaffolds for Tracheal Tissue Engineering

By

Lindsey Marie Ott

B. S., Biological and Agricultural Engineering, Kansas State University, 2008

Submitted to the Bioengineering program and the
Graduate Faculty of the University of Kansas
in partial fulfillment of the requirements for the degree of
Doctor of Philosophy

Committee members

Dr. Michael Detamore, Committee Chair

Dr. Robert Weatherly

Dr. Stevin Gehrke

Dr. Mark Weiss

Dr. Laird Forrest

December 10, 2014
Date defended

The Dissertation Committee for Lindsey Marie Ott certifies that this is the approved version of the following dissertation:

In Vitro and *In Vivo* Characterization of Tunable Fibrous Scaffolds for Tracheal Tissue Engineering

Committee chair

Dr. Michael Detamore, Committee Chair

December 10, 2014

Date approved

ABSTRACT

Laryngotracheal disorders resulting in airway obstruction, although rare, can cause significant morbidity and can be life threatening. Current treatments include augmenting the airway with the patient's own rib cartilage. Specialized surgical technique and an invasive, multi-site surgery are required for this procedure. Thus, an off-the-shelf tissue-engineered product is needed that would replace the need for autologous tissue and eliminate the challenges for the surgeon and patient. The tissue-engineering approach of "scaffold, cells, signals" was used to design a fibrous, graded bilayer scaffold with one layer providing long-term structural support (i.e., polycaprolactone (PCL)) and the other layer allowing for short-term tissue ingrowth and drug delivery (i.e., poly(lactic-co-glycolic) acid (PLGA)). *In vitro* degradation and several *in vivo* studies were completed to evaluate the scaffold performance and refine the design. Incorporating 3-D printed polymeric rings into the fibrous scaffold enhanced mechanical performance and growth factors and cells improved cellular response and tissue ingrowth. Additionally, research techniques were refined to analyze outcomes of these experiments, including microCT and stenosis quantification. The application of electrospun materials to tracheal defect repair was taken from idea to preclinical practice in this thesis and has established a platform for further research and development, with the potential for translation to clinical use.

ACKNOWLEDGMENTS

I gratefully acknowledge support from the NSF CAREER Award and NIH Biotechnology Predoctoral Training Grant. I would like to acknowledge Drs. Michael Detamore, Robert Weatherly, Mark Weiss, Stevin Gehrke, and Laird Forrest for serving on my dissertation committee and their guidance with my thesis research. I had excellent support from the many people has assisted with this research: Dr. David Moore and Heather Shinogle for their training on SEM and microscopy; Mr. Nicholas Hemphill and Lawrence Memorial Hospital for providing technical help with the CT scans; Mrs. Jodi Troup, Mrs. Heidi Lewis, and Dr. Rebecca Henry for their help in coordinating and assisting during the animal surgeries at the Animal Care Unit; Dr. Travis Hagedorn, Mrs. Karen Smith, and all of the staff at the Lab Animal Resources for their assistance with our full-scale animal study. A special thanks to Dr. Robert Weatherly for his continual assistance and surgical skill in all of the *in vivo* studies and for allowing me to observe a pediatric LTR surgery at Children's Mercy Hospital. Thanks to Drs. Mark Weiss and Katrina Fox for their assistance and expertise with animal surgery and bronchoscopy. Thanks to Alan Walker for fabricating the parts of the custom electrospinning equipment. I thank Dr. Qiang Ye and the Bioengineering Research Center for allowing me access to and training me on the microCT. Thanks to Damon Mar and the Orthopedic Research Center for allowing me access to their Instron and for building a custom suture retention fixture. I thank Dr. Richard Galbraith for generously donating his time and expertise in assessing and scoring the histological slides

I would like to acknowledge all of the assistance and hard word from undergraduate researchers: Lauran Byers, Cindy Vu, Ashley Farris, Natalie Walker, and Taylor Zabel. I thank Dr. Nathan Dormer for training me my first few years of graduate school and Dr. AJ Mellott for learning alongside me our first few years. I would like to acknowledge the past and current graduate students in the Biomaterial and Tissue Engineering lab who have been encouraging and helpful through this PhD process. Thanks to Peggy Keefe for being a wonderful lab manager who genuinely cares for all of the graduate and undergraduate students in lab. I also thank my industrial mentors, Dr. Jed Johnson and Katelyn Zak, for showing me how to scale-up electrospinning and build a business around electrospun materials for tissue engineering.

I am very grateful for my advisor, Dr. Michael Detamore, for his guidance and mentorship through this PhD process. He has been an excellent example of productivity, ambition, and hard work. I will forever be thankful for the training he has given me in all aspects of academia and research, from grant writing to management skills.

Finally, I would like to thank God for his grace and for giving me inspiration, comprehension, and eloquence in my research. Special thanks goes to my parents, Kent and Rebecca, my sister, Rachael, and my extended family and friends for their love and support that has seen me through to the completion of my Ph.D. I couldn't have done it without them!

TABLE OF CONTENTS

LIST OF FIGURES

Chapter 1
No Figures

Chapter 2
No Figures

Chapter 3

Chapter 4

Chapter 5

LIST OF TABLES

CHAPTER 1: Introduction

My dissertation encompasses the characterization of electrospun scaffolds for tracheal tissue engineering. Tracheal stenosis or obstruction can occur in the pediatric and adult population, with occurrences due to congenital or acquired development. Although this disease is rare, it is highly fatal. Current treatment of small defects is laryngotracheal reconstruction (LTR), where autologous rib cartilage is used to augment the airway and increase the circumference. Treatment for long-segment defects is slide tracheoplasty which involves removing the stenosed segment and joining the two ends of the trachea in a specialized way. These treatments are limited by donor tissue availability, surgical procedure difficulty, and added complications for patients. A tissue engineered scaffold that is not reliant on donor tissue or complicated surgeries is needed. I used an electrospun scaffold with gradient layers of poly(lactic-co-glycolic) acid (PLGA) and polycaprolactone (PCL). Reinforcing rings were added to assist with mechanical support. Growth factors and cells were incorporated into these scaffolds to determine their effect on cartilage-formation. The aims of this research were to, 1) synthesize and characterize mechanically reinforced scaffolds with radial gradients of materials and encapsulated growth factors and 2) to evaluate the tissue engineered tracheal constructs *in vivo.*

The first aim was to develop the electrospinning technology for the research group and to establish the parameters required to obtain the tracheal scaffolds. Once the scaffold technology was developed, the scaffolds were characterized to determine how the organization of the polymer gradient and how *in vitro* aging affected mass

loss, molecular weight, porosity, fiber morphology, and mechanical properties. The second aim was to determine the functionality of the scaffolds in an *in vivo* model. Several pilot studies and one full-scale study were performed. The thesis chapters follow the progression of the aims.

Chapter 2 is a thorough literature review of the status of tracheal tissue engineering research. The chapter elucidates all of the approaches used to create a tissue engineered trachea, including biomaterials/scaffolds, cells, and culture conditions. A clinical perspective was imparted in the review to bridge the bench top research and clinical need, in part with the assistance of collaborator and committee member, Dr. Robert Weatherly. The knowledge and perspective gained from writing Chapter 2 inspired the pursuit of electrospun scaffolds for tracheal applications, as little research had been done in this space.

While the *in vivo* pilot studies were conducted first to establish functionality of the scaffolds, Chapter 3 provides the basis for *in vitro* characterization of the fibrous scaffolds. Several different scaffold designs were subjected to simulated physiological conditions and characterized through the 12 week degradation. Scaffold morphology, fiber diameters, porosity, mass loss, molecular weight, and mechanical properties (i.e., tensile, tube flattening, suture retention, and burst pressure) were tested.

Chapter 4 and 5 address the second aim to characterize the scaffolds in an *in vivo* model. Chapter 4 is a compilation of all of the pilot studies, including 1) the first *in vivo* study by our research group with the trachea, which was an evaluation of a

monolayer, electrospun scaffold in a patch-type defect (n=2), 2) evaluation of polymer gradients and growth factor encapsulation in patch-type defects (3 groups with n=2), and 3) evaluation of mechanically reinforced tubular scaffolds in circumferential defects (2 groups with n=2). With the positive results of the patch-type defect studies (e.g., no fatalities), a full-scale *in vivo* study (n=5) with the gradient, mechanically reinforced scaffolds was performed (Chapter 5).

Chapter 6 provides a summary of my thesis work and highlights any trends and observations from the research. With the informed perspective obtained from conducting this research, I identify areas of improvement for this technology and future directions for this research.

CHAPTER 2: Overview of tracheal tissue engineering: clinical need drives the laboratory approach[1]

ABSTRACT

Breathing is a natural function that most of us do not even think about, but for those who suffer from disease or damage of the trachea, the obstruction of breathing can mean severe restrictions to quality of life or may even be fatal. Replacement and reconstruction of the trachea is one of the most difficult procedures in otolaryngology/head and neck surgery, and also one of the most vital. Previous reviews have focused primarily on clinical perspectives or instead on engineering strategies. However, the current review endeavors to bridge this gap by evaluating engineering approaches in a practical clinical context. For example, although contemporary approaches often include *in vitro* bioreactor pre-culture, or sub-cutaneous *in vivo* conditioning, the limitations they present in terms of regulatory approval, cost, additional surgery and/or risk of infection challenge engineers to develop the next generation of biodegradable/resorbable biomaterials that can be directly implanted *in situ*. Essentially, the *functionality* of the replacement is the most important requirement. It must be the right shape and size, achieve an airtight fit, resist restenosis and collapse as it is replaced by new tissue, and be non-immunogenic. As we look to the future, there will be no one-size-fits all solution.

---

[1]Published as Ott L.M., Weatherly R.A., and Detamore M.S., "Overview of tracheal tissue engineering: clinical need drives the laboratory approach," Invited review for Annals of Biomedical Engineering, 39(8) 2091-2113, 2011.

INTRODUCTION

Tracheal repair procedures date back to the late 19th century, and yet no predictably effective treatment for tracheal stenosis has been established that easily returns normal function to the trachea.[115] Although tracheal stenosis is a rare disease, the mortality rates for long-segment tracheal stenosis (abnormal narrowing) and atresia (abnormally closed or absent trachea) are nearly 77% and 100%, respectively, as summarized by Fuchs *et al.*[26] Many issues such as neoplasms, tracheotomy, congenital disorders, prolonged endotracheal intubation, and other types of tracheal trauma affect the tracheal lumen and can cause stenosis or tracheomalacia. As a result, any damage to the trachea can compromise speech, deglutition (swallowing), respiration, mucociliary clearance, and immune protection from inhaled or ingested antigens[39]—all important functions for survival.

This review seeks to summarize tissue engineering's role in tracheal defect repair with a specific focus on the biomaterials and culture conditions used to create a tissue engineered trachea. While much research has developed in airway tissue engineering (vocal fold, lung, etc.), the purpose of this review is to give an in-depth view of tracheal tissue engineering. Many excellent trachea tissue engineering reviews exist,[5, 7, 14, 22, 114] but the focus is either clinical or experimental. The purpose of this review is to combine both aspects, and to highlight studies with approaches that are clinically translatable.

SURGICAL STANDARDS

Replacement or reconstruction of the trachea is one of the most difficult procedures in otolaryngology—head and neck surgery.[85] An optimal treatment has not yet been found, but current treatments for tracheal disease involve surgical repair.[32] The most common surgical procedures for severe stenosis are resection of the affected areas followed by end-to-end anastamosis[37] (surgical joining of two trachea ends to allow air flow from one segment to the other), or cartilage augmentation of a focal region of stenosis. For determining the appropriate surgical approach based on the affected area, a general algorithm can be applied as follows:

(1) in short segment stenosis involving the larynx, augmentation is preferred over resection and re-anastamosis.

(2) for short segments not involving the larynx, resection and re-anastamosis are preferred over augmentation, and

(3) in long segment stenosis, a patch (augmentation), usually with fascia or pericardium, or slide tracheoplasty are typically used.

Resection and primary anastamosis can create tension in the trachea, and are only recommended for defects less than half of the length of the adult trachea and one third of pediatric trachea.[34] Long segment defects (greater than 50% of trachea length) make up approximately half of trachea stenosis cases.[26] In many cases, therefore, replacement tissue is utilized to expand the size of the tracheal lumen.

In 2002, Grillo[34] summarized all tracheal replacement methods either in use or under investigation, and divided them into five categories: foreign materials,

nonviable tissues, autogenous tissues, tissue engineering, and tracheal transplantation. Kucera *et al.*[55] and Doss *et al.*[22] also provided a two part summary of tracheal reconstruction using replacement materials and tissues. Each replacement possesses problems when implanted. One example of a common replacement material, used in the laryngotracheal reconstruction (LTR), is costal cartilage. Costal cartilage is the current "gold standard" material for LTR;[27] however, harvesting costal cartilage can cause donor site morbidity, including pneumothorax, pneumonia, and changes in the thorax contour.[65, 81, 121] Shape and length constraints are also drawbacks to the use of costal cartilage in some cases. According to Grillo,[33] tissue engineering techniques show promise for creating a usable tracheal graft.

CLINICAL NEED

Neville *et al.*[76] outlined characteristics for ideal tracheal replacements that are also applicable to tissue engineered trachea constructs (Table 2.1). In addition to that list, tissue engineering techniques will preferably produce a construct that is ready for immediate implantation (i.e., "off-the-shelf" accessibility). To meet this goal, the construct must either have a short fabrication time or be capable of being preserved for future use (i.e., reasonable shelf-life). Materials and cells for the tracheal construct should also be easily accessible (little to no donor site morbidity) and available (overcome the limited supply of transplantable tissue and organs). Along with accessibility of materials, the construct should be easily implanted into the patient, without need for complex, invasive or multi-stage surgeries. The construct

must also be easily vascularized for nutrient transport, have the ability to grow with the patient (especially in pediatric cases), have relatively low cost, and be noncarcinogenic. Tissue engineering of the trachea using the appropriate scaffold, cells, and culture conditions could possibly meet all of these requirements, but all of these characteristics must still be optimized.

The first tissue engineered trachea experiment was published in 1994 by Vacanti *et al.*,[124] where polyglycolic acid (PGA) fibers seeded with chondrocytes were implanted into the cervical trachea of the rat. Since then, a myriad of groups have designed tissue engineered tracheas using a wide variety of techniques. To readily describe these studies, the remainder of this review is divided into three primary sections: (1) Biomaterials, (2) Cells, and (3) Culture Conditions for Tissue Engineered Tracheas.

BIOMATERIALS FOR TISSUE ENGINEERED TRACHEA

In the history of trachea replacement, numerous materials have been utilized to repair segments of the trachea, ranging from stainless steel[122] to collagen. These materials typically have been bio-inert and not resorbable or biodegradable. One historic example of these prosthetic materials is the Neville prosthesis, which was used clinically until dehiscence occurred at the interface between the prosthesis and host tissue.[122] With the advent of tissue engineering, biodegradable and/or porous materials with the ability to support tissue in-growth became the focus. There are four categories of such scaffolds that have been employed in trachea tissue

engineering to date: “scaffold-free”, naturally-derived materials, synthetic materials, and a combination of materials.

“Scaffold-free” approaches

Scaffold-free culture, in this context, involves any approach (e.g., cell sheet or aggregate technologies) that develops tissue-like constructs without the use of biomaterial scaffolding. Scaffold free culture for trachea replacement has only been evaluated within the last 6 years.

The primary advantage of this method is less inflammation since foreign biomaterials are not included in the construct. This approach may, however, compromise mechanical integrity. Most scaffold-free approaches rely on a temporary stent to maintain the shape of the trachea. In one example using an LTR patch procedure, Gilpin et al.[29] did not include a stent when they implanted their chondrocyte sheet in rabbits. The construct exhibited no signs of inflammation, but the graft buckled and migrated into the laryngofissure. In another study, Tani et al.[117] wrapped a chondrocyte sheet around a silicon tube and tested the construct in a rotating bioreactor. While the construct maintained shape after the silicon tube was removed, the elastic intensity (measured with a rheometer) was only one-third of native trachea cartilage, while the GAG content was 72% of native trachea cartilage. Wu et al.[132] created a chondrocyte macroaggregate, which was wrapped around a silicon tube and implanted subcutaneously in 8 rabbits for a period of 8 weeks.

Cartilage formation was evident, but the mechanical properties were significantly lower than native cartilage and epithelialization was not addressed.

In an orthotopic application, Weidenbecher et al.[129] developed bioreactor-formed chondrocyte sheets that were layered with a strap muscle flap around a silicon tube, which were then inserted into a circumferential defect in a rabbit trachea for a period of up to 39 days after first being allowed to mature in a paratracheal position. While the construct was vascularized and cartilage-tissue was detected, fibrous tissue developed in the lumen, causing a fatal airway obstruction in all animals in the study.

Although chondrocytes have been the main focus of scaffold-free trachea constructs, Zhang et al.[143] used a bone-marrow derived chondro-induced cell sheet wrapped around a poly(lactic-co-glycolic acid) (PLGA) tube and cultured it in a spinner flask.

After 8 weeks of culture, histology and GAG content analysis revealed cartilage-like tissue. An epithelial cell based aggregate was formed on temperature responsive dishes, and then placed into the lumen of a Dacron support prosthesis. After heterotopic (subcutaneous) implantation for 4 weeks, followed by orthotropic implantation in rabbits, the epithelial cell sheets formed pseudostratified columnar epithelial cells on the lumen of the construct.[47]

Overall, there have only been a few studies that have utilized the scaffold-free or cell sheet approach for tracheal tissue engineering. Different techniques were used to create these cell-sheets/microaggregates, but they have not yet been fully studied and compared to determine whether these techniques are capable of producing a

construct ideal for trachea tissue engineering. The main disadvantage of this approach is an apparent inability of the construct to maintain the shape of the trachea.

Naturally-derived materials

Naturally-derived materials have been applied to trachea tissue engineering; specifically, decellularized tissue, collagen, hyaluronic-acid, and silk fibroin. Decellularized tissue scaffolds have been used in multiple areas of tissue engineering, and Macchiarini *et al.* [66] proved that they could also be used in a clinical trachea tissue engineering paradigm. Decellularized aortic grafts,[102] jejunum,[67, 126, 127] bladder,[28] and trachea[28, 30, 43, 66] have been utilized for tracheal replacement. These scaffolds have been used with or without cells; however, Go *et al.*[30] observed contamination and infection in constructs not seeded with epithelial cells in their pig model after a period of 11 days. Remlinger *et al.*[93] observed scaffold degradation after they implanted hydrated xenogeneic decellularized trachea extracellular matrix in dog tracheas for 8 weeks. For future studies, the authors suggest adding chondrocytes to the scaffolds, with the goal of replacing the degrading scaffold with cartilage. Preservation methods of such scaffolds also seem to have an effect on regeneration. Gilbert *et al.*[28] did not observe any cartilage formation in their decellularized trachea and bladder constructs when implanted in dogs for 6 months, and they hypothesized this may possibly have been due to lyophilization and freeze-drying of their construct before implantation. Seguin *et al.*[102] studied how cryopreserved, decellularized, and glutaraldehyde-treated aortic grafts behaved as

stents in the sheep trachea for a period of up to 12 months. They observed that the cryopreserved grafts regenerated respiratory epithelium and cartilage better than the other two grafts.

Other naturally-derived scaffolds include hyaluronan-based scaffolds, which have been shown to support chondrocyte growth in bioreactor culture.[37] However, *in vivo* rabbit implantation of allogeneic chondrocyte-seeded hyaluronan-based scaffolds (12 weeks) caused a nonspecific foreign body response and eventual degradation of tissue engineered cartilage.[128] As this reaction has not been observed in knee articular cartilage defects, the authors hypothesized that an unfavorable microenvironment may exist in the neck (i.e., vascularized environment with different immunological properties than the knee).[128] Lastly, silk fibroin has also been proven to be biocompatible in rabbit tracheas for 12 weeks, with fibroblasts and capillary vessels integrating into the material.[77]

Synthetic materials

Synthetic scaffold materials have been used since the advent of tissue engineering. The synthetic scaffold materials used individually (not in combination with other materials) in tracheal tissue engineering have included polyglycolic acid (PGA),[35, 51, 124] polylactic acid/polyglycolic acid (PLA/PGA),[64] poly(lactic-co-glycolic acid) PLGA, polyester urethane,[139] poly(ethylene oxide)-terephthalate/poly(butylene terephthalate)(PEOT/PBT),[73, 113] gelatin sponge,[40] polyethylene oxide/polypropylene oxide copolymer (Pluronic F-127), and

polytetrafluoroethylene (PTFE).[68] Biocompatibility and immune response to synthetic materials are concerns.

Vacanti *et al.*[124] observed no immune response to PGA in nude mice; however, Kojima *et al.*[51] observed poor cartilage formation in the same PGA constructs in an immunocompetent animal (sheep) for 7 days, which the authors concluded could have been due to an inflammatory response. A similar immune response was observed in PLA/PGA constructs in rabbits.[64] However, pre-culturing the PLA/PGA construct for two weeks before implantation allowed for ECM formation and cell in-growth.[64] Luo *et al.*[64] hypothesized that inflammatory acidic degradation products were cleared from the scaffold and cells had begun to fill the scaffold, thereby preventing blood cells from invading the construct and triggering an immune response. Other synthetic materials, like Pluronic F-127, do not have acidic degradation products, and have been shown to support cell attachment and growth. For example, chondrocyte seeded Pluronic F-127 was pre-cultured subcutaneously in three pigs, and then moved to an anterior defect in the trachea.[46] The pigs survived for 3 months, and excellent neocartilage formation and graft integration into cricoid area were observed.

Combination of materials

Finally, combinations of materials, both synthetic and natural, have been investigated for tracheal tissue engineering. The majority of tissue engineered tracheas have been combinations of two or more materials, usually involving a coated

or layered construct. Collagen-coated polypropylene mesh reinforced with a polypropylene mesh cylinder is a trachea prosthetic that has been extensively studied.[74, 75, 78, 82-86, 98, 103, 109, 111, 120, 137] There have also been many alterations on the basic collagen/polypropylene scaffold, by adding a cell loaded collagen gel to the outer surface of the construct,[78, 109] coating vitrigel on the epithelium,[111] and coating poly (L-lactic acid-co-ε-caprolactone) on the lumen.[98]

Coating scaffolds with peptides, like the RGD cell adhesion ligand, is another approach used to enhance cell attachment. For example, chondrocyte-loaded, RGD-modified alginate was coated on PGA mesh and implanted in rabbit trachea for up to 20 weeks.[35] Mature cartilage was formed in the constructs, however, the RGD did not have an effect on cartilage formation. Another composite culture study compared coating a polyurethane sponge (PS) with collagen, fibronectin, RGD, or apatite.[138] Some inflammation occurring in the RGD constructs, and the apatite and fibronectin scaffolds appeared to perform better dog tracheas. Although all constructs were inundated by sputum absorption.

Other combination materials used a multi-layered approach. For example, Komura *et al*.[53] designed a 3-layer construct: a collagen sheet on the luminal side to support epithelial ingrowth, a PGA nonwoven mesh inside, and an L-lactide/ε-caprolactone coarse mesh on the outer surface for mechanical support. In addition, basic fibroblast growth factor (bFGF)-loaded gelatin microspheres were added to the outer surface, which the authors used with the intent of enhancing chondrogenesis.[53] After the construct was implanted in rabbit tracheas for 3 months, some morbidity

occurred due to surgical issues, and in the surviving animals, it appeared that bFGF increased cartilage formation; however, the efficacy of the multi-layered design was not determined (i.e., no comparison to a control). Another three layer construct was evaluated in circumferential defect repair, consisting of a silicon stent, collagen sponge, and gelatin sponge loaded with bone morphogenetic protein (BMP)-2.[136] The silicon stent was removed at 8 weeks and the trachea maintained patency after 6 months of observation. However, this was only evaluated in one dog.

Aside from the composition of scaffold materials, the actual design of the scaffold has received some attention. A majority of tracheal tissue engineering studies are focused on developing scaffolds for large circumferential defect repair, as these type of defects typically cannot be repaired with autografts or end-to-end anastomosis. Less common are the "Y"-shaped defects for bifurcation repair. Sekine *et al.*[103] attempted to implant a "Y" shaped construct in dogs for up to 7 months. However, the survival rate was low due to air leaks. In a long-term follow-up study, 1 dog survived for 5 years with this construct.[75]

In addition, a biomimetic approach in scaffold design and geometry has been considered by some groups. For example, Moroni *et al.*[73] explored how macroscopic topology (i.e., discrete cartilage arches) affected cellular metabolism and ECM production, and established that an anatomically designed scaffold (created from a CT image) created an environment for a high degree of chondrocyte differentiation *in vitro* as compared to cylindrical and toroidal tubular scaffolds. The authors suggested that the imperfections in the anatomical construct created local niches for increased

cell-cell contact and thinner fibers for better chondrocyte attachment.[73] The cause for increased cell performance in these anatomically shaped scaffolds requires further assessment, particularly in an *in vivo* model. Other groups have focused on creating distinct ring shapes in the scaffold to mimic a native cartilage ring. Kojima *et al.*[52] created a construct with a chondrocyte-PGA mesh inserted into helical grooves in a silicon tube, and the outer surface was coated with transforming growth factor (TGF)-β2-loaded hydrogel microspheres.[52] Cartilage formation was evident after 6 weeks of subcutaneous implantation in nude rats; however, the relationship between the geometry and mechanical properties was not evaluated. Lin *et al.*,[61] recreated the tracheal ring structure by inserting chondrocyte-seeded collagen in the grooves of a tubular PCL scaffold. The relationship between construct design and performance was not the focus of this study, but the construct resisted collapse and neocartilage was formed when implanted into rabbit tracheas for 52 days. In another trachea ring replacement approach, Igai *et al.*[40] removed the trachea rings in dogs without disturbing the mucosa, and then filled the gaps with BMP-2-loaded gelatin. Histological analysis revealed cartilage and bone infiltration in the ring-shaped defects after 12 months.

Summary

Many different scaffold materials have been utilized for tracheal tissue engineering, each with their own inherent strengths and weakness. By combining materials (or layering materials), the limitations of one material can be compensated

for by another material. However, this added complexity may require more fabrication time, cost, regulatory approval time and cost, and/or advanced fabrication techniques to assemble the layers. Scaffold design has not been extensively addressed, so the importance of mimicking the biological structure on a macroscopic level has yet to be proven. In translating to clinical utility, the most *straightforward* approach that imparts requisite structure, function, and integration with host tissue until replaced by cellularized tissue may be the most successful.

CELLS LINES USED IN THE TISSUE ENGINEERED TRACHEA

Native trachea tissue is composed of hyaline cartilage, trachealis muscle, fibrous tissue, mucosal tissue, and a delicate vasculature. Thus, some of the more common cell types found in the trachea include chondrocytes, smooth muscle cells, ciliated pseudostratified columnar epithelial cells, goblet cells, fibroblasts, and endothelial cells. Tracheal tissue engineering has utilized a range of cell types, from chondrocytes to mesenchymal stem cells, obtained from many different donor tissues. The use of cells in a tissue engineered trachea can be divided into three strategies: acellular, single cell type, and multi-cell types. In addition, more recent studies using stem cells will be highlighted in an additional subsection.

Acellular constructs

Acellular constructs rely on the biomaterial and any added growth factors to harness the body's ability to allow cells to populate and integrate into the material. In

these constructs, all cells must migrate into the material from the surrounding native tissue. This strategy is often used for proof-of-concept materials that incorporate cells in later studies. Examples of acellular constructs are decellularized tissue matrix[43] and collagen coated polypropylene mesh.[82] The influence of growth factors on tissue in-growth has also been evaluated acellularly, with some cartilage and bone formation observed in the implants in dog tracheas after harvest and examination .[40, 136]

Single cell type

Bioengineered trachea research has primarily employed the one-cell-type strategy. Many studies have utilized chondrocytes or epithelial cells to populate trachea constructs. Chondrocytes were used in Vacanti's first attempt at tracheal tissue engineering,[124] and have been used extensively since then, in hopes of creating functional bioartificial cartilage. Creating functional cartilage provides the needed support to prevent tracheal collapse. Chondrocyte culture is a well established procedure, however, de-differentiation of chondrocytes during culture is a limitation.[125] Often, creating a three-dimensional environment using coated culture dishes (agar[139]) or bioreactors, may help to preserve the chondrocyte phenotype.

While native epithelial cells have been shown to migrate onto the lumen of tissue engineered constructs, re-epithelialization and mucosalization takes a considerable length of time. For large segment reconstruction, mucosal growth over a construct is even slower, and represents a significant problem. Without epithelium,

constructs can be susceptible to bacterial invasion, granulation tissue formation, and restenosis.[34]

The source of chondrocytes and epithelial cells is a crucial consideration for researchers, as an immune response (autologous versus allogeneic source) or donor site morbidity would be highly undesirable. Human tracheal chondrocytes may have the chondrogenic potential to form tissue-engineered cartilage for clinical use.[54] However, obtaining tracheal chondrocytes involves an invasive harvesting procedure from the tissue that is targeted for regeneration, so the clinical relevance of this approach may be limited. After multiple side-by-side comparisons of chondrocyte sources (nasal, articular, auricular, tracheal, costal),[37, 49, 127] the difference in donor site morbidity seems to be the main disparity. The only quantitative difference between isolation locations was seen by Henderson *et al.*,[37] where improved mechanical properties and ECM production were observed in auricular chondrocytes, but this was not confirmed by other studies. While the best source for chondrocytes has not been agreed upon, avoiding the removal of trachea cells would be advantageous. In general, the best method would involve easy retrieval of a relatively small number of donor cells that could be expanded *in vitro* or even directly seeded into the scaffold in the operating room, resulting in limited donor site morbidity.

Multiple cell types

The most complex approach for populating trachea constructs is to create a composite of cell types. Prior to adding the cells to the scaffolding, researchers have

cultured the cells together or separately. Sometimes, the co-culturing of cell types can be synergistic. Chondrocytes and respiratory epithelial cells have been co-cultivated for trachea replacement, and many different methods have been investigated. One study evaluated the performance of (1) epithelial cells on chondrocyte pellets, (2) epithelial cells on native cartilage explants, and (3) co-culture on separate sides of collagen membranes.[89] Immunohistochemical staining revealed expansion and differentiation in the epithelial layer of the third method. The authors of this study concluded that the culture conditions of the third method (collagen membrane system); a basal lamina equivalent, fibroblast conditioned medium, and air-liquid interface; were required for epithelial cell proliferation and differentiation.[89] Another group cultured human respiratory epithelial cells and chondrocytes separately on 3D scaffolds, and then fused the two constructs together with fibrin surgical adhesive. After 5 days in culture, the constructs remained viable and the layers were appropriately adhered to each other.[20]

Chondrocyte and epithelial cell constructs have been seeded abluminally and luminally, respectively, to create a biomimetic construct. These constructs have been introduced into subcutaneous pockets of nude mice.[50, 97] At the conclusion of 6 weeks, the ECM content of the tissue engineered cartilage was similar to native cartilage, and histology revealed mature cartilage and pseudostratified columnar epithelium.[50] The function of these chondrocyte/epithelial cell constructs still needs to be evaluated in the *in vivo* trachea. However, this biomimetic seeding strategy has

had repeated success in human, when seeding chondrocytes differentiated from MSCs on the exterior surface and epithelial cells on the interior surface.[66]

Other combinations of cells utilized for trachea repair are epithelial cells and fibroblasts,[31] endothelial cells and epithelial cells,[142] chondrocytes and fibroblasts,[51] fibroblasts and muscle cells,[67] and bone marrow stromal cell-derived chondrocytes and epithelial cells.[30, 66] Walles *et al.*[126] evaluated an even greater number of cell types; seeding chondrocytes, bone marrow-derived smooth muscle cells, bone marrow-derived endothelial cells, or respiratory epithelium on a decellularized matrix. More research is needed to determine whether multiple cell types can be incorporated onto one construct at one time and whether this approach is clinically beneficial or practical (i.e., multiple biopsy sites). This elaborate approach would need to be justified and the benefits must outweigh any additional costs.

Stem cells

The most ideal cell type is one that comes from a single source and can differentiate into the required cell types. Adipose-derived stem cells,[109] bone marrow stromal cells,[25, 52, 66, 74, 126, 143] and amniocytes[56] have been utilized for chondrogenesis in the tissue engineered trachea. Cell sources for airway epithelium include respiratory tract endogenous cells and exogenous cells from other tissues in the body (embryonic, bone marrow, amniotic fluid, etc.)[96] For example, fully differentiated airway epithelium has been generated from embryonic stem cells through an *in vitro* culture process.[15]

Summary

Although three major approaches exist for populating a tissue engineered trachea (acellular, single-cell, or multi-cell composite), a single source of cells harvested with little to no donor site morbidity or immunogenicity, with lineage specific differentiation capabilities, would be the most promising and clinically relevant approach. With increasing efforts in stem cell research, technologies like induced pluripotent stem cells may hold great potential for tracheal tissue engineering. However, regulatory challenges may postpone their introduction into mainstream use, and the leading candidate cell source today may be the patient's own bone marrow.

CULTURE CONDITIONS FOR TISSUE ENGINEERED TRACHEAS

Once the materials and cells have been determined, a decision must be made regarding culture conditions, if any. Culture techniques can be used to prepare the constructs for tracheal implantation or to simulate the *in vivo* conditions. These techniques include using *in vitro* culture, *in vivo* implantation, or a combination of these steps. When deciding on culture conditions, researchers have to determine whether to use growth factors, certain revascularization techniques, and the location and type of implantation. Summaries of tracheal tissue engineering studies are

provided in Table 2.2 through Table 2.5, where Table 2.2 summarizes *in vitro* studies, Table 2.3 outlines orthotopic *in vivo* studies, Table 2.4 includes heterotopic (subcutaneous) *in vivo* studies, and Table 2.5summarizes *in vivo* studies that implant the construct heterotopically and orthotopically.

Growth factors

Various research groups have exposed their constructs to growth factors at some point in the duration of the study. While growth factors are a common culture medium component in trachea tissue engineering studies, only a few studies have included growth factors in the scaffold materials. One method by which growth factors have been placed into a scaffold is by encapsulation in gelatin microspheres [52, 53] or in gelatin sponges[40, 53, 136] and coated on the trachea construct. Another approach has been to perfuse growth factors into the construct.[113, 116] Vascular endothelial growth factor (VEGF) perfusion through a Degrapol scaffold resulted in increased tissue ingrowth and capillary formation in an *ex ovo* chorioallantoic membrane (CAM) model, as compared to a VEGF precoated scaffold.[116] The growth factors utilized in these studies were used to enhance angiogenesis (VEGF)[116] or to improve chondrogenesis with bFGF,[53] TGF-β2,[52] or BMP-2.[40, 136]

***In vitro* culture and *in vivo* implantation**

Once cells are added to the scaffold, through static or dynamic seeding, the constructs can then be exposed to various *in vitro* and/or *in vivo* conditions before

implantation. Bioreactor and static culture have been used independently or in conjunction with each other. One group showed that bioreactor versus static culture did not have an effect on the GAG content and mechanical properties of scaffold-free chondrocyte constructs.[117] While constructs have been extensively evaluated in static or dynamic *in vitro* culture, ultimately they must be placed in an *in vivo* model to determine functionality and performance in a living organism. Animal models used for tracheal tissue engineering vary from nude mice to pigs, and as of yet a standard animal model for tracheal research has not been established.[118]

Before implantation into an animal model, pre-culturing the constructs *in vitro* may be an important step. For example, Luo *et al.*[64] suggested that *in vitro* pre-culture of constructs may reduce inflammation of biomaterial-based constructs and promote better ECM formation once implanted *in vivo*. A chondrocyte seeded collagen-PCL tubular construct was exposed to a rotating wall bioreactor *in vitro*, followed by orthotopic implantation in rabbits. Unfortunately, formation of granulation tissue caused stenosis in all animals.[64] Tan *et al.*[113, 116] suggested implanting an intra-scaffold perfusion bioreactor, which combines *in vitro* seeding and culture with *in vivo* implantation, in emergency patients who cannot wait for the time consuming construct preparation. The authors proposed to implant the bioreactor system into a patient, supported by an extracorporeal portable system pump. This *in vivo* bioreactor concept has been practiced *in vitro*, but *in vivo* testing remains for future research.

In a unique approach to tracheal tissue engineering, one group evaluated the feasibility of surgically repairing tracheal defects in fetal sheep while *in utero*.[25, 26, 56] In three different studies, allogeneic chondrocytes, bone marrow stromal cells, or amniocytes were seeded onto PGA mesh and implanted in fetal tracheal defects approximately 3 weeks before birth. This approach was feasible with a majority of the lambs surviving and able to breathe at birth. Fetal sheep have been shown to tolerate non-allograft materials,[60] so regeneration and integration of the TE constructs may have a better chance when performed *in utero*. This *in utero* technique is a way to address tracheal stenosis early, but the ability to detect tracheal stenosis *in utero* and the overall risk of such an operation still remain as obstacles to the clinical use of such an approach.

While sequence of culture conditions can vary, the size and location of implantation for *in vivo* studies can also differ. Some studies implanted the tissue engineered trachea subcutaneously.[49] In these cases, survival rates were usually high and tissue in-growth was observed; however, the *functionality* of the construct cannot be analyzed with subcutaneous implantation. A majority of the tracheal tissue engineering studies placed the construct in a patch or circumferential defect in the trachea (orthotopically). Survival rate and performance of the constructs were typically good in patch (or window) defects, while lower survival rates and more complications occurred in circumferential defect repair. Alternatively, some researchers implanted the construct subcutaneously to precondition the construct, and then transplanted the construct orthotopically.[46] An intricate approach was recently

introduced, where tracheal constructs were cultured in a perfusion bioreactor *in vitro*, followed by paratracheal implantation, and finally implanted orthotopically.[129] While this is an elegant and complex approach, stenosis was observed in all cases, and the authors suggested this may have been due to the lack of epithelial lining.

Revascularization

In a recent ground-breaking transplantation study, an allograft trachea was implanted in a patient's forearm for 4 months to revascularize the trachea construct.[18] Then, the allograft trachea was placed into the recipient's tracheal defect. Not only was the trachea revascularized, the patient eventually did not require immunosuppressive therapy after 229 days. This clinical study was only one method of providing for enhanced vascular ingrowth *in vivo*. Similar pre-conditioning approaches have been used for tissue engineered tracheas in animal studies (Table 2.4).

Walles *et al*.[70, 100, 126] addressed vascularity concerns by preserving the vascular pedicle in decellularized intestine grafts, and perfusing the pedicle with endothelial cells. Surrounding the construct with vascularized tissue is another revascularization technique. For example, a PLGA-gelatin/polypropylene prosthesis construct was attached to omentum (highly vascular tissue) and then implanted in a circumferential defect in the dog tracheas.[48] Obtaining an omentum/scaffold construct was challenging due to complicated isolation techniques (success rate 53%), however, once the omentum/scaffold constructs were implanted into the trachea, they

maintained an adequate inner diameter and had stable surfaces after 1 month. Matloub and Yu[68] performed an acellular study with a polytetrafluoroethylene (PTFE) scaffold lined with a fascial flap and skin grafts in 20 rats for 3 weeks. The fascial flap promoted blood vessel formation across the PTFE scaffold.

Tan *et al*.[112] addressed oxygen diffusion by incorporating an oxygen carrier (Oxygent) in their *in vitro* culture medium, and found that it enhanced epithelial cell metabolism. However, reduced GAG content and histology revealed that Oxygent may have interfered with cartilage formation. The authors noted that further testing would need to be done to evaluate the long term effects of Oxygent on cartilage.

Summary

In this final and most important step, constructs must be exposed to optimal culture conditions in order to maximize their performance in living organisms. Culture techniques for tracheal tissue engineering range from simple to very complex. In addition to common static or dynamic *in vitro* culture and subcutaneous or orthotopic *in vivo* implantation techniques, researchers have occasionally combined these techniques to advance tissue regeneration or overcome drawbacks of using one technique alone. The benefit of combining the techniques into a more complex sequence may have advantages to construct survival, but further side-by-side comparisons of these new combination techniques are needed to determine the best culture conditions, in order to prepare the constructs for human implantation. As

tracheal constructs enter the clinical setting, a simple, expedient, and user-friendly approach would be ideal.

CLINICAL STUDIES OF TRACHEA REGENERATION

Only two groups have implanted a tissue engineered trachea in humans. A group in Japan created a polypropylene reinforced mesh coated with collagen and preclotted with autologous blood, which has been implanted in eight human cases with a 4 year follow-up.[83, 86] In contrast, a European team of collaborators from Spain, Italy, and the UK developed a decellularized donor trachea seeded with autologous cells, which has been implanted in one human case with an 18 month follow-up.[6, 66]

The Japanese group has since added cells to their constructs, including bone marrow aspirate, bone marrow-derived stem cells, and fibroblasts.[74, 78] They have also coated the lumen of the polypropylene/collagen construct with poly (L-lactic-acid-co-ε-caprolactone) to delay degradation of the underlying collagen layer, which is intended to allow time for the host's epithelium to migrate onto the collagen layer.[98] According to news reports[1, 2] and the medical literature,[44] the European group has since repeated the decellularized trachea transplantation in additional patients, including two cancer patients and a pediatric patient. In the pediatric case, the transplanted segment was lengthy (7 cm), so a polydioxanone (PDS) stent was placed in the lumen and successfully removed after 2 months.[44] The patient was reported to be healthy.[44] In an attempt to reduce construct preparation time, the European group

incorporated cells and growth factors (erythropoietin, granulocyte colony stimulating factor, and beta-transforming growth factor) into the decellularized scaffold intra-operatively.[44] This *in situ* approach followed the bionic tissue engineering concept proposed by Bader,[6] where a cocktail of growth factors was used to prompt cell growth and differentiation (i.e., boosting factors, recruitment factors, and commitment factors).

Summary

Two approaches to the use of tissue engineered tracheas have reached the clinical arena, and have been successful in humans. While there has been some success, researchers continue to improve upon their respective approaches to address issues like complex preparation time, revascularization, and matching scaffold degradation to tissue integration. These techniques are still in the case-by-case investigational phase, so a full scale clinical trial will be needed to determine functionality in a larger population with a more diverse set of trachea defect types.

DISCUSSION

Great amounts of time and research have been invested into tracheal tissue engineering, and the constructs that have been developed show promise for a clinically-useful tissue engineered replacement. However, many problems have arisen, such as how to maintain structural support of the tissue-engineered construct,

controlling the resorption processes,[14] minimizing the rejection response,[14] optimizing re-epithelialization, and promoting revascularization.

Even the first clinically transplanted tissue engineered trachea,[66] which has functioned successfully in patients thus far, was limited by a long-preparation time, revascularization, and reliance on donor tissue.[99, 106, 133] Even though some limitations exist with decellularized tissue, it is a short term solution that is helping patients with devastating tracheal diseases. The reliance on donor tissue, however, for the decellularized scaffolds is a major limitation, and a synthetic construct may be a better long-term goal of this technology. This obstacle could be overcome by fabricating a scaffold that mimics the decellularized tissue. For example, using fibrous based scaffolds created through techniques like electrospinning could simulate the nanometer scale of the extracellular matrix.[91] By further understanding the microscopic properties of the decellularized tracheal tissue, researchers may be able to use a biomimetic hierarchical approach to reverse-engineer these structures.

Revascularization is another major concern and needs to be addressed, as it is a crucial step in the translation of the tissue engineered trachea from the lab to the clinical arena. While the tissue engineered tracheas that have been implanted in humans seem to be successful, they were not vascularized prior to implantation. Some researchers are concerned that the body cannot successfully revascularize these implants when placed orthotopically, and as a result the constructs may undergo some degree of necrosis.[17] Many methods have been employed to revascularize tissue engineered tracheas, ranging from special surgical procedures (i.e., heterotopic

implantation[18]), to growth factors (e.g., VEGF[116]), to endothelial cell perfusion into the decellularized vascular pedicle.[126] There is no simple and straightforward answer to revascularization, and researchers are not yet in agreement with regard to whether a pre-vascularized construct is needed.[17] At the very least some vascularization is needed in tracheal tissue engineering to maintain construct viability, and future tissue engineered tracheas must include a plan for vascularization.

Growth potential is another important aspect of tracheal tissue engineering. If an implanted construct is vascularized, integration into the native tissue should follow and cells will slowly replace the biomaterial. With the construct fully integrated into the tissue, it should have the potential for growth with the patient. This growth potential has been assessed in vascular grafts.[105] Growth potential in tracheal tissue engineering has not been extensively studied. With the recent implantation of a decellularized donor trachea-based construct in a pediatric patient,[44] this phenomena has to be accounted for in humans.

A large number of studies in this review have investigated a composite of materials and/or cells to address the existing problems of tissue engineered tracheas. Birchall and Macchiarini[10] suggested that a successful trachea construct should not rely on only one tissue type, but instead be a composite tissue that incorporates the mucosa, connective tissue, cartilage, etc. Whether this means multiple cells types are needed, or one cell type could function with the ability to ideally be guided into different lineages according to spatial location, remains to be determined. Stem cells have this differentiation potential, and further use of stem cells in trachea tissue

engineering warrants further investigation. Specifically, stem cells have the potential to overcome invasive harvesting procedures, and the pluripotent characteristics could reproduce the diverse population of cells found in the trachea. Utilizing stem cells with a scaffold that releases growth factors in a gradient manner,[21] could regionally cue the cells to differentiate into the required cartilage, epithelium, and other tissues that exist in the native trachea.

Combining scaffold materials could also be useful, where a composite of materials would be more biomimetic, with one type of material providing mechanical integrity of the construct, and the other materials creating a degradable, biocompatible environment for cells. Multitudes of materials have been used in the trachea, and new material fabrication techniques and materials need to be considered and applied to tracheal tissue engineering. For example, bioprinting of tissue is a relatively new fabrication technique,[72] which could be applied to tracheal patches.

While the literature claims that there are no optimal replacements for large circumferential defects, tissue engineering studies are evaluating both partial and circumferential defects. So the question is, what types of trachea replacements are really needed? And if repair of both types of defects (partial and circumferential) may be based on each individual case, then can a tissue-engineered trachea be tailored for both applications? This one-size-fits-all approach is attractive from a fabrication, mass production, cost, and ease of use perspective; however, a patient specific solution may be more clinically applicable. The technology does exist to create

patient specific tracheal replacement scaffolds; as seen in the CT generated, anatomically designed tissue engineered trachea.[73]

Lastly, the types of culture conditions also need further development. A longer time in an *in vitro* bioreactor or the use of *in vivo* subcutaneous pre-conditioning would allow for tissue formation prior to implantation; however, this requires time and money, introduces regulatory challenges, and introduces risk for bacterial contamination. Bader and Macchiarini[6] suggested eliminating any culturing of cells or constructs, and implanting the construct with a special mix of growth factors used to induce physiological regeneration. Tan *et al*.[113, 116] attempted to eliminate the *in vitro* seeding and culture step by implanting a bioreactor with the trachea construct directly into an animal. The value of *in vitro* culture needs to be further elucidated in side-by-side comparisons of constructs implanted *in vivo* with and without the *in vitro* pre-culture step.

As the optimal construct is developed experimentally, regulatory considerations must also be kept in mind. According to the FDA, a product can either be submitted as a device or as a drug-related item for ultimate approval. The constructs mentioned throughout this review include biomaterials, cells, and proteins (growth factors), and as a result they could fall into both categories as a combination product. As the complexity of the product increases, more regulatory standards and test methods are needed to evaluate the safety and efficacy of such products. Thus, it could become more difficult to achieve regulatory approval and investment funding for commercialization of these combination products. As a result, researchers are

challenged to find a tracheal construct that has a straightforward design. Currently, decellularized tissue is FDA approved for a few applications, for example decellularized heart valves are approved for valve replacement. Approval of such products is promising for allograft and tissue engineering products.

As there is no preferred treatment for tracheal stenosis, there exists a clinical need for tracheal replacement options. As the field of tissue engineering attempts to develop tracheal replacements, multiple types and combinations of cells, scaffold materials, and/or culture conditions have been used. The constructs that have reached clinical application thus far involve a combination of materials or a combination of cells, with and without *in vitro* preculture. Critical assessment of the progress of tracheal tissue engineering provided in this review will hopefully illuminate methods to address vascularization, mechanical stability, fabrication time, and reepithelialization. As we strive to bring trachea regeneration to the clinic, the most direct route would be to employ an off-the-shelf biomaterial, classified by the FDA as a medical device, capable of supporting cell infiltration without the need for any pre-seeding, pre-culture or bioreactors. However, additional layers of complexity may be required, such as seeding the construct with the patient's own stem cells in the operating room, or incorporating growth factors into the construct, which if necessary would justify the associated pursuit of a more lengthy and costly regulatory process. The community has yet to establish an agreed-upon animal model, which will be necessary for initial screening of candidate products and treatment strategies for the clinic. Recognizing that there is unlikely to be a "one-size-fits-all" approach, it is

possible that simpler strategies for tracheal patches may provide a more straightforward route to the clinic, whereas more complex strategies (e.g., cell seeding, heterotopic implant preculture, growth factor release, etc.) may be justified in terms of additional time and cost if they are necessary for regeneration of large circumferential defects.

CHAPTER 3: *In vitro* characterization of gradient electrospun scaffolds for tracheal defect repair

ABSTRACT

Tracheal stenosis and obstruction is a fatal condition, and current treatments include augmentation of the airway with autologous tissue. A tissue-engineered approach would not require a donor source, while providing an implant that meets surgeon's and patient's needs. A fibrous, polymeric scaffold organized in gradient bilayers of polycaprolactone (PCL) and poly-lactic-co-glycolic acid (PLGA) with 3-D printed structural ring supports, inspired by the native trachea rings, could meet this need. *In vitro* degradation of various scaffold designs over 12 weeks revealed that scaffolds with the bioprinted rings had superior properties in tensile and radial compression, with at least a 3-fold improvement and 8.5-fold improvement, respectively, relative to the other scaffold groups. The ringed scaffolds produced tensile moduli, radial compressive forces, and burst pressures similar to or exceeding physiological forces or native tissue data. Scaffolds with a thicker PCL component had better suture retention and tube flattening recovery properties, with the monolayer of PCL (PCL-only group) exhibiting 2.3-fold increase in suture retention strengths. Tracheal scaffolds with ring reinforcements have improved mechanical properties, while the fibrous component increased porosity and cell infiltration potential. These scaffolds could be used to treat various trachea defects (patch or circumferential) or in other tissue engineering applications.

INTRODUCTION

Tracheal tissue engineering is of particular importance because of the high mortality rates due to tracheal stenosis or obstruction. Electrospun scaffolds gained attention for their biomimetic fibrous microenvironment and relative ease of fabrication. These materials have excellent potential for tracheal application, as they are easily shaped into tubular structures for circumferential applications or into sheets for segmental patch applications. Degradable polymers were chosen for their lack of reliance on donor tissues and ability to be replaced and regenerated by host tissue. Our scaffolds are designed into a graded bilayer with one layer providing long-term structural support (i.e., polycaprolactone (PCL)) and the other layer allowing for short-term tissue ingrowth and drug delivery (i.e., poly(lactic-co-glycolic) acid (PLGA)). A polymeric ring of PCL) was incorporated into the fibrous scaffold for added structural integrity. In the current study, seven different permutations of the scaffold were tested, 1) PCL alone, 2) PLGA alone, 3) PCL/PLGA co-spun/blend, 4) PCL/PLGA co-spun/blend, 5) PCL/PLGA bilayer, 6) PCL/PLGA graded bilayer, and 7) PCL/PLGA graded bilayer with incorporated rings. We evaluated the porosity, fiber morphology, molecular weight, mass loss, and mechanical properties of our scaffolds under *in vitro* degradation conditions (Figure 3.1). *In vitro* characterization is crucial for scaffold design and pre-clinical efficacy building. The purpose of the current study is to characterize the tracheal scaffolds and determine the design that meets physiological requirements. We hypothesized that the PLGA would affect porosity and mass loss/molecular weight properties, the PCL component would

provide consistent elastic properties, and the ring would dramatically improve mechanical properties.

MATERIALS AND METHODS

Material fabrication

Using a custom designed electrospinning apparatus, 2 mm thick electrospun fiber hollow cylinders (in all groups except for ring containing scaffolds) were fabricated following a slightly modified protocol established in a previous publication for our group [58]. A 7 wt% polycaprolactone (PCL; inherent viscosity 1.0-1.3 dL/g, LACTEL, Birmingham, AL) solution in hexafluoro-2-propanol (HFIP; Oakwood Chemical; Columbia, SC) and a 14 wt% poly(D,L-lactide-co-glycolic acid) copolymer (PLGA; 50:50 lactic acid : glycolic acid, acid end group, inherent viscosity 0.35 dL/g, Evonik Industries, Birmingham, AL) solution in HFIP were mixed. Safety precautions, personal protective equipment and a well ventilated working environment were used when handling toxic solvents. The solutions were placed in 20 mL syringes and fitted into programmable syringe pumps (PhD Ultra, Harvard Apparatus, Holliston, MA) set to extrude the solution at 5 mL/hr. As the solution was extruded through a charged 20 gauge needle (+12 kV; Glassman High Voltage, High Bridge, NJ), the charged polymer was drawn from the needle tip to a negatively charged (-6 kV) rotating cylindrical stainless steel mandrel (7 mm diameter).

To create the monolayer groups (Figure 3.1), 40 mL of PCL solution and 40 mL of PLGA solution were electrospun to create the PCL monolayer and PLGA monolayer groups, respectively. The PCL/PLGA co-spun monolayer group was created by electrospinning separate solutions of 20 mL of PCL and 20 mL of PLGA at the same time from opposite sides of the mandrel, simultaneously, collecting both fiber types on the mandrel. The PCL/PLGA blend monolayer group was created by mixing equal volumes (20 mL each) of 7 wt% PCL and 14 wt% PLGA solutions prior to electrospinning (creating a 3.5 wt% PCL and 7 wt% PLGA solution for a total polymer solution of 10.5 wt%).

To create the bilayer group, 20 mL of PCL solution was electrospun onto the mandrel followed by 20 mL of PLGA solution.

To create the gradient interface group, 12 mL of PCL was deposited, followed by co-spinning 8 mL of PCL and 8 mL of PLGA from two different needles on opposite sides of the mandrel to create the interface layer, followed by 12 mL of PLGA.

To create the 3-D printed rings, a 3D CAD image was used to print 7 mm ID, 11 mm OD, 2 mm thick PCL (MP05188, MakerBot filament, Brooklyn, NY) rings with a circular cross section(RepRapPro printer, Briston, UK).

To create the gradient interface group with circumferential rings, 6 mL of PCL was deposited, the PCL rings were cut open on one end and wrapped around the cylindrical stainless steel mandrel at 3-4 mm intervals, 6 mL of PCL was deposited

over the rings, followed by co-spinning 8 mL of PCL and 8 mL of PLGA to create the interface layer, followed by 12 mL of PLGA.

To prevent delamination of the layers, in between the deposition of layers, HFIP was lightly misted with an atomizer onto the outer surface of the scaffold to prepare the surface for the next layer. Once the 2 mm wall thickness was achieved, the electrospun tube was removed from the collecting rod, lyophilized for 24 hours, sterilized using ethylene oxide, and aired in a fume hood for 24 hours.

Degradation conditions

Following ASTM F1635-11, the scaffolds were degraded in simulated physiological conditions. Scaffolds were immersed in phosphate-buffered saline (PBS; P5386, Sigma, St. Louis, MO) at 7.4 ± 0.2 at 37°C. To maintain stable aging conditions, the PBS-to-scaffold volume ratio was 100:1. The pH was measured periodically and if an excursion beyond the specified pH range occurred the PBS was removed and refreshed with new PBS for all samples. Samples were collected and washed at specific time points (0, 1, 2, 3, 4, 6, or 12 weeks) for analysis.

SEM

The scaffolds used for imaging represented all seven groups at the 0, 6, and 12 week time points (n=3). All scaffolds were lyophilized overnight before being cut with a scalpel and placed on a specimen holder. The samples were sputter coated (Q150T ES, Quorum Technologies, East Sussex, England) with 30 nm of gold before being positioned in the SEM (Leo 1550 field emission, Carl Zeiss, Oberkochen, Germany).

They were subsequently placed under high vacuum at an accelerating voltage of 10 kV and working distance between 11.5-12.5 mm using the SE2 detector. Each sample was imaged at 500x, 1500x, 2500x, and 5000x magnification with a line integration time of 45 seconds.

Porosity

The scaffolds used for porosity calculation represented all seven groups at the 0, 6, and 12 week time points (n=3). Porosity calculation was determined using the gravimetric method. The mass of the sample was measured (scale ± 0.0001 g), followed by the inside diameter, outside diameter, and height (calipers ± 0.01 mm). Using this information, the apparent density and porosity were calculated according to the equation: $\rho_{app} = 4m/\pi d^2 h$, $Porosity\ (\%) = (1-\rho_{app}/\rho) \times 100$, with m, d, h, and ρ as the mass, diameter, height, and bulk density, respectively. The bulk density (ρ) of PCL and PLGA were 1.081 ± 0.003 gm/cc and 1.324 ± 0.004 gm/cc, respectively.

Mass loss

The scaffolds used for mass loss represented all seven groups at the 0, 1, 2, 3, 4, 6, and 12 weeks (n=3). The mass loss was determined from the initial mass before degradation and the residual mass after rinsing with distilled water and lyophilizing. The results were reported as a percent mass loss versus degradation time.

Size exclusion chromatography

The scaffolds used for molecular weight analysis represented all seven groups at the 0, 1, 2, 3, 4, 6, and 12 weeks (n=3). The residual mass of each scaffold were rinsed with distilled water, lyophilized, completely dissolved in chloroform (at 5

mg/mL), and filtered with a 0.02 μm filter (6809-2002; Whatman; Buckinghamshire, UK). An HPLC system (CBM-20A, LC-20AB, SIL-10AF, CTO-20AC; Shimadzu; Kyoto, Japan) equipped with a column (PL1110-1520, PL1110-6504 (rated for 200-400,000 g/mol); polystyrene/divinylbenzene matrix packing, Agilent Technologies; Santa Clara, CA) and multi-angle light scattering (MALS) (miniDAWN TREOS; Wyatt Technology; Santa Barbara, CA) and refractive index (RI) (RID-10A; Shimadzu; Kyoto, Japan) detectors was used. Samples were eluted at 1 mL/min and the column was maintained at 35° C. A series (530, 3350, 30,000, 105,000, and 245,000 Da) of narrow polydispersity polystyrene standards (TDS-PS-NB; Malvern; Malvern, Worcestershire, UK; 41930, 41925; Alfa Aesar; Ward Hill, MA; PL2012-2001; Agilent Technologies; Santa Clara, CA) were used for calibration.

After data collection, the RI and MALS data were analyzed for weight average molecular weight (M_w) values. MALS data was analyzed with light scattering equations and Zimm plots using ASTRA 5 software (Wyatt) [134]. The *dn/dc* values for PCL and PLGA were empirically determined using the RI detector (RID-10A; Shimadzu; Kyoto, Japan) (PCL = 0.0386 ± 0.0047 mL/g, PLGA = 0.0243 ± 0.0025 mL/g). RI data were analyzed with the polystyrene calibration curve using LC Solutions software (Shimadzu). Mark-Houwink-Sakurada correction was not performed because the *a* and *K* constants for PCL and PLGA were not available in the literature [11].

Tensile testing

The scaffolds used for tensile testing represented all seven groups at the 0, 3, 6, and 12 weeks (n=3). The testing method is similar to a previously published study from our group [107]. Briefly, tensile tests were performed using a uniaxial testing apparatus (Instron Model 5848, Canton, MA) with a custom-made stainless steel bath and grip assembly. The grip faces were covered with 220-grit waterproof sandpaper that provided extra traction without damaging the specimens.

Before testing, each specimen was thawed and equilibrated in 0.01M PBS at 37 ± 1° C for 1 hour. Prior to degradation, the specimens were cut into long rectangular strips from the tubular scaffolds, in a circumferential direction. Prior to testing, the specimens were cut into 2 mm width strips using parallel razor blades. The average specimen thickness of 1.26 ± 0.39 mm and average width of 1.96 ± 0.16 mm. Specimen dimensions were measured using calipers (± 0.01 mm). After specimens were secured between the grips, a tare load of 0.03 N was applied to remove the laxity of the specimen. The bath was then filled with PBS at 37° C and the specimen was allowed to re-equilibrate under this tare load for 10 min. The average initial specimen length was 7.6 ± 1.0 mm. Preliminary studies determined that preconditioning is not required to obtain repeatable stress-strain curves and that a stress relaxation phase of 30 min was sufficient for the samples to reach equilibrium. Preliminary testing showed that 15% strain was safely below the onset of failure or slippage from grips (as indicated by sudden drops in force during step strain).

A buoyant force correction was performed as described by Detamore and Athanasiou [19]. Briefly, the load exerted by the PBS on the top grip (F_b) was

measured empirically as a function of grip-to-grip separation (d). The measured force (F_m) was adjusted to the actual force experienced by the sample (F) by subtracting the effect of buoyancy, i.e., $F(d) = F_m(d) - [F_b(d) - F_b(L_0)]$, where L_0 is the initial specimen length. For a consistent buoyant profile, the bath height was held constant throughout all experiments and the bath was covered with parafilm to reduce evaporation. The change in bath height was observed to be negligible at the end of each test.

The testing protocol involved two phases: 1) applying a tensile load of 1% strain/sec to a 15% strain endpoint and 2) holding for 30 minutes at 15% strain. Stress-strain curves were generated from the continuous pull during the step strain to 15%. Young's moduli were obtained from the linear regions of the stress-strain curves (no toe region observed). Equilibrium moduli were obtained by dividing the average stress during the last 30 seconds of the relaxation phase by the step strain (15%).

Burst pressure

The scaffolds used for burst pressure testing represented all seven groups at 0, 3, 6, and 12 weeks (n=3). In accordance with ISO 7198:1998(E) and a previously published method [23], a 60 mL syringe (Becton-Dickenson, USA) was filled with water and placed in a syringe pump (KD Scientific, USA) set to run at a constant rate of 20 mL/min. The syringe was attached to a length of surgical tubing, which was attached to a custom pressure sensor. This pressure sensor was attached to another length of surgical tubing, which in turn was connected to a pediatric Foley catheter

(Coloplast, Denmark). The catheter's balloon was placed in the view field of a High Accuracy CCD Micrometer (Keyence, USA). Pressure and scaffold diameter readings were measured and recorded at time intervals of 0.25 seconds as the tests took place using Labview 2010 software.

Before the first test, the second length of surgical tubing was disconnected from the catheter. To ensure no air was present inside the testing apparatus, water from the syringe was pumped through the apparatus and allowed to exit from the open end of the second length of surgical tubing into a separate container. A separate syringe was used to repeatedly fill the Foley catheter with water and draw a vacuum until nothing but water was left inside. At this time the catheter was also inspected to make sure the balloon filled evenly. The catheter and second length of surgical tubing were then reconnected prior to testing.

Frozen scaffolds were allowed to thaw before they were removed from their sterile containers. Scaffolds were submerged in a 37° C warm water bath for 3 minutes. They were then removed from the water bath and placed over the balloon of the pediatric Foley catheter.

The Labview 2010 recording program was initiated, and the syringe pump was run. The pressure and width of the scaffold were monitored and recorded. The syringe pump was deactivated and testing ceased when the scaffold failed or the pressure reached 30 psig. The maximum pressure of 30 psig was chosen based on the physical constraints of the catheter, tubing connections, and syringe pump.

Using Microsoft Excel, pressure and change in diameter were plotted by group and by week. The average change in diameter at 30 psig or failure for each group was calculated by week and recorded in a table.

Suture retention

The scaffolds used for suture retention testing represented all seven groups at 0, 3, 6, and 12 weeks (n=3). Suture retention tests were performed using a uniaxial testing apparatus (Instron Model 3342, Canton, MA) with a custom-made suture fixture (a hook attached to the top fixture). Before testing, each specimen was thawed and equilibrated in 0.01M PBS at 37° C for 15 min. The specimen geometry was elliptical with a 2.5 cm length and 1 cm width. The elliptical shaped specimens were cut in half using a scalpel, so that the specimens were 1.25 cm length and 1 cm width. Specimens were oriented in the bottom grip in such a way that testing was done in two directions to simulate the suture forces in the radial and axial direction. Specimen dimensions were measured using a caliper (± 0.01 mm). The average specimen thickness was 1.67 ± 0.71 mm. A 4-0 PDS suture (M315A; Patterson Veterinary; Devens, MA) was placed 3 mm from the edge of the scaffold, tied into a loop and knotted 7 times. The suture loop was attached to the suture holder and testing commenced. The testing protocol involved pulling the suture loop at 1% strain/second (with the strain based on the length between bottom grip and the suture hole) until the sutured pulled through the scaffold (no tare load applied as the only measurement obtained was the final force). The testing was not done under hydrated conditions as the scaffold was pre-hydrated and testing time was short enough to

ensure specimen remained hydrated during testing. The force required to pull the suture through the scaffold was classified as the suture holding capacity (SHC) and the SHC divided by the scaffold thickness multiplied by the suture thickness was classified as the suture retention strength (SRS) [80].

Tube flattening

The scaffolds used for tube flattening testing represented all seven groups at 0, 3, 6, and 12 weeks (n=3). Unconfined compression testing was performed using a uniaxial testing apparatus (Instron Model 5848, Canton, MA) with a custom-made stainless steel bath and compressive platen assembly. Before testing, each specimen was thawed and equilibrated in 0.01M PBS at 37° C for 1 hour. Specimen dimensions were measured using a caliper (± 0.01 mm). The specimen geometry was tubular with a 21.0 ± 1.7 mm length and an average inner diameter of 6.5 ± 1.3 mm and average outer diameter of 9.6 ± 1.6 mm. The specimens were placed on the bottom platen and a tare load of 0.1 N was applied. The bath was filled with PBS at 37° C and the specimen was allowed to re-equilibrate under this tare load for 10 min. Then the specimen was compressed in the radial direction at 0.1667% strain/second until reaching 80% strain (based on outer diameter) or until the load reached 45 N. The buoyant force was empirically determined to be negligible, a result of the top platen having a smaller volume and shorter distance traveled as compared to the tensile testing grips, resulting in a smaller buoyant force change as the fixture traveled through the PBS. To account for specimen recovery, the sample outer radiuses were measured 1 hour after testing.

The tube flattening force at 100% strain (for inner diameter) was determined by examining the load-extension profile, where the scaffold compression region was linear and deviated from linearity at the point of flattening (100% strain based on inner diameter). After the point of flattening, the load-extension profile exponentially increased as force from the bottom platen overtook the measured load. To isolate the point of flattening, a linear regression of the compression region was established and the point of flattening was established to be at 15% deviation. 15% deviation represented a reasonable value to allow a reproducible value and objective basis for identification of flattening. As a check, the extension at this point was compared to the caliper measured inner diameter to ensure a reasonable value had been identified. The actual caliper measurement was not used because the 100% strain could not be accurately determined by caliper measurements, due to difference in caliper and extension measurements after tare load. Percent recovery was determined by taking a ratio of the pre- and post-test outer diameter based on caliper measurement.

Statistical analysis

Using one-way ANOVA and Tukey's post-hoc analysis for SEM fiber diameter, porosity, Young's modulus, equilibrium modulus, burst pressure diameter change, suture retention strength, tube flattening force, and tube recovery differences were determined to be significant if $p<0.05$.

RESULTS

Gross morphology

Gross morphological images of scaffolds were collected through the course of degradation (0, 1, 2, 3, 4, 6, and 12 weeks) (Figure 3.3). The PCL component of the scaffolds was preserved through the course of 12 weeks, while the PLGA layer degraded (to a point that it could not be extracted from a tube) between 2 and 3 weeks (PLGA-only). The PLGA component in the combination groups (Co-spun through Gradient+Rings) were preserved longer with the support of the intertwined or underlying PCL, as evident by a translucent layer at week 3 through 6 in Bilayer and 7 images. Sample degradation for other analyses followed a similar trend, where the PLGA-only scaffolds were completed degraded by 3 weeks.

Fiber morphology

The average fiber diameter of the scaffolds ranged from 1.5-6.3 μm across groups (Table 3.1). There was a distinct difference between the PCL and PLGA fiber appearance and diameters. The PCL fibers (PCL-only and Bilayer) had 75% smaller diameter fibers than the PLGA fibers (PLGA-only) at week 0 ($p<0.05$). In addition, the PLGA fibers had a smoother, flatter surface with junctions between fibers deformed and fused together, while the PCL fibers were distinctly separate (Figure 3.3).

As the scaffold degraded, the PLGA component completely degraded after week 0 (in PLGA-only and Bilayer), lost its fibrous appearance and become an amorphous mass (Gradient), or retained its fibrous appearance up to Week 12 (Gradient+Rings). In the cases of blending or combining fiber types (Co-spun and Blended), the fiber morphology was unique. Co-spun fiber morphology became more

irregular and distorted as the sample degraded (week 6) and regained a normal fibrous morphology at the final time point (week 12). Blend fibers had a unique morphology upon degradation, where the length of a single fiber transitioned between one large diameter fiber to a bundle of smaller fibers (week 6 and 12).

The sample cross-sections at week 0 revealed a fibrous cross-section in all groups, except for PLGA-only, which appeared to be more of a porous polymer mass. The layered scaffolds had a noticeable demarcation, indicating a transition between polymer types (Bilayer, Gradient, and Gradient+Rings).

Polymer degradation

The mass loss data analysis shows the change in mass over degradation time (Figure 3.4). All groups experienced significant mass loss except for PCL-only, which is expected due to the slow degradation of PCL. For the Co-spun, Blended, Bilayer, Gradient, and Gradient+Rings groups, the mass loss dropped off significantly after 3 weeks, which was attributed to the degradation of the PLGA component. The blended and mixed scaffolds (Co-spun and Blended) experienced similar mass loss. Gradient scaffolds had the largest mass loss, while Gradient+Rings, a similar group with the exception of a PCL ring, had a much lower mass loss. This is expected since the PCL component was preserved over 12 weeks and comprised a larger part of the mass of the Gradient+Rings samples. No statistically significant differences were derived from these data.

The PCL component of the scaffolds in all groups maintained a similar molecular weight over the 12 week degradation (Figure 3.5). The pure PCL scaffold

(PCL-only) group had a consistent profile, maintaining a molecular weight around 117 kDa (MALS) or 146 kDa (RI). In contrast, the other treatment groups had molecular weight profiles that varied slightly more over time with a reduction in molecular weight at week 0 in the RI data, which could be due to PLGA and PCL chromatogram overlap thus reducing the M_w at week 0.. The Co-spun group degraded to a larger extent than any of the other groups.

The PLGA profile revealed that the molecular weight significantly decreased over 12 weeks (Figure 3.5). The pure PLGA scaffolds (PLGA-only) exhibited a rapid decrease from 64 kDa at 0 weeks to 6.5 kDa at 2 weeks (MALS) or 65.9 kDa at 0 weeks to 4.3 kDa at 2 weeks (RI). While processing the PLGA SEC data, it was difficult to distinguish between the PLGA and PCL at 0 weeks, so no data were collected for combination scaffolds at week 0. In the MALS profile, measurable PLGA was retained for 6 weeks in the blend Blend group, for 4 weeks in Bilayer, Gradient, and Gradient+Rings groups, and for 3 weeks in the Co-spun group. In the RI profile, measurable PLGA was retained for 6 weeks in all Co-spun, Blend, and Gradient groups, for 4 weeks in the Bilayer group, and only 2 and 4 week data points for the Gradient+Rings group.

Porosity

Calculated porosity values revealed that the percent porosity significantly increased by 17-31% from 0 to 6 weeks for all groups ($p<0.05$), except for PCL-only and Gradient+Rings (Figure 3.6). The porosity remained in the same range from 6 to 12 weeks for all groups (no week 6 or 12 data for PLGA-only).

At 0 weeks, all groups had porosities in the range of 55-70% except for the PLGA-only group. PLGA-only had the lowest porosity of all other groups at the week 0 ($p<0.05$). The Gradient scaffolds had a higher porosity at week 12, as compared to the PCL-only group at week 12 ($p<0.05$).

Mechanical properties

Tensile Testing: Stress-strain curves were linear through the tensile pull to 15% strain. The Young's modulus data showed that Gradient+Rings scaffolds outperformed by 5- to 250-fold increase moduli over all other scaffolds at the corresponding time points ($p<0.05$), except for PCL-only and Bilayer samples at week 0 ($p<0.05$) (Figure 3.7). Equilibrium modulus was used to evaluation viscoelasticity of the scaffolds, by determining how much the scaffolds relaxed during a hold at constant strain. The equilibrium modulus data followed trends similar to the Young's modulus data where the Gradient+Rings samples outperformed all of the other groups (3-fold improvement over the PCL-only and Bilayer group) ($p<0.05$) (Figure 3.7). Within the groups, the Young's moduli and equilibrium moduli did not significantly change over time.

Burst Pressure: None of the scaffolds failed during testing (max-out pressure of 30 psig) except for the Blend group at week 12. The Blend, week 12 scaffolds average burst pressure was approximately 19.7 psig. The change in scaffold diameter was measured from beginning of testing to the end of testing and a trend was observed across all groups in which the average change in diameter increased with degradation time (Figure 3.8). No statistically significant differences were established.

Suture Retention: Suture pull-out testing results had an overall general trend of decreasing suture holding capacity (SHC) (data not presented) and suture retention strength (SRS) over degradation time (Figure 3.9). The direction of testing (circumferential and axial) did not affect SHC or SRS.

SRS data for circumferential direction revealed that within groups, Blend SRS decreased by 97% from 0 to week 3, 96% to week 6, and 99% to week 12 ($p<0.05$). Gradient SRS also had degradation dependent decline in SRS (~66%) from week 0 to week 3 ($p<0.05$). Between groups, PCL-only, week 12 SRS were 2-fold or 400-fold higher than Co-spun and Blend scaffolds at week 12, respectively ($p<0.05$). PLGA-only SRS at week 0 were lower than all groups at week 0 ($p<0.05$). Blend, week 3 SRS were lower than PCL-only, Bilayer, and Gradient+Rings at week 3 ($p<0.05$). Blend, week 6 SRS were lower than PCL-only, Bilayer, Gradient, and Gradient+Rings at week 6 ($p<0.05$). Gradient+Rings, week 12 SRS were higher than Co-spun at week 12 ($p<0.05$).

Analysis of the SRS data in the axial direction revealed that within groups, Blend and Gradient scaffolds were affected by degradation with the SRS decreasing over time (Blend, week 0-week 6 and week 0- week 12; Gradient, week 0-week 3) ($p<0.05$). Among groups, PCL-only and Gradient+Rings, week 12 had greater SRS than Co-spun and Blend at week 12 ($p<0.05$). PLGA-only, week 0 SRS were lower than Blend, Bilayer, and Gradient at week 0 ($p<0.05$).

Tube Flattening: The load required to flatten the scaffolds followed an overwhelming trend, where Gradient+Rings scaffolds outperformed all other groups

at corresponding time points (denoted by #, $p<0.05$) (Figure 3.10). Degradation had no significant impact on tube flattening force within the groups.

The recovery of scaffolds after flattening revealed that Co-spun and Blend scaffolds at 3, 6, and 12 weeks remained in a flatter state (or recovered less) than PCL-only, Bilayer, Gradient, and Gradient+Rings at the corresponding time points ($p<0.05$). Gradient+Rings scaffolds at week 0 recovered better than Co-spun and Blend at week 0 ($p<0.05$). The blending or co-spinning of polymers resulted in tubular scaffolds that deform more permanently than other groups.

Within the groups, PCL-only, week 0 scaffolds recovered less than at week 6 ($p<0.05$). Co-spun, week 0 scaffolds recovered better than week 6 ($p<0.05$). Blend, week 0 scaffolds recovered better than week 6 and week 12 ($p<0.05$). Degradation of the blended or co-spun groups drastically reduced the scaffolds' ability to recover, as compared to other groups.

DISCUSSION

A comparison among the groups and their outcome measures was developed to determine the optimal scaffold design (Table 3.2).

Fiber diameter, pore size, porosity, and their interconnected relationship affect cell response. Submicron PCL fibers, in a range from 0.25-2 μm have been shown to improve cell attachment and proliferation due to the increased surface area that enhanced protein binding [110]. However, this relationship has not been seen with other polymers [110]. The scaffolds in the current study exhibited fiber diameters in the

micron range, with PCL-only scaffolds exhibiting a slightly lower fiber diameter than other groups. Fiber morphology and diameter can be tuned with the electrospinning fabrication process (e.g., solution concentration, solution conductivity, needle to collector distance, ambient conditions) [90]. In our process, these parameters were empirically selected to produce uniform submicron-micron fibers in the range of 0.5-1.5 μm (data not shown). However, fiber morphology altered significantly after sterilization, specifically in the case of PLGA fibers, which appeared to have melted after sterilization (flattened appearance in SEM images). This phenomenon is not mentioned greatly in the electrospinning literature, except for one study that found that ethylene oxide can damage fragile structures found in electrospun materials [92]. Further investigation is needed to determine how the ethylene oxide sterilization process can be altered (e.g., concentration, temperature, humidity, time) to preserve scaffold architecture or to determine better sterilization methods.

The blending of two polymer prior to electrospinning created a distinctive fiber morphology which could be due to phase separation where the two polymers assumed distinct spatial organization with-in one fiber when electrospun, where the PCL component could be the spindle-like fibers in the interior of the fibers and the PLGA component filling around through PCL fibers. The difference in polymer properties (e.g. conductivity) could have affected how the two polymers electrospun together. The unique fiber morphology created by polymer blending could be used beneficially in specific tissue applications.

Porosity is another important factor that affects cell infiltration and diffusion. All of the groups, except for the PLGA-only group, at some point during degradation had the recommended range of 70-90% porosity [110]. All groups became significantly more porous after 6 weeks due to the degradation of the PLGA component. The Gradient+Ring group had a decline in porosity due to the retention of the solid PCL ring. To obtain more accurate porosity measurement, other techniques could be employed (e.g., gas adsorption or flow porosimetry) [38], although our work with microCT revealed that the submicron pore sizes in electrospun materials were not detectable.[62] Techniques to increase porosity can be employed with electrospinning, like salt leaching, sacrificial-fiber incorporation, 3D printing, or phase separation.[62] The PCL ring's porosity could be increased to allow for cellular infiltration prior to degradation; however, mechanical properties would need to be maintained with the increase in porosity.

Molecular weight change and mass loss of the scaffolds were used to assess how the tunable properties (i.e., polymer mixing and layering) affect degradation. Since static degradation conditions were employed, as compared to dynamic mechanical loading, chemical degradation was the primary degradation mechanism. PCL and PLGA degrade through hydrolysis of the aliphatic ester linkages and undergo bulk erosion.[123] We hypothesized that fiber mixing (Co-spun, Gradient, and Gradient+Rings) would slow PLGA degradation due to limited diffusion of water to the internalized PLGA fibers. Indeed, the molecular weight profile for PLGA was slightly higher in combination groups as compared to PLGA-only (variation in M_W in

MALS data due to signal overlap). The decrease in PLGA molecular weight had a direct impact on suture retention strength, and less so on tensile or compressive properties. The dispersion of PLGA throughout the bulk of the scaffold (Blend and Co-spun) resulted in worsened tube flattening recovery, indicating that a thick PCL layer contributed to the elastic recovery of the scaffolds. Should the mechanical or drug delivery properties need to be tailored, the degradation of the PLGA can be controlled by LA/GA ratio, molecular weight, and shape/structure of matrix.

Desired mechanical properties for scaffolds usually rely on mimicking physiological conditions or empirical data derived from native tissue, although biomimicry may not necessarily result in functional *in vivo* performance. Tensile properties in the circumferential direction have no analog *in vivo,* besides inhalation/exhalation force, which will be discussed in the burst pressure section. Tracheal cartilage, crucial to the structural integrity of the trachea, exhibits a nonlinear stress-stain behavior with tensile forces from 0.02 to 0.01 N (porcine cartilage) [119]. The superficial zone of human tracheal cartilage (collagen dense region) resists tension, while the inner layer (proteoglycan rich) resists compression (equilibrium tensile modulus was 13.6 ± 1.5 MPa for abluminal superficial zone and 4.6 ± 1.7 MPa for middle zone) [95]. Rabbit tracheal cartilage exhibits an ultimate tensile strength of $4.08 \pm 0.96 \times 10^2$ kPa and elastic modulus of $3.5 \pm 1.1 \times 10^2$ kPa [141]. Comparing these data to our data, our scaffolds exceeded the Young's modulus of the native rabbit trachea, except for PLGA-only. Gradient+Rings scaffolds

possessed an equilibrium modulus similar to human tracheal tissue (in the abluminal superficial zone).

Physiological expiration and inspiratory pressures for adults and kids are in the range of 60-150 mm H_2O (or 0.853-2.133 psi) [131]. Bursting strength of the porcine trachea has been reported to be 180 mmHg (3.48 psig) in the pharyngeal portion (dorsal or top of trachea) and progressively decreased down the trachea length to 110 mmHg (2.13 psig) in the tracheal carina (ventral or bottom of trachea before bifurcation) [104]. Our implant was tested in its tubular form, not sutured into a native trachea. Testing the implant alone revealed that the scaffolds in all of the groups far exceeded any forces exerted by breathing or pressures required to burst native porcine tracheas. If more complex *in vitro* characterization were to be employed, dynamic degradation conditions could mimic breathing forces and would likely speed degradation of the scaffolds thus altering mechanical properties.[140] *In vivo,* if any failure occurred it would likely be at the suture line, thus future testing could involve testing the scaffolds sutured into cadaveric tracheas.

Suture retention is crucial as failure at the suture line would be catastrophic. Maximum suture retention in an anastomosis model using a single-interrupted PDS suture, placed around the circumference of the trachea, was 123 N (sheep trachea) [9]. Native trachea suture retention for our testing method was not found in the literature. Our suture holding capacities were at a much lower range than an anastomosis model, due to the inequivalent comparison of one single-interrupted suture (our testing) to a series of single-interrupted sutures (anastomosis model). The PLGA-only and Blend

had poor suture retention strengths, while the other groups performed in a range of 20-70 MPa.

Tube flattening or radial compression of the trachea is comparable to a situation where an external force compressed the airway (i.e., during trauma). Porcine tracheas withstand compression (across the diameter) to 50% strain, which results in an average radial pedestal force of 10 N [104]. The rabbit trachea had a compressive strength of 2.1 N at 50% compressive displacement [41]. Our scaffolds were tested to 100% strain (completely flattened), with that in mind, our Gradient+Rings scaffolds far exceeded the native porcine and rabbit trachea's ability to resist radial force. The PCL-only and Bilayer scaffolds had an average tube flattening force of 3.8 N, which could be comparable to the rabbit trachea compressive strength. This tube flattening property of the scaffolds will be crucial to tracheal patches that exist for the purpose of holding open a stenosed trachea that has been opened to widen the airway.

The application of these materials will impact interpretation of the results. Tracheal materials can be implanted in small, patch-type defects and in long, circumferential defects. Each scenario demands slightly different properties of our scaffolds and should be considered when utilizing our data and materials. Additionally, these scaffolds could have other applications, specifically vascular and intestinal tissue engineering.

In conclusion, we evaluated the fiber morphology, polymer degradation, porosity, and mechanical properties of seven variations of our fibrous trachea

scaffolds under *in vitro* degradation conditions. While all scaffolds had at least one favorable characteristic, the graded scaffolds with rings had improved tensile and radial compression properties, largely due to the 3-D printed PCL rings. And we can assume that the rings would have an impact on burst pressure if testing could exceed 30 psig. The fibrous PCL component also plays an important role in recovery properties and suture retention, with the tensile equilibrium moduli and percent recovery after tube flattening being much higher in the PCL containing groups. Additionally, the fibrous materials are an excellent suture holding substrate. We can conclude that the addition of a structural and flexible fibrous component is crucial for tracheal scaffolds to recapitulate the function of the native trachea cartilage and connective tissue. Therefore, our reinforce, fibrous scaffolds have the potential to be utilized for trachea tissue engineering applications, after further *in vitro* and *in vivo* testing.

CHAPTER 4: Electrospun Fibrous Scaffolds for Tracheal Defect Repair: Pilot Studies

ABSTRACT

Current treatments for tracheal stenosis do not predictably return normal function to the trachea, thus new treatment solutions may be useful. Synthetic tissue engineered scaffolds could provide otolaryngologists with an important new technique, if it can be easily implemented. We undertook three preliminary investigations during which polymeric electrospun fibrous scaffolds were sutured into induced defects in rabbit tracheas. The studies utilized 1) polycaprolactone (PCL) scaffolds implanted in a patch-type application, 2) trilayer gradient scaffolds of polylacticcoglycolic acid (PLGA) and PCL with encapsulated growth factors implanted in a patch-type defect, and 3) bilayer gradient scaffolds with incorporated rings in a circumferential segment-type defect. In the patch-type defects, the animals were thriving, showing no signs of infection or air leakage into their wounds, and no signs of respiratory distress. CT scans and histology confirmed that the airways remained patent, with some cell infiltration and re-epithelialization on the scaffolds using standard tissue processing and staining. The current study demonstrates for the first time that tracheal defect repair with biodegradable polymeric scaffolds with fibers is feasible and life-sustaining in an animal model. In the circumferential segment-type defect, severe stenosis caused fatalities in all animals. Scaffold use in this model should be redesigned, and the surgery method should be reassessed.

INTRODUCTION

Tracheal stenosis is a rare but often fatal disease with a mortality rate as high as 77%.[26] Current treatments for tracheal stenosis alleviate the effects of the stenosis using specialized surgical procedures (e.g., slide tracheoplasty) or cartilage augmentation of a focal region of stenosis. There is not, however, a treatment that completely returns normal function to the trachea.[32] Furthermore, some donor site morbidity occurs with augmentation techniques, and size or shape mismatches are not uncommon. Tissue engineering has the potential to create effective replacement trachea-like tissue for procedures like laryngotracheal reconstruction, and may circumvent these problems.

Fibrous electrospun materials have been used in various realms of tissue engineering, but have not been extensively utilized in trachea regeneration (Brizzola *et al.*[12] conducted a trachea study with unaligned fibers). Electrospinning is one of the most efficient fabrication techniques to create microscale and nanoscale fibers. Electrospun fiber based materials create favorable microenvironments that closely mimic native extracellular matrix (ECM) and support cell attachment, differentiation, and growth.[71] Circumferentially aligned fibers further mimic the collagen in native tracheal cartilage, where the outer superficial zones of cartilage have circumferentially aligned collagen fibers (which are active in tensile resistance and combat inward collapse).[95] These scaffolds are biomimetic in their structure, and they are based on synthetic materials that are not reliant on donor tissue for tracheal regeneration.[99, 106, 133] Thus, the theoretical benefits of electrospun fibrous scaffolds

are their ability to allow tissue ingrowth, their lack of reliance on donor tissue, and their ability to be created in a variety of sizes and shapes.

The objective of these studies was to demonstrate the feasibility of our concept. We hypothesized that cellular infiltration and a favorable tissue response to the scaffold would be observed. A feasibility study of this nature is warranted in order to demonstrate a promising new technology, and to establish a foundation for larger studies, if successful. Three pilot studies were performed on: 1) polycaprolactone (PCL) scaffolds implanted in a patch-type application, 2) trilayer gradient scaffolds of polylacticcoglycolic acid (PLGA) and PCL with encapsulated growth factors implanted in a patch-type defect, and 3) bilayer gradient scaffolds with incorporated rings in a circumferential segment-type defect (Figure 4.1).

METHODS

Material fabrication

Using a custom designed electrospinning apparatus, 2 mm thick electrospun fiber sheets were fabricated following a slightly modified protocol established in a previous publication.[57] Briefly, liquid polymeric solutions were mixed and placed in a 20 mL syringe and fitted into a programmable syringe pump (PhD Ultra, Harvard Apparatus) set to extrude the solution at a set flow rate. As the solution was extruded through a charged 20 gauge needle, the charged polymer was drawn from the needle tip to the rotating cylindrical stainless steel mandrel. The electrospun tube was removed from the collecting rod by cutting with scalpel (biomaterial sheet observed

in Figure 4.2, sterilized using ethylene oxide, and aired in a fume hood for 24 hours. Safety precautions, personal protective equipment and a well ventilated working environment were used when handling toxic solvents.

For the first pilot study (2 rabbits), we used a 23% w/v solution consisting of polycaprolactone (Intrinsic viscosity= 1.0-1.3 dL/g, Lactel) in methylene chloride (Fisher Scientific). Extrude the solution at 1.3 ml/hr and charged to 20 kV (Glassman High Voltage, High Bridge, NJ) onto a 6.35 mm diameter cylindrical stainless steel mandrel rotating at 10,000 rpm.

For the second pilot study (6 rabbits), a 18% w/v polycaprolactone (PCL; intrinsic viscosity 1.0-1.3 dL/g, LACTEL, Birmingham, AL) solution in dichloromethane (DCM; Fisher Scientific, Hampton, NH): dimethylformamide (DMF) (80:20) and a 30% w/v poly(D,L-lactide-co-glycolic acid) copolymer (PLGA; 50:50 lactic acid : glycolic acid, acid end group, MW 50,000 Da, intrinsic viscosity 0.35 dL/g, Evonik Industries, Birmingham, AL) solution in DCM:DMF (80:20). Extruded the solution at 5 ml/hr and it was charged to 20 kV (Glassman High Voltage, High Bridge, NJ) and collected on a rotating cylindrical stainless steel mandrel (6.35 mm diameter; 10,000 rpm measured with tachometer).

To create the protein-loaded PLGA solutions, transforming growth factor beta 3 (TGF-B3; Peprotech, Rocky Hill, NJ) and epidermal growth factor (EGF; Peprotech, Rocky Hill, NJ) were reconstituted in 0.1% bovine serum albumin (BSA) in phosphate buffered saline (PBS). The reconstituted protein solutions were individually mixed with the PLGA solutions to reach a final loading ratio of 1.5 ug of

TGF-B3 or 6.0 ug of EGF per 1.0 mg of PLGA. The final mixtures were then sonicated over ice (50% amplitude, 20 s). The solutions were electrospun immediately after preparation.

To create the sharp interface group, 6 mL of PLGA was electrospun on to the collecting mandrel (0.5 layer thickness), then 10 mL of PCL was electrospun on to the PLGA layer (1 mm layer thickness), and finally 6 mL of PLGA was electrospun on to the PCL layer (0.5 mm layer thickness). The final wall thickness was 2 mm.

To create the gradient interface group, 2 mL of PLGA was electrospun (0.25 mm layer thickness), then 2 mL of PLGA and 2 mL of PCL was simultaneously electrospun on to the PLGA layer (0.5 mm layer thickness), followed by 4 mL of PCL electrospun on to the PLGA/PCL layer (0.5 mm layer thickness), then 2 mL of PLGA and 2 mL of PCL was simultaneously electrospun on to the PCL layer (0.5 mm layer thickness), and finally 2 mL of PLGA was electrospun on to the PLGA/PCL layer (0.25 mm layer thickness).

To create the scaffolds for the circumferential defect study (4 rabbits) (Figure 4.12), the using a 7 wt% polycaprolactone (PCL; intrinsic viscosity 1.0-1.3 dL/g, LACTEL, Birmingham, AL) solution in hexafluoro-2-propanol (HFIP; Oakwood Chemical; Columbia, SC) and a 14 wt% poly(D,L-lactide-co-glycolic acid) copolymer (PLGA; 50:50 lactic acid : glycolic acid, acid end group, MW 50,000 Da, intrinsic viscosity 0.35 dL/g, Evonik Industries, Birmingham, AL) solution in HFIP. The solution was extruded at 5 mL/hr and the 20 gauge needle was charged at +12 kV (Glassman High Voltage, High Bridge, NJ) and the rotating cylindrical stainless steel

mandrel (7 mm diameter) was charged to -6 kV. To create the gradient interface group with circumferential rings, 6 mL of PCL was deposited, the PCL or Bioglass Rings rings (PCL-created by mixing 15 w/v% PCL in 1:1 DCM:DMF solution, pouring solution into flat plate and allowing solvent to evaporate forming a polymer sheet; rings were cut to 1-2 mm width, approx. 1.5 mm thickness; Bioglass provided by MO-SCI, MO) were wrapped around the cylindrical stainless steel mandrel at 3-4 mm intervals, 6 mL of PCL was deposited over the rings, followed by co-spinning 8 mL of PCL and 8 mL of PLGA to create the gradient layer, followed by 12 mL of PLGA.

Surgical procedure

Animal experiments were approved by the Institutional Animal Care and Use Committee of the University of Kansas (2 rabbit study= #175-06, 6 rabbit study= #175-13, 4 rabbit study= #175-15).

For the first pilot study (2 rabbits), prior to the procedure, routine antibiotics and analgesics were administered to male New Zealand White rabbits (9-10 lbs) (n=2), and general anesthesia was induced with a combination of ketamine (40 mg/kg) and xylazine (5 mg/kg). The surgical sites were cleaned and disinfected after removal of hair. Once ready, the rabbits were laid in the supine position and an incision along the neck region was made to access the trachea. In each rabbit, an elliptical defect (approximately 0.5 by 2 cm with the long axis oriented vertically along the main axis of the trachea) was created in the tracheal wall and the biomaterial graft was placed, partially overlapping the tracheal wall to form an

appropriate seal using 4-0 polydioxanone suture material. The scaffold material was sized to 1 by 2.5 cm, and cut from a sheet of the polymer in the operating room. The process is illustrated in more detail in Figure 1. Additionally, a second implant (1 by 1 cm square) was placed subcutaneously along the back of the animal.

For the second pilot study (6 rabbits), following stable general anesthesia, the surgical sites of male New Zealand White rabbits (9-10 lbs) (n=6) were cleaned and disinfected after removal of hair. The bare neck region was disinfected with three alternate scrubs of betadine and 70% ethanol and then draped. Only strict aseptic techniques and sterile instruments were used, and the surgeon wore sterile gowns, masks, and head covers. Once ready, the rabbits were laid in the supine position and an incision along the neck region was made to access the trachea. In each rabbit, an elliptical defect (approximately 0.5 by 2 cm with the long axis oriented vertically along the main axis of the trachea) was created in the tracheal wall and the biomaterial graft was placed, partially overlapping the tracheal wall to form an appropriate seal using 4-0 polydioxanone suture material. The scaffold material was sized to 1 by 2.5 cm, and cut from a sheet of the polymer in the operating room.

For the third pilot study (circumferential defect in 4 rabbits), the procedure was very different than the patch implantation illustrated above. A ventral midline cervical incision was made, including identification and division of the strap muscles. The cervical trachea was then accessed. A defect was marked out on the wall of the trachea with an approximate size of 1 centimeter segment of trachea. The defect was centered approximately 2 centimeters below the cricoid cartilage. The marked area of

trachea was removed with sharp dissection, the ET tube was removed quickly, and the resulting void was replaced with a tube of electrospun graft approximately the same diameter as the rabbit's native trachea, with overlap on both ends to ensure a seal. Absorbable polydioxanone suture (size 4-0) was used for this step. The wound was losed in layers using polyglycolic acid absorbable suture in the muscle layer and the subcuticular or skin closure layer.

Bronchoscopy

Bronchoscopy was performed at 3 and 4.5 weeks for the third pilot study. A video-endoscopy system consisting of a bronchoscope (10020ATA; Hopkins Telescope, 0°, 2.9 mm, 30 cm; Karl Storz Endoskope; Tuttlingen, Germany) and a video processor coupled to a light source (20045020; TelepackX; Karl Storz Endoskope; Tuttlingen, Germany) was used for bronchoscopic evaluation. The degree of reepithelialization over the scaffolded region and appearance of stenotic regions of the trachea were evaluated with a bronchoscope. Procedures were done under anesthesia and analgesics were given post-procedure.

CT scan

Seven weeks after implantation, the first pilot study animals' laryngotracheal complex and subcutaneous implant were harvested following an approved protocol for euthanasia. Prior to storage in formalin and histological staining, the excised tracheas were imaged using a CT scanner system (Siemens Somatom Sensation 64 high resolution scanner) and reconstructed using Inspace software (Siemens).

microCT analysis

After completion of the second and third pilot study, tracheas were excised and fixed in 10% neutral buffered formalin. To aid in soft tissue visualization in the microCT analysis, the fixed tracheas were soaked in 40% Hexabrix (Covidean)/60% PBS for 20 hours.1 All tracheas were secured in a vertical position during scanning, so that the microCT scanner produced transverse cross-sectional slices. To prevent dehydration during scanning, the tracheas were placed in a tube, with PBS at the bottom and sealed with parafilm. All scans were performed using a 3D X-ray imaging system (Xradia MicroXCT-400, Pleasanton, CA) at 40 kV, 8 W, 2 second exposure time, 0.5x objective magnification. For high quality images, 1600 projections were collected with multi reference images selected at 10 images every 400 frames for a total acquisition time of 2.5 hours. After acquisition, the images were manually reconstructed using the Xradia software. The center shift and beam hardening were determined.

To determine percent stenosis, the diameter of the scaffolded and normal regions of trachea were measured in the CT software. The scaffolded trachea diameter (D_s) was divided by normal trachea diameter (D_n) and subtracted by 1, i.e., $Stenosis = 1 - (D_s / D_n)$.

Histological analysis

The tracheas and subcutaneous implants were then placed in formalin. The samples were cryogenically sectioned, and stained with hematoxylin and eosin (H&E). For the second study, hematoxylin and eosin (H&E) and safranin O/fast green were run. Immunohistochemical analysis for collagen I (CI), collagen II (CII;

10 ug/mL; AF5710, Acris Antibodies, San Diego, CA), and actin was done using a secondary antibody peroxidase system kit (ABC Elite Mouse IgG kit, Vector Labs, Burlingame, CA). The presence of antibody was visualized with a AEC peroxidase substrate producing a red color (Vector Labs). As a positive control, trachea without the scaffold was stained. As a negative control, the normal staining protocol was followed, excluding the primary antibody. Photomicrographs were taken of representative sections of the interfaces between the polymer and the animal's native tissue.

RESULTS

Mortality

The implantation of the scaffolds was straightforward, with the scaffolds being easily cut into the desired elliptical shape in the operating room and sutured into the induced defect (Figure 4.3). The segmental defect was a more challenging surgery than the patch-defect surgeries (Figure 4.13). Throughout the course of the first and second pilot studies, the rabbits did not display any signs of distress and ate and breathed normally, with the exception of slight wound opening in one rabbit in the second pilot study. In this event, staples were used to close the wound and antibiotics were administered (Baytril).

The subjects in the third study exhibited more adverse reactions. Throughout the 6 weeks of the study, all of the rabbits displayed signs of distress. In the event of an adverse reaction (i.e., labored breathing, coughing, weight loss, stridor, death), the

rabbit underwent bronchoscopic evaluation, vital sign monitoring, more frequent monitoring, and administration of dexamethasone to alleviate inflammation and stenosis. If the animal's condition was rapidly declining and no intervention methods were available, euthanasia was determined to be the best course of action. There was 0% survival, with Bioglass subject 1 dying 1 day post-op, Bioglass subject 2 dying 17 days post-op, PCL subject 1 and 2 were euthanized 30 days post-op.

Bronchoscopy

The third study subjects underwent bronchoscopy. PCL group tracheas were analyzed after excision and fixation. Bronchoscopy images revealed that Subject 1 had an open airway and Subject 2 had a blocked airway and could not pass endoscope through. We forced a suction tube through the blockage (Figure 4.14). The Bioglass group, subject 3 bronchoscopy revealed severely narrowed trachea on the proximal end of graft. And Bioglass group, subject 4 bronchoscopy revealed narrowing of the trachea on the distal end of the graft. The image also shows yellow region which is the graft (Figure 4.14).

Gross morphological observations

At the time of harvest, the gross morphological observations of the tracheas revealed the presence of polymer and tissue growth around the scaffold (Figure 4.4, Figure 4.7).

The third study, Bioglass, Subject 1 necropsy revealed that the trachea was filled with froth/foam, and the lungs were more congested that what normally see

post-mortem. Bioglass, Subject 2 necropsy nothing significant noted in necropsy (bowel and heart looked normal, did not look down trachea).

CT and histology

For the first study, the CT scans revealed that the airway was widely patent, and the 3-D reconstructions suggested no obvious new cartilage formation (Figure 4.5). The histological sections of the tracheas illustrated several key findings: (1) The lumen of the scaffold was covered with normal ciliated respiratory epithelium, (2) various cells were dispersed throughout the scaffold, with multinucleated giant cells observed among electrospun fibers, (3) there was no cartilage-like tissue within the scaffold (Figure 4.6).

For the second study, the microCT scans revealed acceptable narrowing of the trachea through the grafted sections, but not severe stenosis. Tissue sections revealed the presence of PCL and almost complete resorption of PLGA, as expected. There was coverage of the outer surfaces with a cartilage-like tissue (evidenced by collagen II immunohistochemistry) (Figure 4.10, Figure 4.11), and with normal ciliated epithelium lining the lumen of the scaffold in all groups. These results with the new preliminary study have clearly demonstrated an improvement over the PCL-only scaffold, with intense collagen II immunostaining of the regenerated cartilaginous region.

Tracheal diameter was observed to decrease in the scaffold regions across all groups. The diameters appeared to decrease by approximately 35% (1-2 mm) (Figure 4.8, Figure 4.9). Although narrowing occurred in the scaffold, rabbits were able to

respire without difficulty. The addition of tougher materials, like bioglass ribbons, to the scaffold could alleviate the slight collapse induced by the removal of cartilage ring support. Between groups, no differences in microCT images were observed. A summary of diameters were: Group 1 (Trilayer): diameter=4.4 mm, normal diameter=6.8 mm, 35% decrease in diameter; Group 2 (Trilayer w/GF): diameter=3.5 mm, normal diameter=5.1 mm, 32% decrease in diameter; and Group 3 (Gradient w/GF): diameter=3.2 mm, normal diameter=5.5 mm, 42% decrease in diameter.

For the third study, the microCT scans revealed significant stenosis at the proximal and distal ends of the implant (located at anastomosis sites) (Figure 4.15).

DISCUSSION

The electrospun scaffolds maintained the shape and airtight seal of the trachea in the first two pilot studies. Keeping the airway open is crucial for a tracheal prosthesis to perform properly, which has been a major issue in prior tracheal tissue engineering studies. Further mechanical testing of these scaffolds is needed, but this *in vivo* study demonstrated effective mechanical performance of the scaffold material.

In the first pilot study, the presence of multinucleated giant cells could indicate a multitude of issues; however, we believe that the presence of these cells within our scaffold indicates “non-immune” chronic inflammation. These cells are reactive to relatively inert foreign materials (e.g., suture fragments) and can be classified as foreign body granulomas (as opposed to immune granulomas.)

Multinucleated giant cells are commonly observed in implanted tissue engineered scaffolds.[3] These cells are known to be mediators in biomaterial degradation[4] and indicators of a foreign body reaction. Within this 7 week time period, the rabbit appeared to tolerate the scaffolds with only a low level inflammation response based on the presence of the multinucleated giant cells. However, further evaluation of the degree of inflammation and longer time points in follow-up studies will better confirm the true immunogenic properties of the scaffolds.

The native rabbit trachea possesses a distinct cartilaginous character.[130] Replicating this cartilaginous component within a tracheal repair site would seem to be desirable. Cellular infiltration and fibrous-type tissue were observed within the scaffolds in the first two studies, which may indicate a favorable environment for chondrogenesis. No new cartilage formation in the histological evaluation of our specimens was a shortcoming of the first pilot study. Utilizing alternative techniques like including growth factors (e.g., transforming growth factor-β3) could provide the desired degradation kinetics, chemotactic effects, and accelerated tissue growth for cartilage tissue regeneration in future tracheal defect repair studies. And we did observe increased CII staining on the external surface of the implant in the second pilot study. Further analyses of techniques to improve chondrogenesis are needed. Chondrogenesis in scaffolds is possible, as observed in other tissue engineering studies,[45, 59, 88] but it remains a major challenge to achieve robust chondrogenesis.

In the segmental, circumferential study, the defect creation and reanastomosis of a tracheal scaffold was highly traumatic and induced granulation tissue that

occluded the airway. Different surgical techniques and scaffold design are needed to improve outcomes in future studies (Figure 4.16). Instead of fitting the scaffold over the trachea, we should place the scaffold inside the trachea to block inflamed tissue from gathering in the trachea lumen (causing stenosis). The limitation of this technique is a reduction in the scaffold diameter, which significantly encroaches on the airway in a small animal model (or patient) with a small airway. Re-designing the scaffold to accommodate for this is necessary **(**Figure 4.16**)**. Other re-design considerations include making the adaptor portion of the scaffold out of a woven/mesh material, similar to a metallic stent. Short-term use of steroids or other anti-inflammatories in the scaffold or delivery upon implantation could be another technique to reduce early inflammation associated with defect creation.

We investigated alternative surgical techniques to join scaffold and trachea, and we made the following observations. End-to-end anastomosis resulted in a misalignment of the trachea and scaffold **(**Figure 4.16**)**. When sutured together, the scaffold was partially pulled inside the trachea and partially outside the trachea. This is demonstrated in the endoscopy image, where the trachea is observed in the scaffold (on the left side of the image). We investigated scaffold inside trachea suturing. Scaffold diameter is crucial, where the scaffold should seamlessly fit inside the trachea without buckling and folding. We looked at hemi-circular scaffolding, and we determined that removing a hemi-circular patch of the trachea completely disrupts the mechanical stability of the trachea. As a result, the remaining trachea tissue

cannot support suturing of the scaffold material. In conclusion, scaffold inside trachea suturing is the ideal technique.

In conclusion, this preliminary study revealed that a polymeric, electrospun scaffold implanted in the trachea allowed for tissue overgrowth and survival of the rabbits (except for circumferential defects), demonstrating feasibility of this technology and a platform for expanded studies with more advanced designs.

CHAPTER 5: Functional reconstruction of tracheal defects by protein-loaded, cell-seeded, fibrous constructs in rabbits

ABSTRACT

Tracheal stenosis is a life-threatening disease and current treatments include surgical reconstruction with autologous rib cartilage. We propose using a sustainable implant, composed of a tunable, fibrous scaffold with encapsulated chondrogenic growth factor (TGF-B3) or seeded bone marrow mesenchymal cells (BMSCs). *In vivo* functionality of these constructs was determined by implanting them in induced tracheal defects in rabbits for 6 or 12 weeks. Our scaffolds maintain functional airways in a majority of cases, with the cell-seeded group having an improved survival rate and the acellular group had a higher occurrence of more patent airways. The BMSC group had a more severe accumulation of immune cells over the graft, while also exhibiting more normal epithelium, subepithelium and cartilage formation. This leads us to conclude that a simple, acellular scaffold is a viable option for tracheal tissue engineering, with the intraoperative addition of cells being an optional variation to the scaffolds.

INTRODUCTION

Laryngotracheal disorders resulting in airway obstruction, although rare, can cause significant morbidity and can be life threatening. These disorders are the result of congenital (laryngo/tracheomalacia, congenital subglottic stenosis) or acquired (prolong intubation, traumatic injury, tracheotomy, tumors) causes. The estimated incidence of stenosis in post intubation or tracheotomy patients is 10-20% with only 1-2% being symptomatic or having severe stenosis (estimated 4.9 severe stenosis cases per million per year in the general population.) [79, 144]. Due to the congenital occurrences and increased survival of pre-mature infants requiring prolonged intubation, the pediatric population makes up a significant portion of patients requiring treatment.

Treatment options include balloon dilation, laser surgery, stenting, and surgical resection and reconstruction; with reconstruction being the preferred alternative for severe stenosis, though there are limitations to this treatment. Laryngotracheal reconstruction (LTR) involves augmenting the stenotic region with autologous costal cartilage. Specialized surgical technique and an invasive, multi-site surgery are required for this procedure. Thus, an off-the-shelf tissue-engineered product is needed that would replace the need for autologous tissue and eliminate the challenges for the surgeon and patient.

Various tissue engineered trachea replacements exist[87], including human trials with decellularized donor tissues re-cellularized with autologous cells[66] and non-degradable polypropylene scaffolds coated with natural materials.[83] Approaches

utilizing degradable synthetic materials are gaining popularity due to the limited availability, specialized preparation, and storage of donor tissues, and the limited regenerative capacity of non-degradable materials.[16] We endeavor to use biomimetic, polymeric scaffolds for trachea repair, utilizing electrospun poly-lactic-co-glycolic acid (PLGA) and polycaprolactone (PCL) graded, biphasic scaffolds reinforced with PCL rings for tracheal defect repair. Our hypothesis is that the scaffold will provide an airtight, biocompatible prosthesis with potential for cartilage-like tissue replacement. Our preliminary pilot studies in rabbits indicated that the scaffolds were functional in patch-type tracheal defects (not published). Thus, a larger study *in vivo* study is needed to establish statistically significant efficacy. Three groups were designed for the current study: 1) the gradient scaffold with reinforced rings, 2) the scaffold with TGF-β3 encapsulated in the PLGA, and 3) the scaffold with rabbit bone marrow mesenchymal stem cells (BMSCs) seeded intraoperatively (Figure 5.1). The objective of the current study was to supplement the pre-clinical data available for tracheal tissue engineering. The following paper includes a description of the materials and materials used to create the scaffolds and surgically implant them, the results will further highlight the more pertinent findings from our study, and the discussion will assess the significant and implications of the data.

MATERIALS AND METHODS

Material fabrication

Using a custom designed electrospinning apparatus, 2 mm thick electrospun fiber sheets were fabricated following a slightly modified protocol established in a previous publication.[58] A 7 wt% polycaprolactone (PCL; intrinsic viscosity 1.0-1.3 dL/g, LACTEL, Birmingham, AL) solution in hexafluoro-2-propanol (HFIP; Oakwood Chemical; Columbia, SC) and a 14 wt% poly(D,L-lactide-co-glycolic acid) copolymer (PLGA; 50:50 lactic acid : glycolic acid, acid end group, MW 50,000 Da, intrinsic viscosity 0.35 dL/g, Evonik Industries, Birmingham, AL) solution in HFIP. The solutions were placed in 20 mL syringes and fitted into programmable syringe pumps (PhD Ultra, Harvard Apparatus, Holliston, MA) set to extrude the solution at 5 ml/hr. As the solution was extruded through a charged 20 gauge needle (+10 kV, Glassman High Voltage, High Bridge, NJ), the charged polymer was drawn from the needle tip to a negatively charged (-6 kV) rotating cylindrical stainless steel mandrel (6.35 mm diameter). Safety precautions, personal protective equipment and a well ventilated working environment were used when handling toxic solvents.

To create the graded, biphasic group, 8.33 mL of PCL was electrospun (0.34 mm layer thickness), then PCL rings (created by mixing 15 w/v% PCL in 1:1 DCM:DMF solution, pouring solution into flat plate and allowing solvent to evaporate forming a polymer sheet; rings were cut to 1-2 mm width, approx. 1.5 mm thickness.) were affixed to the PCL and arranged 3-4 mm apart along the length of the cylindrical stainless steel mandrel. Another 0.34 mm layer of PCL was electrospun over the rings, thus encapsulating the rings between layers. 6.67 mL of PLGA and PCL (total of 13.33 mL total polymer) was simultaneously electrospun on to the PCL

layer (0.67 mm layer thickness), followed by 8.33 mL of PCL electrospun on to the PLGA/PCL layer (0.67 mm layer thickness).

To create the protein-loaded PLGA solutions, transforming growth factor beta 3 (TGF-β3; Peprotech, Rocky Hill, NJ) were reconstituted to 1 mg/mL with 10 mM citric acid (251275; Sigma; Milwaukee, WI) and further diluted to 0.8 mg/mL with 0.1% bovine serum albumin (BSA; BP9706; Fisher Scientific; Waltham, MA) in phosphate buffered saline (PBS; P5368; Sigma; Milwaukee, WI). The reconstituted protein solutions were individually mixed with the PLGA solutions to reach a final loading ratio of 30 ng of TGF-β3 per 1.0 mg of PLGA (approx. 126 μg of TGF-β3 per scaffold). The final mixtures were then sonicated over ice (50% amplitude, 20 s). The solutions were electrospun immediately after preparation.

Once the 2 mm wall thickness was achieved, the electrospun tubes were removed from the collecting rod, lyophilized for 24 hours, sterilized using ethylene oxide, and aired in a fume hood for 24 hours.

Cell source

Bone marrow was harvested from the femur and tibia of 6-8 week old New Zealand White rabbits (n=3) under Institutional Animal Care and Use Committee of the University of Kansas (protocol #175-08). Bone marrow stromal cells (BMSCs) were isolated by density gradient centrifugation (Histopaque; 10771; Sigma; Milwaukee, WI) and culture in alpha-MEM (12571; Gibco; Carlsbad, CA), 10% FBS (12662; Gibco; Carlsbad, CA), and 1% penicillin/streptomycin (15140; Gibco; Carlsbad, CA). Cells were passaged to P4 (frozen at P2) prior to implantation.

Surgical procedure

Animal experiments were approved by the Institutional Animal Care and Use Committee of the University of Kansas Medical Center (protocol #2012-2099). Following the induction of stable general anesthesia (ketamine, xylazine, and glycopyrrolate administered) and analgesic delivery (buprenorphine), hair was shaved from the area around the neck/trachea region of male New Zealand White rabbits (7-8 lbs) (n=5). The rabbit was intubated to deliver isoflurane (the defect was created above the end of the ET tube, so isoflurane could be reliably delivered). Intubation was assisted with a brochoscope. Inhaled isoflurane was used to maintain anesthesia. Before the procedure, the rabbit was provided with a warmed saline bolus (60mL, subcutaneous) to ensure proper hydration and to maintain blood pressure. The surgical area was disinfected with alternate scrubs of surgical scrub (povidone scrub or chlorhexidine scrub) and 70% ethanol, and then draped. Only strict aseptic techniques and sterile instruments were used, and the surgeons were wearing sterile gown, masks and head covers, as practiced.

A ventral midline cervical incision was made, including identification and division of the strap muscles. The cervical trachea was accessed. Lidocaine/bupivicaine was delivered directly to the defect site or subcutaneously prior to surgery to alleviate discomfort associated with defect creation. An elliptical defect was marked out on the wall of the trachea with an approximate size of 0.5 by 1.5 centimeters (with the long axis oriented along the length of the trachea). The defect was centered approximately 2 centimeters below the cricoid cartilage. The

marked area of tracheal wall was removed with sharp dissection, and the resulting hole was patched with a biomaterial scaffold slightly larger than the defect itself in order to create an airtight seal (1 by 2.5 cm).

In the cell seeded group, approximately 25 million cells per rabbit/scaffold were prepared with 7-10% of cells labeled with near-infrared fluorescent quantum dots (Q25071MP; Life Technologies; Carlsbad, CA) for *in vivo* cell imaging (data not shown) and stored in 37°C media in polypropylene tubes until needed for surgery. Prior to seeding, the cell media was removed through centrifugation and cells were suspended in 200 uL of PBS. Once one side of the scaffold was sutured in place, the cell slurry was pipetted directly onto the exterior surface of the scaffold and exposed side of the scaffold. Cells were allowed to soak for 5 minutes, excess fluids were suctioned from the trachea lumen, and the other edge of the scaffold was sutured in place.

Absorbable polydioxanone suture (size 4-0) was used to suture the scaffold to the trachea in all groups. The wound was then closed in layers using running polyglycolic acid absorbable suture in the strap muscle layer and the skin closure layer. After the procedure was finished and the rabbit recovered from anesthesia, they were administered meloxicam and returned to their cage once they remained sternal.

Bronchoscopy

A video-endoscopy system consisting of a bronchoscope (10020ATA; Hopkins Telescope, 0°, 2.9 mm, 30 cm; Karl Storz Endoskope; Tuttlingen, Germany)

and a video processor coupled to a light source (20045020; TelepackX; Karl Storz Endoskope; Tuttlingen, Germany) was used for bronchoscopic evaluation. The degree of reepithelialization over the scaffolded region and appearance of stenotic regions of the trachea were evaluated with a bronchoscope at 3, 6, 9, and 12 weeks after implantation. Procedures were done under anesthesia and analgesics were given post-procedure.

Bronchoscopic images were visually assessed and assigned a semi-quantitative score by the following criteria: severity of lumen narrowing (none, slight, moderate, severe), progression of lumen narrowing (none, slight, moderate, severe), direction and type of narrowing (side-to-side, graft collapse, swelling), and re-epithelalization of the graft (none, slight, moderate, complete).

***In vivo* imaging**

A pre-clinical *in vivo* fluorescence imaging system (IVIS Spectrum, PerkinElmer, Waltham, MA) was used to detect the quantum dot labeled cells. *In vivo* cell tracking was planned at 3, 6, 9, and 12 weeks post-operation. Briefly, the subjects were anesthetized and positioned in the imaging system to visualize the neck region. The system was set to sweep at excitations of 400, 450, and 550 nm and emission collection at 480 and 820 nm. Fluorescence could not be detected through the animal's skin and muscle (data not shown). Further cell tracking was not pursued during this experiment.

microCT analysis

At 6 or 12 week, tracheas were excised and fixed in 10% neutral buffered formalin. To aid in soft tissue visualization in the microCT analysis, the fixed tracheas were soaked in 40% Hexabrix (Mallinckrodt, St. Louis, MO)/60% PBS for 10 hours.[135] All tracheas were secured in a vertical position during scanning. To prevent dehydration during scanning, the tracheas were placed in a sealed tube with PBS at the bottom. All scans were performed using a 3D X-ray imaging system (Xradia MicroXCT-400, Pleasanton, CA) at 40 kV, 8 W, 2-4 second exposure time, 0.5x objective magnification. For high quality images, 1600 projections were collected with multi reference images selected at 10 images every 400 frames for a total acquisition time of 2.5-5 hours. After acquisition, the images were manually reconstructed using the Xradia software. The center shift and beam hardening were determined.

Volume quantification

Following microCT reconstruction, the resulting AmiraMesh files were processed in the Avizo Fire software to quantify luminal volume. A modified pore quantification procedure was used. Briefly, interactive thresholding was used to define the void space in the CT image creating a binary image. The quantification command I_Analyze was used to obtain quantitative date (volume, area, length) for each void space. The image was then filtered based on volume, resulting in the isolation of the lumen void space from other void space in the image. Once the lumen space was isolated, the volume and length of the 3D image and max/min area of the 2D slices were recorded for statistical analysis. To account for variation in

trachea length measured in software, the length was divided by the lumen volume creating a normalized volume in cross-sectional units.

Histological analysis

Following microCT analysis, the tracheas were soaked in PBS for 24 hrs to remove contrast agent and then placed in formalin. The samples were dehydrated in graded ethanol and paraffin embedded. Transverse sections were taken on a Microm HM 355S microtome using a low-profile disposable blade (3052835, Thermo Scientific, Waltham, MA) with a sample thickness of 5 μm. Sections were placed on positively charged slides, heated to 60°C for 1 min, and allowed to dry at room temperature overnight. Prior to staining, the slides were heated to 60°C for 45 min. After drying, the paraffin was removed from the slides and the tissue was rehydrated using CirtiSolv (22143975, Fisher Scientific, Waltham, MA) and a graded series of ethanols.

Hematoxylin and Eosin (H&E) staining for cell nuclei and general tissue visualization was performed using the following protocol. Slides were stained with Harris Hematoxlylin (SH30-4D, Fisher Scientific, Waltham, MA) for 3 min, rinsed with water, dipped in acid ethanol, rinsed in water, and stained with Eosin Y (119830-25g, Sigma-Aldrich, St. Louis, MO) for 30 seconds. Safranin-O/Fast Green staining for GAGs was performed using the following protocol. Slides were stained with Harris Hematoxlylin (SH30-4D, Fisher Scientific, Waltham, MA) for 3 min, rinsed with water, dipped in acid ethanol, rinsed with water, stained in Fast Green (F7258, Sigma-Aldrich, St. Louis, MO) for 3 min, dipped in 1% acetic acid (537020,

Sigma-Aldrich, St. Louis, MO), stained in 0.1% Safranin-O (S8884, Sigma-Aldrich, St. Louis, MO) for 10 min, and rinsed with water. Alcain Blue staining for GAGs was performed using the following protocol. Slides were stained with Alcain Blue solution (A3157, Sigma-Aldrich, St. Louis, MO) for 30 min, rinsed in water, stained with Nucler Fast Red solution (IW-3021, IHC World, Woodstock, MD), and rinsed with water. Verhoeff-Van Gieson staining was performed using the following protocol. Slides were stained with Verhoeff's solution (hematoxylin-ferric chloride-iodine solution) (H9627, 157740, 207772, 221945, Sigma-Aldrich, St. Louis, MO) for 1 hour, rinsed with water, dipped in 2% Ferric Chloride (157740, Sigma-Aldrich, St. Louis, MO) for 2 min, rinsed with water, dipped in 5% sodium thiosulfate (S7026, Sigma-Aldrich, St. Louis, MO) for 1 min, rinsed in water, and stained in Van Gieson's solution (1% aqueous acid fuschin in picric acid) (F8129, Sigma-Aldrich, St. Louis, MO; 80456, Fluka, Buchs, Switzerland) for 5 min. Sudan Black B for residual polymer was performed according to manufacturer's instructions (IW-3021, IHC World, Woodstock, MD).

All sections were then dehydrated in graded alcohol and then cleared in Citrisolv and mounted, with the exception of Sudan Black where the sections remained hydrated and were mounted with aqueous mounting medium (E01-15, IHC World, Woodstock, MD). Photomicrographs were taken of representative sections.

Histological scoring

The histological sections were scored blind by a pathologist (RG). The scoring system was developed to evaluate inflammation, vascularization,

epithelialization, cartilage formation, and residual polymer. The location of inflammation was determined by the spatial organization of inflammatory cells/tissue (diffuse or on outer surface of scaffold) and severity of inflammation was determined by the thickness of the "cap" like tissue on the exterior surface of the scaffold, none (0), thin layer (1), moderate layer (2), and thick layer (3). Immune cells types were differentiated into multi-nucleated giant cells (MNG cells), mononuclear cells (macrophages, lymphocytes, plasma cells), heterophils (rabbit analog of neutrophils) [108], and eosinophils and quantity of cells observed were categorized into none (0), mild (1), moderate (2), severe (3), and extreme (4). To determine vasculature, four representative fields of inflamed tissue were examined at 40x and vessel cross sections containing erythrocytes were counted.

Epithelialization was analyzed by simply categorizing it into two groups—presence or absence of epithelium (yes or no). The epithelial character were described and categorized into pseudostratified columnar, simple cuboidal, stratified cuboidal, simple columnar, squamous, and ulcer formation. Subepithelial character was described as fibrous, vascular, inflamed, or a combination. Cartilage formation was assessed by detecting new or immature cartilage and by assessing collagen staining (Verhoeff-Van Gieson) and collagen location. The presence of obvious fibroblasts and their location were also noted. The amount of polymer present was ranked from no polymer (0), 25% (1), 50% (2), 75% (3), and 100% of polymer present (4).

Statistical analysis

Using one-way ANOVA and Tukey's posthoc analysis, the bronchoscopy rating, lumen volume, and histological scoring were determined to be significant if $p<0.05$.

RESULTS

Mortality

The implantation of the scaffolds was straightforward, with the scaffolds being easily cut into the desired elliptical shape in the operating room and sutured into the induced defect (Figure 5.2). Throughout the 6 or 12 weeks of the study, a majority (73%) of the rabbits did not display any signs of distress. In the event of an adverse reaction (i.e., labored breathing, coughing, weight loss, stridor, death), the rabbit underwent bronchoscopic evaluation, vital sign monitoring, and more frequent monitoring. If the animal's condition was rapidly declining and no intervention methods were available, euthanasia was determined to be the best course of action. Adverse events occurred in 27% of the total study population, with a breakdown of 10% occurring in the scaffold only group (3% of 6 wk and 7% of 12 wk), 13% occurring in the TGF-β3 group (6.5% of 6 wk and 6.5% of 12 week), and 3% occurring in the BMSC group (3% of 6 wk and 0% of 12 wk). 13% fatality (4 out of 30 subjects) occurred during the first 6 week time point and 27% fatality (4 out of 15 subjects) occurred during the final 6 weeks (Figure 5.3).

Bronchoscopy

The purpose of the bronchoscopic analysis was to reveal the real-time morphology of the airway through the course of the study (Figure 5.4). Images were compared side-by-side and assigned a stenosis severity, progression of stenosis, re-epithelization rating, and type of narrowing (Figure 5.5).

Severity of stenosis was assessed on a scale from none (1), slight (2), moderate (3), to severe (4). We observed that the later time point subjects (12 week) had a higher severity rating than the earlier time point (6 week). Additionally, the adverse events all exhibited the most severe level of stenosis, although no statistical analysis could be done due to group size limitations.

Of the cases exhibiting slight to severe stenosis, the progression of the stenosis over time was evaluated on a scale from none (0), slight (1), moderate (2), to severe (4). Similar to the stenosis severity rating, we observed that the later time point subjects (12 week) exhibited a more extreme progression of stenosis as compared to the earlier time point (6 week). Between the groups, the week 12 and adverse event cases in the TGF-β3 group had a more rapid progression of stenosis as compared to the other groups, although statistical analysis could not be done due to group size limitations.

Re-epithelialization was assessed on a scale from none (0), slight (1), to moderate (2). All subjects exhibited some degree of epithelialization over the implant area. The degree of epithelialization seemed to decline over time in the TGF-β3 subjects, where a moderate degree of epithelialization was observed at week 6 and a slight degree of epithelialization was observed at week 12. Between the groups, the

BMSC cases displayed more epithelialization than the Scaffold-only cases. The fatal cases appeared to have a lesser degree of epithelialization, all scoring at slight epithelialization.

The types of stenosis (of the stenotic cases) were categorized into side-to-side narrowing, in-folding of one of the tracheal walls, and scaffold displacement into the airway. It is important to note that no granulation tissue (obvious protrusion of granular tissue) was observing on the lumen surface of the implants, indicating that inflammatory tissue overgrowth occluding the airway was not the type of stenosis observed. A large majority of the subjects exhibited a side-to-side narrowing (84% of total subjects with stenosis), with fewer subjects exhibiting one-wall in-folding (8% of total subjects with stenosis) and scaffold obstructing airway (8% of total subjects with stenosis). The two cases of scaffold obstruction occurred in the Scaffold-only group and the two cases of one-wall in-folding occurred in the Scaffold-only and BMSC group.

In summary, bronchoscopy data indicated that stenosis progressed over time, fatality is linked to stenosis, and epithelium was present in all groups.

Gross morphological observations

At the time of harvest, the gross morphological observations of the tracheas revealed the presence of polymer and tissue growth around the scaffold, for all groups. Some narrowing in the scaffolded region was observed, in most cases.

microCT and volume quantification

Visual inspection of the microCT scans revealed that all groups have some degree of stenosis as compared to a native, unaltered trachea. Analysis with specialized imaging software provided quantitative lumen volume data (Figure 5.6).

Volume quantification indicated that the Scaffold-only and TGF-β3 groups performed similarly to the native trachea at both 6 and 12 weeks. In contrast, the adverse events (fatalities) in the Scaffold-only and TGF-β3 group have a reduced lumen area ($p<0.05$) as compared to a native trachea. The BMSC group at week 6 and 12 had a lesser lumen area ($p<0.05$) as compared to the native trachea (Figure 5.7).

Statistical comparison within groups and between groups was performed. Within the Scaffold-only group, the week 12 subjects had a lumen area that was significantly larger than the adverse events. For this group, the normalized lumen area that is indicative of fatality was approximately 0.19 ± 0.02 cm^2. Among groups, the Scaffold only-week 12 scaffolds had significantly larger lumen than the BMSC-week 12 scaffolds ($p<0.05$).

In addition, the 2-D CT slice data was analyzed (data not shown) and the location (cranial, middle, caudal) of the narrowest region of the trachea were summarized. The point of greatest stenosis occurred exclusively at the midpoint of the implant (data not shown).

In summary, CT quantification data indicated that the Scaffold only group had larger tracheal volumes, and thus less stenosis, than the BMSC group. The BMSC group and adverse events in all groups has significantly smaller airways than the

normal trachea. And finally, adverse event subjects had smaller lumen area, indicating there could be a threshold associated with fatality.

Histology

Macroscopic assessment of immune cells involved evaluating thickness (linked to severity) and location of the immune cell containing region. Immune cells were mainly located on the outer layer of the scaffold, forming a "cap" over the scaffold (Figure 5.8)**.** Diffuse distribution of immune cells was only observed in two subjects (scaffold-only and TGF- β3 adverse events). Although no statistically significant difference could be determined for inflammation severity, a trend of increasing severity over time and in the adverse events was observed (Figure 5.10). BMSC seeded scaffolds at week 12 had more severe inflammation (a thicker layer of inflammatory tissue) than the scaffold-only group at week 6 ($p<0.05$).

Microscopic assessment of immune cell types showed that MNG cells are severely present in all groups, except for a few adverse event cases (Figure 5.10). Mononuclear cells are also moderately to severely present in all groups. Heterophils were moderately present. Eosinophils were not present except for a single case in the scaffold-only group and a single case in the BMSC group (Figure 5.9).

The quantification of blood vessels shows that the TGF-β3, week 6 group had a significantly higher quantity of vasculature than other groups and at other time points (and adverse events) within the TGF-β3 group ($p<0.05$) (Figure 5.10). It appears that the TGF-β3 treatment increases vasculature at early time points but the vasculature declines at later time points. Adverse events in the scaffold-only group

and TGF-β3 group had more vasculature than at non-fatal cases within their respective groups ($p<0.05$).

Epithelium assessment revealed that all scaffolds had epithelium, except for 5 adverse event cases. Of the case with epithelium, a variety of epithelium was present. Epithelium was ciliated to some degree in all subjects. Pseudostratified columnar epithelium was the most common epithelium, with 21 subjects exhibiting this morphology (Figure 5.9). Of the 21 cases, 15 subjects only possessing this epithelium and 6 of those cases had a combination of other types of epithelium—cuboidal, simple cuboidal, stratified cuboidal, and simple columnar. A majority of the pure pseudostratified columnar cases were from the BMSC group (7 cases) and the week 12 cases (9 cases). This is suggestive that cell-seeding and time encourage normal epithelial formation. The simpler epithelium (e.g., simple columnar, cuboidal, and squamous types) was observed in 5 cases and those cases were in different treatment groups but all at 6 weeks. This could indicate that more complex epithelium takes time to migrate and develop on the scaffold lumen [34]. Ulcers were observed in the adverse events subjects (4 cases), indicating that granulation tissue was present in the airway (that could not be determined with bronchoscopy).

The subepithelium was assessed for its vascular and fibrous nature (Figure 5.9). Inflammation was also noted. A large majority of subjects had a fibrous character (10 purely fibrous and 16 in combinations with vascular or inflamed tissue). BMSC seeded scaffolds made up the majority of fibrovascular subepithelium (6 of 9 cases), suggesting cells could positively influence a normal subepithelial appearance.

Subepithelial vasculature was observed in 13 cases and inflammation was observed in 7 cases. The scaffold-only subjects did not have any occurrence of inflamed subepithelium, while adverse event cases usually had inflamed subepithelium (6 of 8 cases).

Regions of immature cartilage formation were observed at defect edges and over the defect (in a couple cases) (Figure 5.9). Scaffold-only subjects had 3 cases of immature cartilage formation, with 2 cases at 6 weeks and 1 case at 12 weeks. TGF-β3 subjects also had 3 cases, with 2 occurring at 12 weeks and 1 occurring in an adverse event case. The cell seeded group had 6 instances of new cartilage formation, occurring mainly at 12 weeks (4 cases).

Assessment of obvious fibroblast appearance and location reveal that fibroblasts were observed in all subjects, usually oriented in a layer around the scaffold, between scaffold layers, and in the subepithelium (Figure 5.9). Unique fibrous, connective tissue was observed inside the scaffold in the 6 week BMSC cases located inside the scaffold, indicating that the BMSCs could have formed or recruited cells to form this tissue (Figure 5.9). Amount of collagen and location of the deposited collagen were assessed. Collagen was moderately present, with no particular difference between groups, and was located in similar regions as the fibroblasts (i.e., around the scaffold) (Figure 5.10).

Though no statistically significant difference could be gathered from this data, there is a decreasing amount of polymer remaining over time and the BMSC group had fewer polymer present as compared to the other groups (Figure 5.10).

In summary, the outer surface of the scaffold was covered by a layer of inflammatory cells, with a thicker layer of these cells occurring in the BMSC group than the Scaffold-only group. The immune cells present (as can be determined with H&E staining) were MNG cells, mononuclear cells, and heterophils. Degree of vascularization was higher in the TGF-B3 group (when compared to the other groups), but the vasculature diminished by 12 weeks. Normal epithelium (pseudostratified columnar) presented more often in the BMSC groups and at later time points. Fibrovascular subepithelium occurred more often in the BMSC groups, while the Scaffold-only group had no incidences of inflamed subepithelium. Immature cartilage was observed across all groups, but with a higher occurrence in the BMSC group. Fibroblasts and collagen were present in all subjects, mainly organizing around the scaffolds and within the scaffold. Normal connective fibroblastic tissue was observed inside the BMSC group scaffolds.

DISCUSSION

We observed that severe stenosis did not always result in fatality. Of the bronchoscopy images scored as severe, approximately half were fatal. Severe stenosis appears to be necessary for fatality, but does not necessarily lead to fatality. The animal model for the current study, the rabbit, was chosen because the trachea is similar in size to a pediatric trachea. We observed that the predominant type of stenosis was tracheal wall deformation and migration of native trachea wall into the laryngofissure, not graft dislodgement occluding the airway. This wall deformation

could be due to 1) the scaffold weakness and inability for construct to adequately support the surrounding tissue, 2) inflammatory response, or 3) the innate fragility of the rabbit trachea wall that is compounded by the defect creation. An understanding for the reason for fatality is needed.

After seeing this variable response to stenosis and delicate nature of the rabbit trachea, this leads us to reassess our animal model. There is no agreed upon animal model for tracheal research, and the animals have ranged from nude mice to pigs.[118] Recently it was determined that the rabbit trachea has a reduced capacity to resist compressive or tensile forces as compared to a sheep or human trachea.[42] The rabbit was an adequate model for small animal work, but future *in vivo* work could include a more mechanically robust trachea (e.g., sheep or pig).

The CT lumen quantification data suggested that the TGF-β3 group (and the Scaffold Only group) has a significant similar lumen area to the native trachea. Also the scaffold-only group had a statistically significant improved lumen area as compared to the BMSC-seeded group. The native trachea-like performance of the scaffold-only group and TGF-β3 group indicates that an acellular approach is a viable option for trachea defect repair. Reasons that the BMSC group had a reduced performance could be linked to the more severe inflammatory response present around those scaffolds.

Acute inflammatory cells (heterophils) and chronic inflammatory cells (mononuclear, MNG cells) were present in all cases [69]. As tissue was collected at later time points (6 and 12 weeks) the later stages of the inflammation response were

captured with histology—small population of heterophils and larger population of mononuclear and MNG cells. In the fatality cases, the inverse was observed with higher populations of neutrophils and lower populations of MNG cells. The inverse cell profile in fatal and nonfatal cases indicates that fatal cases had an acute inflammatory reaction, which could be related to 1) the earlier collection of tissue or 2) the host cells could not transition to chronic inflammation with potential for healing. No clear trend in cell types was observed between groups, except that the inflammation severity (thickness of inflammatory cell layer) was higher in the BMSC group than other groups. Although an immune response severity occurred in the BMSC group, survival was the highest in this group. Thickness of accumulated immune cells over the implant may not be linked to survival, although this indicates a heightened immune response.

Immature cartilage was observed in all groups, but more often in the BMSC group. This could indicate that the cartilage is either an artifact of the histology section or the BMSCs contributed to cartilage formation.[101] Vasculature was observed in all subjects, and the TGF-β3 treatment increased vasculature at early time points but the vasculature declines at later time points, which is expected as TGF-B3 induces angiogenesis [94]. Angiogenesis occurs in granulation tissue and the normal healing process.

Less residual polymer was present in the BMSC group, indicating that the addition of cells could speed degradation, which could be potentially related to increase phagocytosis of polymer material by immune cells. The amount of

inflammatory tissue was increased in the BMSC group. Although no statistically significant difference was observed in this observation, so trends are not conclusive.

The difference between the bronchoscopy rating and the CT lumen quantification, specifically in regards to the TGF-β3 loaded scaffolds, could occur because 1) of the subjective nature of the bronchoscopy rating, 2) the lumen quantification's ability to account for the length of stenosis which can be difficult to determine from the 2D fixed view of the bronchoscopic images, and 3) tissue distortion occurring during the excision and fixation processes. Furthemore, the airway is dynamic, so the lumen can change shape and size based on inspiration and expiration. These static testing methods, like microCT, only evaluate the trachea dimensions at one morphology. If live CT methods are employed in the future, four-dimensional dynamic volume multidetector computed tomography (4D-CT) could be used to account for variation in airway diameter.

The reason for fatality the large study as compared to the pilot studies needs to be investigated. The possible reasons could be: 1) the low statistical power in the pilot studies undermining the true effect of our scaffolds or 2) an experimental variation between the pilot studies and this large scale study. The latter seems more likely as some degree of adverse reaction would have occurred in the pilot studies that would have been comparable to the reactions observed in the current study. The variation between the pilot and large experiments are: 1) change in electrospinning solvent from dichloromethane (DCM) to HFIP, 2) variable electrospinning parameters that affect scaffold thickness or morphology, 3) animal size changed from

8-9 lb in pilot study to 7-8 lb animals in large study, or 4) variation in surgical technique. The most likely from this list could be the solvent change, although any residual solvent should be removed as the scaffolds are lyophilized and fumed for 2 days, or the difference in animal size. As mentioned previously, the rabbit trachea walls have reduce mechanical properties and thus a smaller animal could have more fragile walls than a larger animal. Cytotoxicity testing should be done to determine solvent effects.

Future directions and improvements for this work include measuring the stenosis during bronchoscopy (with a balloon or other method) so we should calculate a percent reduction in area of a finite segment of the tracheal cylinder encompassing the stenosis site. Additionally, an estimate of the added airway resistance over what the normal resistance would have been without the narrowing. While these two approaches would be much more difficult, they would add more data obtained from bronchoscopy. Further histological and immunohistological staining to clarify the specific immune cells types, for example, determining the type of macrophage which could illuminate the direction of healing [13]. In addition, a different surgical technique could be used to induce defects (e.g., laser or brush stenosis) , to implant scaffold (in line with trachea rather than overlap), and to revascularize (pedicle flap over implant). Most importantly, the scaffold could be redesigned to anchor the tracheal walls and prevent any wall migration into the airway. Success has been seen in extra-tracheal tracheal splints.[145] We are designing the next generation of implant that will incorporate extra external support rings that would extend from the patch and could

be additional suture points to anchor the tracheal wall to the scaffold. A tubular scaffold is also in development that could expand this research from small, patch type defects to larger segmental defects.

We have illustrated that our scaffolds maintain functional airways in a majority of cases. While the cell-seeded group had an improved survival rate, the acellular group had a higher occurrence of more patent airways and the BMSC group has reduced areas. The BMSC group had a more severe accumulation of immune cells over the graft, while also exhibiting more normal epithelium, subepithelium and cartilage formation. This leads us to conclude that a simple, acellular scaffold is a viable option for tracheal tissue engineering, with the intraoperative addition of cells being an optional variation to the scaffolds. In conjunction with work to investigate reasons for tracheal obstruction disease pathology and development preventative treatment, our approach could treat patients that have already developed narrowing. Our fibrous bilayer scaffolds provide a clinically-relevant, off-the-shelf approach to tracheal defect repair.

CHAPTER 6: Conclusion

After the decision to apply electrospun materials to tracheal tissue engineering, this research has established the fabrication methods required to manufacture tracheal scaffolds, characterized the morphological and mechanical properties of these scaffolds under *in vitro* degradation, and demonstrated functionality in an *in vivo* model. The series of *in vivo* studies refined the scaffold design and surgical technique. Overall, this work has characterized the use of reinforced, graded, fibrous materials for tracheal defect repair.

The *in vitro* characterization revealed that the short-term degradation of the fibrous PLGA component increased porosity, while the fibrous PCL component reliably held sutures and contributed to recovery from radial compression. The addition of the 3-D printed PCL ring largely improved mechanical properties under tension and radial compression. When compared to desired outcome measures, the gradient scaffolds with ring supports had superior properties compared to other variations of the scaffold. The limits of this scaffold design were the decreased porosity due to the non-porous PCL ring and the larger fiber diameters due to the PLGA component. Future work should investigate increasing porosity of the ring with 3-D printing and solving the sterilization deformed fibers.

The *in vivo* characterization showed that the scaffolds can maintain a functional airway in a patch-defect, although the large-scale study has more adverse outcomes than the previous two pilot studies. More data was gathered in the full-scale study from bronchoscopy, microCT, and histology to evaluate the scaffolds. I

observed that the scaffold-only subjects exhibited larger tracheal lumen volumes and a lower inflammatory response, the TGF-β3 group also had larger tracheal lumen volumes and had improved vasculature, and the cell-seeded group had less fatality and a promising immature connective tissue growth inside the scaffold. Overall, I observed that cells infiltrated into the scaffolds and replaced the regions of degraded PLGA. The cell types present were immune type cells (indicating an inflammatory process), fibroblasts, and epithelium. The addition of growth factors demonstrated an increase in collagen II (second pilot study) and an increase in vascularity of the tissue (full scale study). The addition of cells produced a slightly higher inflammatory response while producing normal connective tissue in and around the scaffold. A redesign of the scaffolds is needed to improve cell-seeding methods, growth factor delivery, and tracheal reinforcing techniques (i.e., surgical technique and external tracheal splint). Specfic redesign include extending PCL rings beyond fibrous portion to create a cage around the trachea to act as an external splint and suture anchor points (e.g., cage or spider-type design). The results of this study proved that a reinforcing component (e.g., ring) is required for improved mechanical performance and that the graded fibrous component provides desirable degradation properties, porosity, and microenvironment. Therefore, I have demonstrated that a scaffold-only approach can maintain the airway, but the addition of growth factors and cells could improve upon the scaffold-only approach.

After in-depth analyses of our scaffold system, areas that require further study include determining cytotoxicity of scaffolds to determine if that could be the cause

of fatality in the *in vivo* study. In the electrospinning field, there is a call for less use of organic solvent (e.g., melt electrospinning), although these solvents contribute to the easy creation of submicron, uniform fibers. Characterization of residual solvent (e.g., HPLC or mass spectroscopy) and a more thorough protocol for solvent removal could also aid in reducing potential cytotoxity.

Other considerations should be the scale up of the scaffold fabrication process. Developing the equipment to make uniform, repeatable scaffolds with less human interaction (e.g., manual addition of PCL rings) is required for marketing and use of the scaffolds.

Characterization of the encapsulated TGF-β3 is needed. Preliminary work quantified growth factor release and bioactivity, although technical and time limitations cut that work short. *In vivo* work demonstrated that TGF-β3 had an effect on collagen II and vascularization of the implant, indicating that the TGF-β3 was bioactive. Further work should be done to refine growth factor release and to identify other beneficial proteins that could reduce severe inflammation and regenerate the complex tracheal tissue (i.e., cartilage, epithelium, glandular-tissue, muscle, vasculature).

My work focused on regenerating the structural component of the trachea, the cartilage. *In vivo,* fibroblasts and collagen were present in and around the scaffold, but normal connective tissue was observed in the cell-seeded group. The presence of normal connective tissue, unique from the fibroblasts that surround the scaffold, indicates that the BMSCs were surviving and populating the implant. Future work

with growth factors and cells should include utilizing no animal products (e.g., BSA carrier for TGF-β3), autologous cells (e.g., bone marrow aspirate or alternative stem cell source), the combination of growth factor and cells for further differentiation of the stem cells, and *in vitro* seeding of the implant prior to implantation.

Future directions for scaffold design would be to investigate other polymer types (e.g., poly(L-lactide-co-caprolactone)) and biological materials (e.g.,. collagen, decellularized tissue). Understanding the immune response to the implant is crucial for implant acceptance and incorporation into the host. Further immune characterization is needed to determine inflammatory cell types (using cell surface marker), which could indicate the type of inflammatory process that is occurring. Innovative research in immunomodulatory tissue engineering approaches could be applied to the scaffolds to control the host's immune response. One such approach could be incorporative antiproliferatives (e.g., rapamycin or paclitaxel) into the electrospun fibers to reduce the inflammatory response.[24] The antiproliferatives prevent smooth muscle cell growth during the first 2-3 weeks after implantation, when risk of inflammation is greatest.

Developing the *in vitro* and *in vivo* models for tracheal implants is crucial for predicting response in humans. Intricate *in vitro* cell culture system could be used to mimic the airway conditions. Once such model could be an air-liquid interface system, where the implant could be exposed to liquid (e.g., cell culture medium) on one side and air on the other. For the *in vivo* model, new defect creation methods should be deployed to create a stenosis model closer to the human occurrence of

stenosis (e.g., laser or brush irritation of the tracheal lumen). Alternative animal models could also be used. The rabbit is an ideal small animal model, but further work should be done in larger animal models such as sheep and pigs. Another avenue for *in vivo* research could be on client-owned animals with naturally occurring tracheal stenosis.[8, 36, 63] Dogs are one such case, where the tracheal cartilage ages and degenerates to a point that it collapses (late stage tracheomalacia). This could be a potential new market for tracheal implants.

The typical strategy for evaluating medical products is to test *in vitro* (with cells), *in vivo* (with a progression from small to larger animals), and finally clinical testing in humans. Pilot *in vivo* studies can be executed first to overstep the inadequacies of *in vitro* testing and to determine if the product functions in its desire application (orthotopic). This pilot study approach is valid for speeding product development by eliminating products/designs that fail in the pilot study stage, with criteria for failure including adverse events, death, or lesser performance to current medical treatment. My pilot studies were successful but when transitioned to a full-scale *in vivo* study, the fatalities caused room for concern. In hindsight, before attempting a large-scale *in vivo* study, I believe that it is wise to check *in vitro* performance before investing in expensive and time consuming full-scale *in vivo* testing. Valuable information can be gathered from *in vitro* testing following a pilot study, such as cytotoxicity (ISO 10993-5 and FDA blue book memorandum #G95-1), cell infiltration, differentiation, etc. In the case of my studies, I believe that the change in electrospinning solvent and decreased rabbit size from pilot to full-scale

study and may be linked to the increased fatalities. In the case of the solvent change, *in vitro* testing could have illuminated the cytotoxicity.

Another observation made from comparing our group's knee research to the trachea research is the dramatically different response to scaffolds *in vivo*. The knee studies have not resulted in fatality, while the trachea models have been less successful. The implantation of tracheal scaffolds is a risky surgery, with a more acute response to implantation (e.g., a compromised airway). It has been reported that an unfavorable microenvironment may exist in the neck (i.e., vascularized environment with different immunological properties than the knee).[128] Thus scaffold development for the trachea should have special consideration.

Translating tracheal tissue engineering into the clinic will require thorough characterization and development of the tracheal constructs, *in vitro* and *in vivo*. Studies like those presented in this thesis refine scaffold design to meet the clinical need. My approach of using fibrous degradable synthetic materials overcomes the limited availability, specialized preparation, and storage of donor tissues, and the limited regenerative capacity of non-degradable materials. Graded, fibrous scaffolds with reinforcing rings can be an alternative to the current standard of care. Although further research and redesign of the scaffold is warranted, these materials can be beneficially incorporated with growth factors and cells. The application of electrospun materials to tracheal defect repair has been taken from idea to practice in this thesis and has established a platform for further research and development, with the potential for translation into clinical use.

REFERENCES

[1]Doctors: Transplant Advance in Windpipe Cancer. *ABC News*. 2010.

[2]Windpipe transplant in UK child. *BBC News*. 2010.

[3]Anderson J. M., W. G. Brodbeck, Y. Nakayama, T. Matsuda, E. Colton, and N. P. Ziats. Biomaterial surface chemistry dictates adherent monocyte/macrophage cytokine expression in vitro. *Cytokine*. 18:311-319, 2002.

[4]Anderson J. M., A. Rodriguez, and D. T. Chang. Foreign body reaction to biomaterials. *Seminars in Immunology*. 20:86-100, 2008.

[5]Asnaghi A., P. Macchiarini, and S. Mantero. Tissue engineering toward organ replacement: a promising approach in airway transplant. *Int J Artif Organs*. 32:763-8, 2009.

[6]Bader A. and P. Macchiarini. Moving towards in situ tracheal regeneration: the bionic tissue engineered transplantation approach. *J Cell Mol Med*. 14:1877-89, 2010.

[7]Baiguera S., M. A. Birchall, and P. Macchiarini. Tissue-engineered tracheal transplantation. *Transplantation*. 89:485-91, 2010.

[8]Becker W. M., M. Beal, B. J. Stanley, and J. G. Hauptman. Survival after surgery for tracheal collapse and the effect of intrathoracic collapse on survival. *Vet Surg*. 41:501-6, 2012.

[9]Behrend M., E. Kluge, W. Schuttler, and J. Klempnauer. Breaking strength of native and sutured trachea. An experimental study on sheep trachea. *Eur Surg Res*. 33:255-63, 2001.

[10]Birchall M. and P. Macchiarini. Airway transplantation: a debate worth having? *Transplantation*. 85:1075-80, 2008.

[11]Brandrup J., E. H. Immergut, and E. A. Grulke. *Polymer handbook*. 4th ed. New York: Wiley. 1999.

[12]Brizzola S., M. de Eguileor, T. Brevini, A. Grimaldi, T. Congiu, P. Neuenschwander, and F. Acocella. Morphologic features of biocompatibility and neoangiogenesis onto a biodegradable tracheal prosthesis in an animal model. *Interact Cardiovasc Thorac Surg*. 8:610-4, 2009.

[13]Brown B. N. and S. F. Badylak. Expanded applications, shifting paradigms and an improved understanding of host-biomaterial interactions. *Acta Biomater*. 9:4948-55, 2013.

[14]Bucheler M. and A. Haisch. Tissue engineering in otorhinolaryngology. *DNA Cell Biol*. 22:549-64, 2003.

[15]Coraux C., B. Nawrocki-Raby, J. Hinnrasky, C. Kileztky, D. Gaillard, C. Dani, and E. Puchelle. Embryonic stem cells generate airway epithelial tissue. *Am J Respir Cell Mol Biol*. 32:87-92, 2005.

[16]Del Gaudio C., S. Baiguera, F. Ajalloueian, A. Bianco, and P. Macchiarini. Are synthetic scaffolds suitable for the development of clinical tissue-engineered tubular organs? *J Biomed Mater Res A*. 102:2427-47, 2014.

[17]Delaere P. Stem-cell "hype" in tracheal transplantation? *Transplantation*. 90:927-8; author reply 928-9, 2010.

[18]Delaere P., J. Vranckx, G. Verleden, P. De Leyn, and D. Van Raemdonck. Tracheal allotransplantation after withdrawal of immunosuppressive therapy. *N Engl J Med*. 362:138-45, 2010.

[19]Detamore M. S. and K. A. Athanasiou. Tensile properties of the porcine temporomandibular joint disc. *J Biomech Eng*. 125:558-65, 2003.

[20]Doolin E. J., L. F. Strande, X. Sheng, and C. W. Hewitt. Engineering a composite neotrachea with surgical adhesives. *J Pediatr Surg*. 37:1034-7, 2002.

[21]Dormer N. H., M. Singh, L. Wang, C. J. Berkland, and M. S. Detamore. Osteochondral interface tissue engineering using macroscopic gradients of bioactive signals. *Ann Biomed Eng*. 38:2167-82, 2010.

[22]Doss A. E., S. S. Dunn, K. A. Kucera, L. A. Clemson, and J. B. Zwischenberger. Tracheal replacements: Part 2. *ASAIO J*. 53:631-9, 2007.

[23]Drilling S., J. Gaumer, and J. Lannutti. Fabrication of burst pressure competent vascular grafts via electrospinning: effects of microstructure. *J Biomed Mater Res A*. 88:923-34, 2009.

[24]Forrest M. L., J. A. Yanez, C. M. Remsberg, Y. Ohgami, G. S. Kwon, and N. M. Davies. Paclitaxel prodrugs with sustained release and high solubility in poly(ethylene glycol)-b-poly(epsilon-caprolactone) micelle nanocarriers: pharmacokinetic disposition, tolerability, and cytotoxicity. *Pharm Res*. 25:194-206, 2008.

[25]Fuchs J. R., D. Hannouche, S. Terada, J. P. Vacanti, and D. O. Fauza. Fetal tracheal augmentation with cartilage engineered from bone marrow-derived mesenchymal progenitor cells. *J Pediatr Surg*. 38:984-7, 2003.

[26]Fuchs J. R., S. Terada, E. R. Ochoa, J. P. Vacanti, and D. O. Fauza. Fetal tissue engineering: in utero tracheal augmentation in an ovine model. *J Pediatr Surg*. 37:1000-6; discussion 1000-6, 2002.

[27]Gerek M. Laryngotracheal reconstruction update. *Current Opinion in Otolaryngology & Head and Neck Surgery*. 9:209-213, 2001.

[28]Gilbert T. W., S. Gilbert, M. Madden, S. D. Reynolds, and S. F. Badylak. Morphologic assessment of extracellular matrix scaffolds for patch tracheoplasty in a canine model. *Ann Thorac Surg*. 86:967-74; discussion 967-74, 2008.

[29]Gilpin D. A., M. S. Weidenbecher, and J. E. Dennis. Scaffold-free tissue-engineered cartilage implants for laryngotracheal reconstruction. *Laryngoscope*. 120:612-7, 2010.

[30]Go T., P. Jungebluth, S. Baiguero, A. Asnaghi, J. Martorell, H. Ostertag, S. Mantero, M. Birchall, A. Bader, and P. Macchiarini. Both epithelial cells and mesenchymal stem cell-derived chondrocytes contribute to the survival of tissue-engineered airway transplants in pigs. *J Thorac Cardiovasc Surg*. 139:437-43, 2010.

[31]Goto Y., Y. Noguchi, A. Nomura, T. Sakamoto, Y. Ishii, S. Bitoh, C. Picton, Y. Fujita, T. Watanabe, S. Hasegawa, and Y. Uchida. In vitro reconstitution of the tracheal epithelium. *Am J Respir Cell Mol Biol*. 20:312-8, 1999.

[32]Grillo H. C. Development of tracheal surgery: a historical review. Part 1: Techniques of tracheal surgery. *Ann Thorac Surg*. 75:610-9, 2003.

[33]Grillo H. C. Tracheal replacement. *J Thorac Cardiovasc Surg*. 125:975, 2003.

[34]Grillo H. C. Tracheal replacement: a critical review. *Ann Thorac Surg*. 73:1995-2004, 2002.

[35]Grimmer J. F., C. B. Gunnlaugsson, E. Alsberg, H. S. Murphy, H. J. Kong, D. J. Mooney, and R. A. Weatherly. Tracheal reconstruction using tissue-engineered cartilage. *Arch Otolaryngol Head Neck Surg*. 130:1191-6, 2004.

[36]Hardie E. M., and B. D. Lascelles. The Honking Dog: Current Controversies in Collapsing Tracheas. *World Small Anim. Vet. Assoc.*, 2002.

[37]Henderson J. H., J. F. Welter, J. M. Mansour, C. Niyibizi, A. I. Caplan, and J. E. Dennis. Cartilage tissue engineering for laryngotracheal reconstruction: comparison of chondrocytes from three anatomic locations in the rabbit. *Tissue Eng*. 13:843-53, 2007.

[38]Ho S. T. and D. W. Hutmacher. A comparison of micro CT with other techniques used in the characterization of scaffolds. *Biomaterials*. 27:1362-76, 2006.

[39]Holt P. G., M. A. Schon-Hegrad, M. J. Phillips, and P. G. McMenamin. Ia-positive dendritic cells form a tightly meshed network within the human airway epithelium. *Clin Exp Allergy*. 19:597-601, 1989.

[40]Igai H., S. S. Chang, M. Gotoh, Y. Yamamoto, M. Yamamoto, Y. Tabata, and H. Yokomise. Tracheal cartilage regeneration and new bone formation by slow release of bone morphogenetic protein (BMP)-2. *ASAIO J*. 54:104-8, 2008.

[41]Jones M. C., F. A. Rueggeberg, H. A. Faircloth, A. J. Cunningham, C. M. Bush, J. D. Prosser, J. L. Waller, G. N. Postma, and P. M. Weinberger. Defining the biomechanical properties of the rabbit trachea. *Laryngoscope*. 124:2352-8, 2014.

[42]Jones M. C., F. A. Rueggeberg, H. A. Faircloth, A. J. Cunningham, C. M. Bush, J. D. Prosser, J. L. Waller, G. N. Postma, and P. M. Weinberger. Defining the biomechanical properties of the rabbit trachea. *Laryngoscope*. 2014.

[43]Jungebluth P., T. Go, A. Asnaghi, S. Bellini, J. Martorell, C. Calore, L. Urbani, H. Ostertag, S. Mantero, M. T. Conconi, and P. Macchiarini. Structural and morphologic evaluation of a novel detergent-enzymatic tissue-engineered tracheal tubular matrix. *J Thorac Cardiovasc Surg*. 138:586-93; discussion 592-3, 2009.

[44]Kalathur M., S. Baiguera, and P. Macchiarini. Translating tissue-engineered tracheal replacement from bench to bedside. *Cell Mol Life Sci*. 2010.

[45]Kalathur M., S. Baiguera, and P. Macchiarini. Translating tissue-engineered tracheal replacement from bench to bedside. *Cell Mol Life Sci*. 67:4185-96, 2010.

[46]Kamil S. H., R. D. Eavey, M. P. Vacanti, C. A. Vacanti, and C. J. Hartnick. Tissue-engineered cartilage as a graft source for laryngotracheal reconstruction: a pig model. *Arch Otolaryngol Head Neck Surg*. 130:1048-51, 2004.

[47]Kanzaki M., M. Yamato, H. Hatakeyama, C. Kohno, J. Yang, T. Umemoto, A. Kikuchi, T. Okano, and T. Onuki. Tissue engineered epithelial cell sheets for the creation of a bioartificial trachea. *Tissue Eng*. 12:1275-83, 2006.

[48]Kim J. H., J. Kim, W. H. Kong, and S. W. Seo. Factors affecting tissue culture and transplantation using omentum. *ASAIO J*. 56:349-55, 2010.

[49]Kojima K., L. J. Bonassar, R. A. Ignotz, K. Syed, J. Cortiella, and C. A. Vacanti. Comparison of tracheal and nasal chondrocytes for tissue engineering of the trachea. *Ann Thorac Surg*. 76:1884-8, 2003.

[50]Kojima K., L. J. Bonassar, A. K. Roy, H. Mizuno, J. Cortiella, and C. A. Vacanti. A composite tissue-engineered trachea using sheep nasal chondrocyte and epithelial cells. *FASEB J*. 17:823-8, 2003.

[51]Kojima K., L. J. Bonassar, A. K. Roy, C. A. Vacanti, and J. Cortiella. Autologous tissue-engineered trachea with sheep nasal chondrocytes. *J Thorac Cardiovasc Surg*. 123:1177-84, 2002.

[52]Kojima K., R. A. Ignotz, T. Kushibiki, K. W. Tinsley, Y. Tabata, and C. A. Vacanti. Tissue-engineered trachea from sheep marrow stromal cells with transforming growth factor beta2 released from biodegradable microspheres in a nude rat recipient. *J Thorac Cardiovasc Surg*. 128:147-53, 2004.

[53]Komura M., H. Komura, Y. Kanamori, Y. Tanaka, K. Suzuki, M. Sugiyama, S. Nakahara, H. Kawashima, A. Hatanaka, K. Hoshi, Y. Ikada, Y. Tabata, and T. Iwanaka. An animal model study for tissue-engineered trachea fabricated from a biodegradable scaffold using chondrocytes to augment repair of tracheal stenosis. *J Pediatr Surg*. 43:2141-6, 2008.

[54]Komura M., H. Komura, Y. Tanaka, Y. Kanamori, M. Sugiyama, S. Nakahara, H. Kawashima, K. Suzuki, K. Hoshi, and T. Iwanaka. Human tracheal chondrocytes as a cell source for augmenting stenotic tracheal segments: the first feasibility study in an in vivo culture system. *Pediatr Surg Int*. 24:1117-21, 2008.

[55]Kucera K. A., A. E. Doss, S. S. Dunn, L. A. Clemson, and J. B. Zwischenberger. Tracheal replacements: part 1. *ASAIO J*. 53:497-505, 2007.

[56]Kunisaki S. M., D. A. Freedman, and D. O. Fauza. Fetal tracheal reconstruction with cartilaginous grafts engineered from mesenchymal amniocytes. *J Pediatr Surg*. 41:675-82; discussion 675-82, 2006.

[57]Lazebnik M., M. Singh, P. Glatt, L. A. Friis, C. J. Berkland, and M. S. Detamore. Biomimetic method for combining the nucleus pulposus and annulus fibrosus for intervertebral disc tissue engineering. *J Tissue Eng Regen Med*. 5:e179-e187, 2011.

[58]Lazebnik M., M. Singh, P. Glatt, L. A. Friis, C. J. Berkland, and M. S. Detamore. Biomimetic method for combining the nucleus pulposus and annulus fibrosus for intervertebral disc tissue engineering. *J Tissue Eng Regen Med*. 5:e179-87, 2011.

[59]Li W. J., R. Tuli, C. Okafor, A. Derfoul, K. G. Danielson, D. J. Hall, and R. S. Tuan. A three-dimensional nanofibrous scaffold for cartilage tissue engineering using human mesenchymal stem cells. *Biomaterials*. 26:599-609, 2005.

[60]Liechty K. W., T. C. MacKenzie, A. F. Shaaban, A. Radu, A. M. Moseley, R. Deans, D. R. Marshak, and A. W. Flake. Human mesenchymal stem cells engraft and demonstrate site-specific differentiation after in utero transplantation in sheep. *Nat Med*. 6:1282-6, 2000.

[61]Lin C. H., S. H. Hsu, C. E. Huang, W. T. Cheng, and J. M. Su. A scaffold-bioreactor system for a tissue-engineered trachea. *Biomaterials*. 30:4117-26, 2009.

[62]Loh Q. L. and C. Choong. Three-dimensional scaffolds for tissue engineering applications: role of porosity and pore size. *Tissue Eng Part B Rev*. 19:485-502, 2013.

[63]Luffy S. A., D. T. Chou, J. Waterman, P. D. Wearden, P. N. Kumta, and T. W. Gilbert. Evaluation of magnesium-yttrium alloy as an extraluminal tracheal stent. *J Biomed Mater Res A*. 102:611-20, 2014.

[64]Luo X., G. Zhou, W. Liu, W. J. Zhang, L. Cen, L. Cui, and Y. Cao. In vitro precultivation alleviates post-implantation inflammation and enhances development of tissue-engineered tubular cartilage. *Biomed Mater*. 4:025006, 2009.

[65]Lusk R. P., D. R. Kang, and H. R. Muntz. Auricular cartilage grafts in laryngotracheal reconstruction. *Ann Otol Rhinol Laryngol*. 102:247-54, 1993.

[66]Macchiarini P., P. Jungebluth, T. Go, M. A. Asnaghi, L. E. Rees, T. A. Cogan, A. Dodson, J. Martorell, S. Bellini, P. P. Parnigotto, S. C. Dickinson, A. P. Hollander, S. Mantero, M. T. Conconi, and M. A. Birchall. Clinical transplantation of a tissue-engineered airway. *Lancet*. 372:2023-30, 2008.

[67]Macchiarini P., T. Walles, C. Biancosino, and H. Mertsching. First human transplantation of a bioengineered airway tissue. *J Thorac Cardiovasc Surg*. 128:638-41, 2004.

[68]Matloub H. S. and P. Yu. Engineering a composite neotrachea in a rat model. *Plast Reconstr Surg*. 117:123-8, 2006.

[69]McNally A. K. and J. M. Anderson. Macrophage fusion and multinucleated giant cells of inflammation. *Adv Exp Med Biol*. 713:97-111, 2011.

[70]Mertsching H., T. Walles, M. Hofmann, J. Schanz, and W. H. Knapp. Engineering of a vascularized scaffold for artificial tissue and organ generation. *Biomaterials*. 26:6610-7, 2005.

[71]Min B. M., G. Lee, S. H. Kim, Y. S. Nam, T. S. Lee, and W. H. Park. Electrospinning of silk fibroin nanofibers and its effect on the adhesion and spreading of normal human keratinocytes and fibroblasts in vitro. *Biomaterials*. 25:1289-97, 2004.

[72]Mironov V., R. P. Visconti, V. Kasyanov, G. Forgacs, C. J. Drake, and R. R. Markwald. Organ printing: tissue spheroids as building blocks. *Biomaterials*. 30:2164-74, 2009.

[73]Moroni L., M. Curti, M. Welti, S. Korom, W. Weder, J. R. de Wijn, and C. A. van Blitterswijk. Anatomical 3D fiber-deposited scaffolds for tissue engineering: designing a neotrachea. *Tissue Eng*. 13:2483-93, 2007.

[74]Nakamura T., T. Sato, M. Araki, S. Ichihara, A. Nakada, M. Yoshitani, S. Itoi, M. Yamashita, S. Kanemaru, K. Omori, Y. Hori, K. Endo, Y. Inada, and K. Hayakawa. In situ tissue engineering for tracheal reconstruction using a luminar remodeling type of artificial trachea. *J Thorac Cardiovasc Surg*. 138:811-9, 2009.

[75]Nakamura T., M. Teramachi, T. Sekine, R. Kawanami, S. Fukuda, M. Yoshitani, T. Toba, H. Ueda, Y. Hori, M. Inoue, K. Shigeno, T. N. Taka, Y. Liu, N. Tamura, and Y. Shimizu. Artificial trachea and long term follow-up in carinal reconstruction in dogs. *Int J Artif Organs*. 23:718-24, 2000.

[76]Neville W. E., J. P. Bolanowski, and G. G. Kotia. Clinical experience with the silicone tracheal prosthesis. *J Thorac Cardiovasc Surg*. 99:604-12; discussion 612-3, 1990.

[77]Ni Y., X. Zhao, L. Zhou, Z. Shao, W. Yan, X. Chen, Z. Cao, Z. Xue, and J. J. Jiang. Radiologic and histologic characterization of silk fibroin as scaffold coating for rabbit tracheal defect repair. *Otolaryngol Head Neck Surg*. 139:256-61, 2008.

[78]Nomoto Y., K. Kobayashi, Y. Tada, I. Wada, T. Nakamura, and K. Omori. Effect of fibroblasts on epithelial regeneration on the surface of a bioengineered trachea. *Ann Otol Rhinol Laryngol*. 117:59-64, 2008.

[79]Nouraei S. A., E. Ma, A. Patel, D. J. Howard, and G. S. Sandhu. Estimating the population incidence of adult post-intubation laryngotracheal stenosis. *Clin Otolaryngol*. 32:411-2, 2007.

[80]Obermiller J. F., J. P. Hodde, C. S. McAlexander, K. Kokini, and S. F. Badylak. A comparison of suture retention strengths for three biomaterials. *Med Sci Monit*. 10:PI1-5, 2004.

[81]Ohara K., K. Nakamura, and E. Ohta. Chest wall deformities and thoracic scoliosis after costal cartilage graft harvesting. *Plast Reconstr Surg*. 99:1030-6, 1997.

[82]Okumura N., M. Teramachi, Y. Takimoto, T. Nakamura, Y. Ikada, and Y. Shimizu. Experimental reconstruction of the intrathoracic trachea using a new prosthesis made from collagen grafted mesh. *ASAIO J*. 40:M834-9, 1994.

[83]Omori K., T. Nakamura, S. Kanemaru, R. Asato, M. Yamashita, S. Tanaka, A. Magrufov, J. Ito, and Y. Shimizu. Regenerative medicine of the trachea: the first human case. *Ann Otol Rhinol Laryngol*. 114:429-33, 2005.

[84]Omori K., T. Nakamura, S. Kanemaru, H. Kojima, A. Magrufov, Y. Hiratsuka, and Y. Shimizu. Cricoid regeneration using in situ tissue engineering in canine larynx for the treatment of subglottic stenosis. *Ann Otol Rhinol Laryngol*. 113:623-7, 2004.

[85]Omori K., T. Nakamura, S. Kanemaru, A. Magrufov, M. Yamashita, and Y. Shimizu. In situ tissue engineering of the cricoid and trachea in a canine model. *Ann Otol Rhinol Laryngol*. 117:609-13, 2008.

[86]Omori K., Y. Tada, T. Suzuki, Y. Nomoto, T. Matsuzuka, K. Kobayashi, T. Nakamura, S. Kanemaru, M. Yamashita, and R. Asato. Clinical application of in situ tissue engineering using a scaffolding technique for reconstruction of the larynx and trachea. *Ann Otol Rhinol Laryngol*. 117:673-8, 2008.

[87]Ott L. M., R. A. Weatherly, and M. S. Detamore. Overview of Tracheal Tissue Engineering: Clinical Need Drives the Laboratory Approach. *Annals of Biomedical Engineering*. 39:2091-2113, 2011.

[88]Ott L. M., R. A. Weatherly, and M. S. Detamore. Overview of tracheal tissue engineering: clinical need drives the laboratory approach. *Ann Biomed Eng*. 39:2091-113, 2011.

[89]Pfenninger C., I. Leinhase, M. Endres, N. Rotter, A. Loch, J. Ringe, and M. Sittinger. Tracheal remodeling: comparison of different composite cultures consisting of human respiratory epithelial cells and human chondrocytes. *In Vitro Cell Dev Biol Anim*. 43:28-36, 2007.

[90]Pham Q. P., U. Sharma, and A. G. Mikos. Electrospinning of polymeric nanofibers for tissue engineering applications: A review. *Tissue Engineering*. 12:1197-1211, 2006.

[91]Pham Q. P., U. Sharma, and A. G. Mikos. Electrospinning of polymeric nanofibers for tissue engineering applications: a review. *Tissue Eng*. 12:1197-211, 2006.

[92]Phillip E., N. S. Murthy, D. Bolikal, P. Narayanan, J. Kohn, L. Lavelle, S. Bodnar, and K. Pricer. Ethylene oxide's role as a reactive agent during sterilization: Effects of polymer composition and device architecture. *Journal of Biomedical Materials Research Part B-Applied Biomaterials*. 101B:532-540, 2013.

[93]Remlinger N. T., C. A. Czajka, M. E. Juhas, D. A. Vorp, D. B. Stolz, S. F. Badylak, S. Gilbert, and T. W. Gilbert. Hydrated xenogeneic decellularized tracheal matrix as a scaffold for tracheal reconstruction. *Biomaterials*. 31:3520-6, 2010.

[94]Roberts A. B., M. B. Sporn, R. K. Assoian, J. M. Smith, N. S. Roche, L. M. Wakefield, U. I. Heine, L. A. Liotta, V. Falanga, J. H. Kehrl, and et al. Transforming growth factor type beta: rapid induction of fibrosis and angiogenesis in vivo and stimulation of collagen formation in vitro. *Proc Natl Acad Sci U S A*. 83:4167-71, 1986.

[95]Roberts C. R., J. K. Rains, P. D. Pare, D. C. Walker, B. Wiggs, and J. L. Bert. Ultrastructure and tensile properties of human tracheal cartilage. *J Biomech*. 31:81-6, 1998.

[96]Roomans G. M. Tissue engineering and the use of stem/progenitor cells for airway epithelium repair. *Eur Cell Mater*. 19:284-99, 2010.

[97]Sakata J., C. A. Vacanti, B. Schloo, G. B. Healy, R. Langer, and J. P. Vacanti. Tracheal composites tissue engineered from chondrocytes, tracheal epithelial cells, and synthetic degradable scaffolding. *Transplant Proc*. 26:3309-10, 1994.

[98]Sato T., M. Araki, N. Nakajima, K. Omori, and T. Nakamura. Biodegradable polymer coating promotes the epithelization of tissue-engineered airway prostheses. *J Thorac Cardiovasc Surg*. 139:26-31, 2010.

[99]Sato T. and T. Nakamura. Tissue-engineered airway replacement. *Lancet*. 372:2003-4, 2008.

[100]Schanz J., J. Pusch, J. Hansmann, and H. Walles. Vascularised human tissue models: A new approach for the refinement of biomedical research. *J Biotechnol*. 2010.

[101]Seguin A., S. Baccari, M. Holder-Espinasse, P. Bruneval, A. Carpentier, D. A. Taylor, and E. Martinod. Tracheal regeneration: evidence of bone marrow mesenchymal stem cell involvement. *J Thorac Cardiovasc Surg*. 145:1297-1304 e2, 2013.

[102]Seguin A., D. Radu, M. Holder-Espinasse, P. Bruneval, A. Fialaire-Legendre, M. Duterque-Coquillaud, A. Carpentier, and E. Martinod. Tracheal replacement with cryopreserved, decellularized, or glutaraldehyde-treated aortic allografts. *Ann Thorac Surg*. 87:861-7, 2009.

[103]Sekine T., T. Nakamura, H. Ueda, K. Matsumoto, Y. Yamamoto, Y. Takimoto, T. Kiyotani, and Y. Shimizu. Replacement of the tracheobronchial bifurcation by a newly developed Y-shaped artificial trachea. *ASAIO J*. 45:131-4, 1999.

[104]Shi H. C., W. J. Deng, C. Pei, D. Lu, X. J. Zhang, X. H. Wang, and Y. J. Zeng. Biomechanical properties of adult-excised porcine trachea for tracheal xenotransplantation. *Xenotransplantation*. 16:181-6, 2009.

[105]Shinoka T., D. Shum-Tim, P. X. Ma, R. E. Tanel, N. Isogai, R. Langer, J. P. Vacanti, and J. E. Mayer, Jr. Creation of viable pulmonary artery autografts through tissue engineering. *J Thorac Cardiovasc Surg*. 115:536-45; discussion 545-6, 1998.

[106]Shoichet M. S. Polymer Scaffolds for Biomaterials Applications. *Macromolecules*. 43:581-591, 2009.

[107]Singh M. and M. S. Detamore. Tensile properties of the mandibular condylar cartilage. *J Biomech Eng*. 130:011009-7, 2008.

[108]Song B. Z., R. B. Donoff, T. Tsuji, R. Todd, G. T. Gallagher, and D. T. Wong. Identification of rabbit eosinophils and heterophils in cutaneous healing wounds. *Histochem J*. 25:762-71, 1993.

[109]Suzuki T., K. Kobayashi, Y. Tada, Y. Suzuki, I. Wada, T. Nakamura, and K. Omori. Regeneration of the trachea using a bioengineered scaffold with adipose-derived stem cells. *Ann Otol Rhinol Laryngol*. 117:453-63, 2008.

[110]Szentivanyi A., T. Chakradeo, H. Zernetsch, and B. Glasmacher. Electrospun cellular microenvironments: Understanding controlled release and scaffold structure. *Adv Drug Deliv Rev*. 63:209-20, 2011.

[111]Tada Y., T. Suzuki, T. Takezawa, Y. Nomoto, K. Kobayashi, T. Nakamura, and K. Omori. Regeneration of tracheal epithelium utilizing a novel bipotential collagen scaffold. *Ann Otol Rhinol Laryngol*. 117:359-65, 2008.

[112]Tan Q., A. M. El-Badry, C. Contaldo, R. Steiner, S. Hillinger, M. Welti, M. Hilbe, D. R. Spahn, R. Jaussi, G. Higuera, C. A. van Blitterswijk, Q. Luo, and W. Weder. The effect of perfluorocarbon-based artificial oxygen carriers on tissue-engineered trachea. *Tissue Eng Part A*. 15:2471-80, 2009.

[113]Tan Q., S. Hillinger, C. A. van Blitterswijk, and W. Weder. Intra-scaffold continuous medium flow combines chondrocyte seeding and culture systems for tissue engineered trachea construction. *Interact Cardiovasc Thorac Surg*. 8:27-30, 2009.

[114]Tan Q., R. Steiner, S. P. Hoerstrup, and W. Weder. Tissue-engineered trachea: History, problems and the future. *Eur J Cardiothorac Surg*. 30:782-6, 2006.

[115]Tan Q., R. Steiner, S. P. Hoerstrup, W. Weder, S. Kanemaru, A. Magrufov, M. Yamashita, and Y. Shimizu. Tissue-engineered trachea: History, problems and the future. *Eur J Cardiothorac Surg*. 30:782-6, 2006.

[116]Tan Q., R. Steiner, L. Yang, M. Welti, P. Neuenschwander, S. Hillinger, and W. Weder. Accelerated angiogenesis by continuous medium flow with vascular endothelial growth factor inside tissue-engineered trachea. *Eur J Cardiothorac Surg*. 31:806-11, 2007.

[117]Tani G., N. Usui, M. Kamiyama, T. Oue, and M. Fukuzawa. In vitro construction of scaffold-free cylindrical cartilage using cell sheet-based tissue engineering. *Pediatr Surg Int*. 26:179-85, 2010.

[118]ten Hallers E. J., G. Rakhorst, H. A. Marres, J. A. Jansen, T. G. van Kooten, H. K. Schutte, J. P. van Loon, E. B. van der Houwen, and G. J. Verkerke. Animal models for tracheal research. *Biomaterials*. 25:1533-43, 2004.

[119]Teng Z., I. Ochoa, J. A. Bea, and M. Doblare. Theoretical and experimental studies on the nonlinear mechanical property of tracheal cartilage. *Conf Proc IEEE Eng Med Biol Soc*. 2007:1058-61, 2007.

[120]Teramachi M., T. Nakamura, Y. Yamamoto, T. Kiyotani, Y. Takimoto, and Y. Shimizu. Porous-type tracheal prosthesis sealed with collagen sponge. *Ann Thorac Surg*. 64:965-9, 1997.

[121]Thomson H. G., T. Y. Kim, and S. H. Ein. Residual problems in chest donor sites after microtia reconstruction: a long-term study. *Plast Reconstr Surg*. 95:961-8, 1995.

[122]Toomes H., G. Mickisch, and I. Vogt-Moykopf. Experiences with prosthetic reconstruction of the trachea and bifurcation. *Thorax*. 40:32-7, 1985.

[123]Ulery B. D., L. S. Nair, and C. T. Laurencin. Biomedical Applications of Biodegradable Polymers. *J Polym Sci B Polym Phys*. 49:832-864, 2011.

[124]Vacanti C. A., K. T. Paige, W. S. Kim, J. Sakata, J. Upton, and J. P. Vacanti. Experimental tracheal replacement using tissue-engineered cartilage. *J Pediatr Surg*. 29:201-4; discussion 204-5, 1994.

[125]von der Mark K., V. Gauss, H. von der Mark, and P. Muller. Relationship between cell shape and type of collagen synthesised as chondrocytes lose their cartilage phenotype in culture. *Nature*. 267:531-2, 1977.

[126]Walles T., B. Giere, M. Hofmann, J. Schanz, F. Hofmann, H. Mertsching, and P. Macchiarini. Experimental generation of a tissue-engineered functional and vascularized trachea. *J Thorac Cardiovasc Surg*. 128:900-6, 2004.

[127]Walles T., B. Giere, P. Macchiarini, and H. Mertsching. Expansion of chondrocytes in a three-dimensional matrix for tracheal tissue engineering. *Ann Thorac Surg*. 78:444-8; discussion 448-9, 2004.

[128]Weidenbecher M., J. H. Henderson, H. M. Tucker, J. Z. Baskin, A. Awadallah, and J. E. Dennis. Hyaluronan-based scaffolds to tissue-engineer cartilage implants for laryngotracheal reconstruction. *Laryngoscope*. 117:1745-9, 2007.

[129]Weidenbecher M., H. M. Tucker, D. A. Gilpin, and J. E. Dennis. Tissue-engineered trachea for airway reconstruction. *Laryngoscope*. 119:2118-23, 2009.

[130]Wemer R. D., Michael Detamore, Robert A. Weatherly. Immunohistochemical characterization of the rabbit tracheal cartilages. *J Biomed Sci and Engg*. 3:1006-1012, 2010.

[131]Wilson S. H., N. T. Cooke, R. H. Edwards, and S. G. Spiro. Predicted normal values for maximal respiratory pressures in caucasian adults and children. *Thorax*. 39:535-8, 1984.

[132]Wu W., X. Cheng, Y. Zhao, F. Chen, X. Feng, and T. Mao. Tissue engineering of trachea-like cartilage grafts by using chondrocyte macroaggregate: experimental study in rabbits. *Artif Organs*. 31:826-34, 2007.

[133]Wu W., Y. Liu, and Y. Zhao. Clinical transplantation of a tissue-engineered airway. *Lancet*. 373:717; author reply 718-9, 2009.

[134]Wyatt P. J. Light-Scattering and the Absolute Characterization of Macromolecules. *Analytica Chimica Acta*. 272:1-40, 1993.

[135]Xie L., A. S. Lin, M. E. Levenston, and R. E. Guldberg. Quantitative assessment of articular cartilage morphology via EPIC-microCT. *Osteoarthritis Cartilage*. 17:313-20, 2009.

[136]Yamamoto Y., T. Okamoto, M. Goto, H. Yokomise, M. Yamamoto, and Y. Tabata. Experimental study of bone morphogenetic proteins-2 slow release from an artificial trachea made of biodegradable materials: evaluation of stenting time. *ASAIO J*. 49:533-6, 2003.

[137]Yamashita M., S. Kanemaru, S. Hirano, A. Magrufov, H. Tamaki, Y. Tamura, M. Kishimoto, K. Omori, T. Nakamura, and J. Ito. Tracheal regeneration after partial resection: a tissue engineering approach. *Laryngoscope*. 117:497-502, 2007.

[138]Yanagi M., A. Kishida, T. Shimotakahara, H. Matsumoto, H. Nishijima, M. Akashi, and T. Aikou. Experimental study of bioactive polyurethane sponge as an artificial trachea. *ASAIO J*. 40:M412-8, 1994.

[139]Yang L., S. Korom, M. Welti, S. P. Hoerstrup, G. Zund, F. J. Jung, P. Neuenschwander, and W. Weder. Tissue engineered cartilage generated from human trachea using DegraPol scaffold. *Eur J Cardiothorac Surg*. 24:201-7, 2003.

[140]Yang Y., G. Tang, Y. Zhao, X. Yuan, and Y. Fan. Effect of cyclic loading on in vitro degradation of poly(L-lactide-co-glycolide) scaffolds. *J Biomater Sci Polym Ed*. 21:53-66, 2010.

[141]Zang M., Q. Zhang, G. Davis, G. Huang, M. Jaffari, C. N. Rios, V. Gupta, P. Yu, and A. B. Mathur. Perichondrium directed cartilage formation in silk fibroin and chitosan blend scaffolds for tracheal transplantation. *Acta Biomater*. 7:3422-31, 2011.

[142]Zani B. G., K. Kojima, C. A. Vacanti, and E. R. Edelman. Tissue-engineered endothelial and epithelial implants differentially and synergistically regulate airway repair. *Proc Natl Acad Sci U S A*. 105:7046-51, 2008.

[143]Zhang J. R., F. L. Chen, W. Wu, J. H. Wei, X. H. Feng, and T. Q. Mao. [Constructing tissue engineered trachea-like cartilage graft in vitro by using

bone marrow stromal cells sheet and PLGA internal support: experimental study in bioreactor]. *Zhonghua Zheng Xing Wai Ke Za Zhi*. 25:124-8, 2009.

[144]Zias N., A. Chroneou, M. K. Tabba, A. V. Gonzalez, A. W. Gray, C. R. Lamb, D. R. Riker, and J. F. Beamis, Jr. Post tracheostomy and post intubation tracheal stenosis: report of 31 cases and review of the literature. *BMC Pulm Med*. 8:18, 2008.

[145]Zopf D. A., C. L. Flanagan, M. Wheeler, S. J. Hollister, and G. E. Green. Treatment of severe porcine tracheomalacia with a 3-dimensionally printed, bioresorbable, external airway splint. *JAMA Otolaryngol Head Neck Surg*. 140:66-71, 2014.

APPENDIX A: Figures

Chapter 3: Figures 3.1-3.10
Chapter 4: Figures 4.1-4.16
Chapter 5: Figures 5.1-5.10

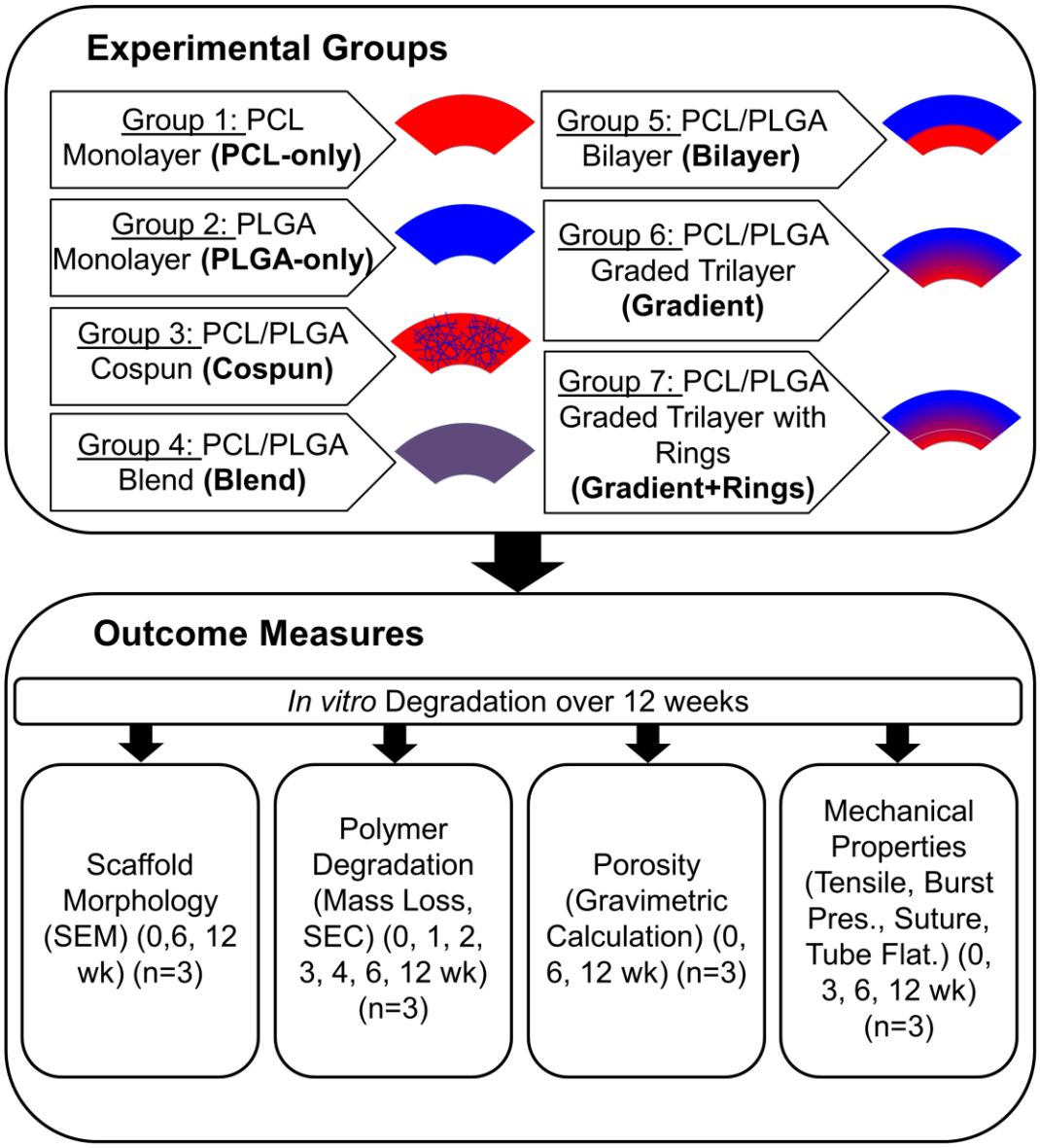

Figure 3.1: *In vitro* characterization of tracheal scaffolds.

Seven different types of scaffolds were tested—1) Polycaprolactone (PCL)-only, 2) poly(lactic-co-glycolic acid) (PLGA)-only, 3) Co-spun, 4) Blend, 5) Bilayer, 6) Gradient, 7) Gradient+ rings. Scaffolds were aged for 12 weeks and the scaffold morphology, degradation, porosity, and mechanical properties were evaluated. [SEM—scanning electron microscopy, SEC—size exclusion chromatography]

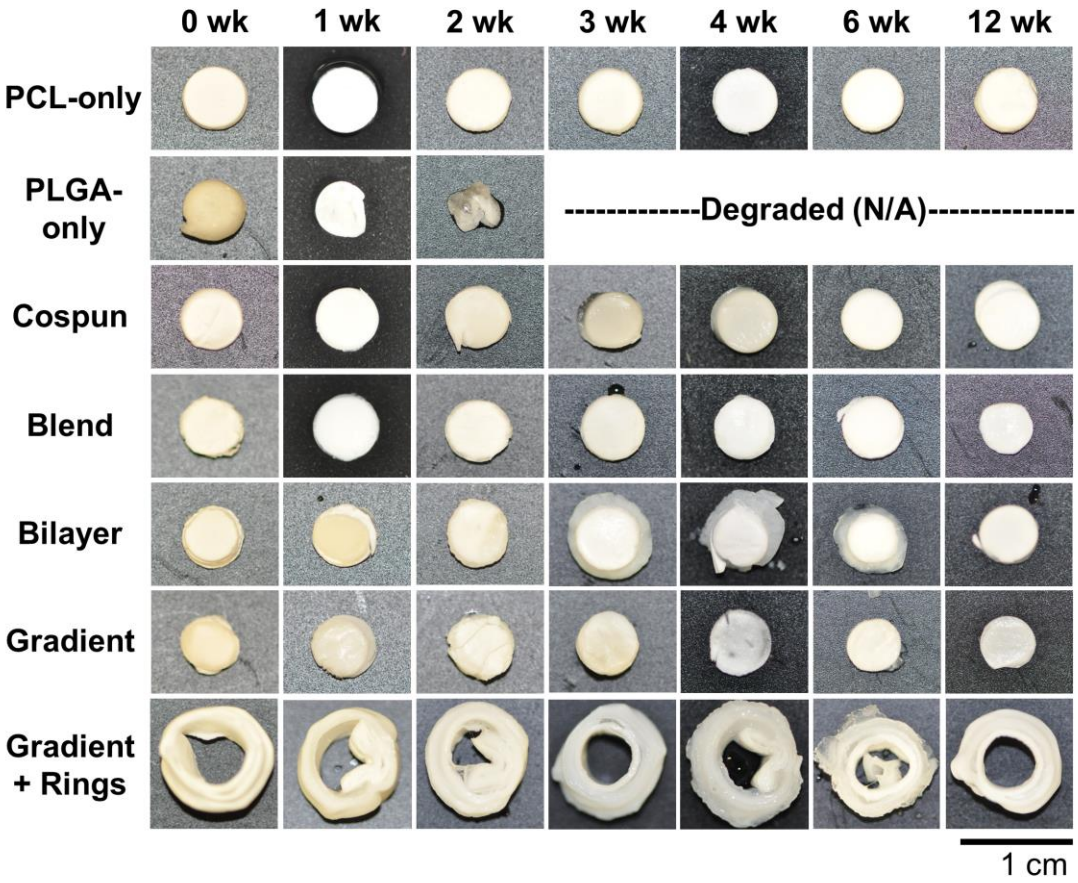

Figure 3.2: Gross morphology of aged scaffolds.

Scaffolds from all groups (except for Gradient+Rings) are presented as an anterior view of disk scaffolds. Gradient+Rings is a cross-section view of tubular scaffolds. The PLGA component degraded after 2 weeks in the PLGA-only group. The PCL component maintained the scaffold shape in all other groups.

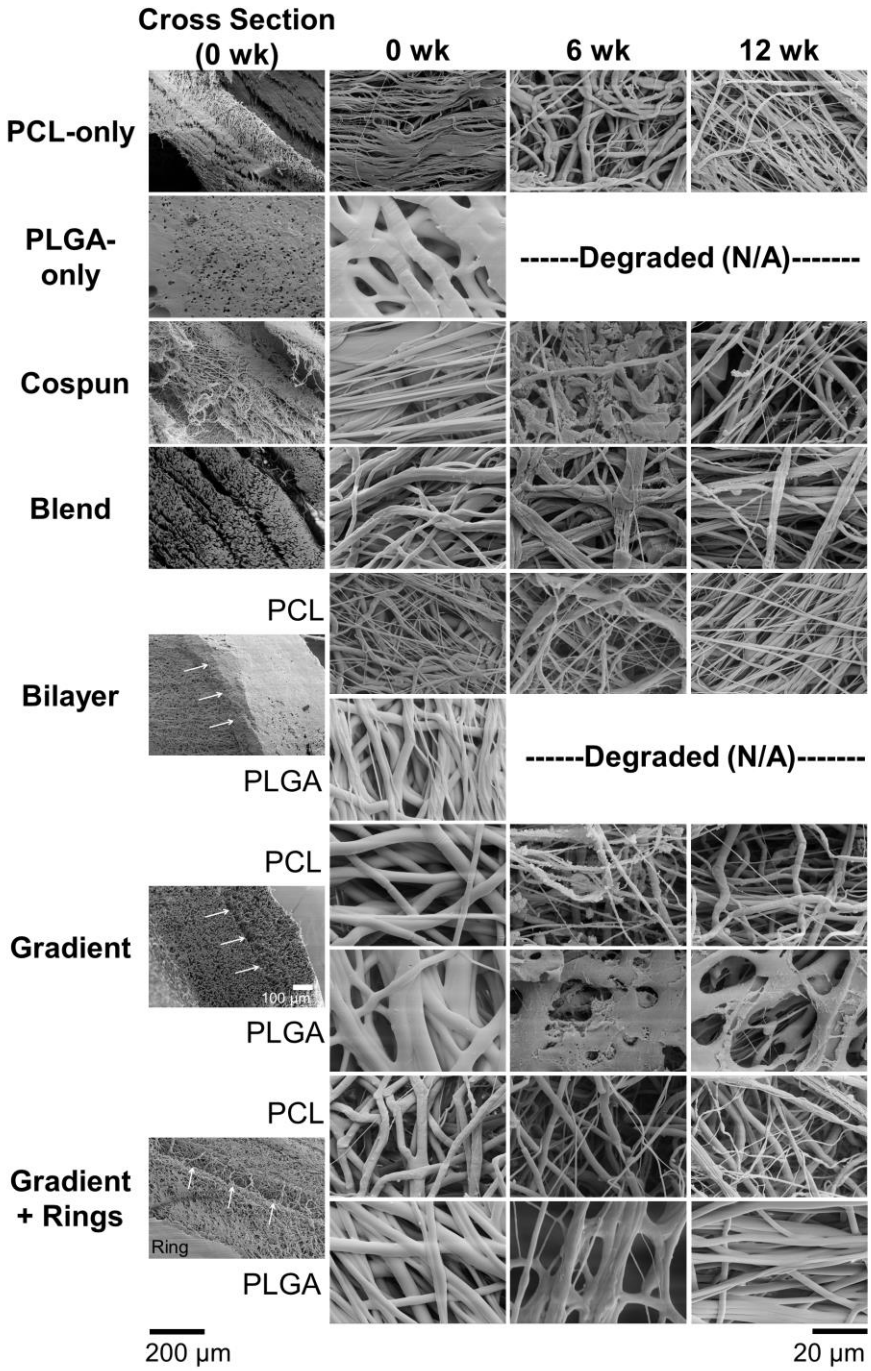

Figure 3.3: SEM images of cross-sections and aged scaffolds.

The PCL fibers are more uniform and the PLGA fibers are flattened and larger. In the cross-section images, arrows indicate the interface between layers and the scale bar is 200 microns. 20 microns represents columns 2-4, which are magnified images of the different treatment groups. The scaffolds with two layers have images for both layers.

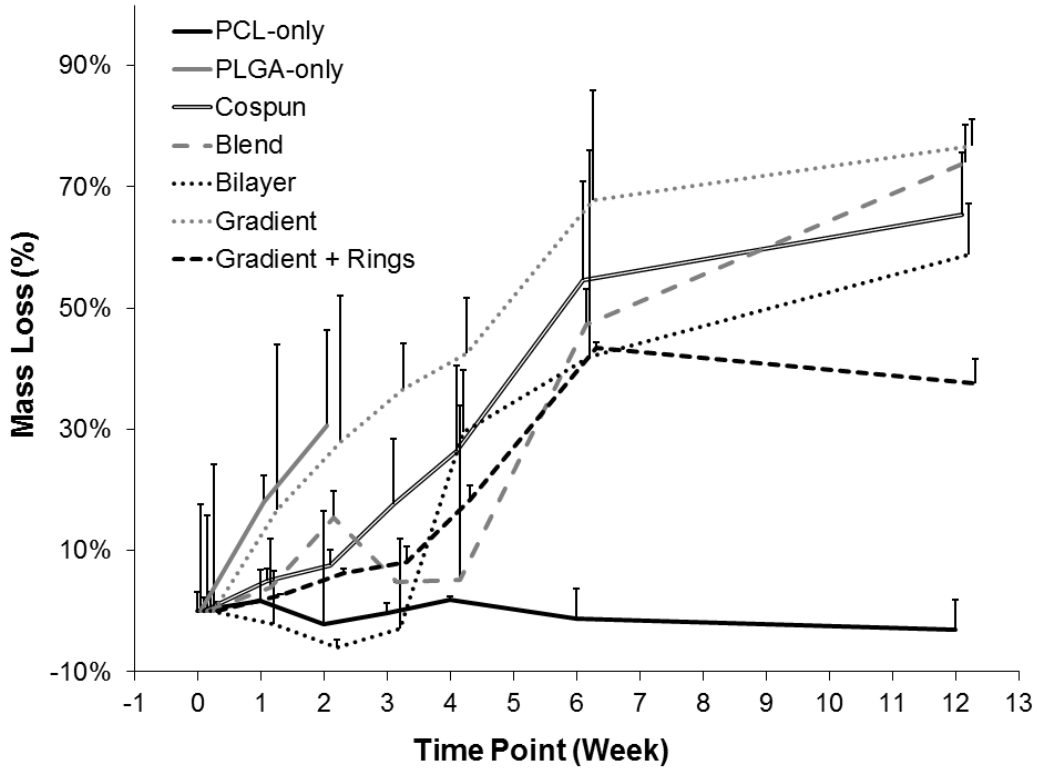

Figure 3.4: Mass loss (%) of aged scaffolds.

All PLGA containing scaffolds exhibited significant mass loss, while the PCL-only group did not lose mass. Data represents averages and error bars represent one standard deviation (n=3).

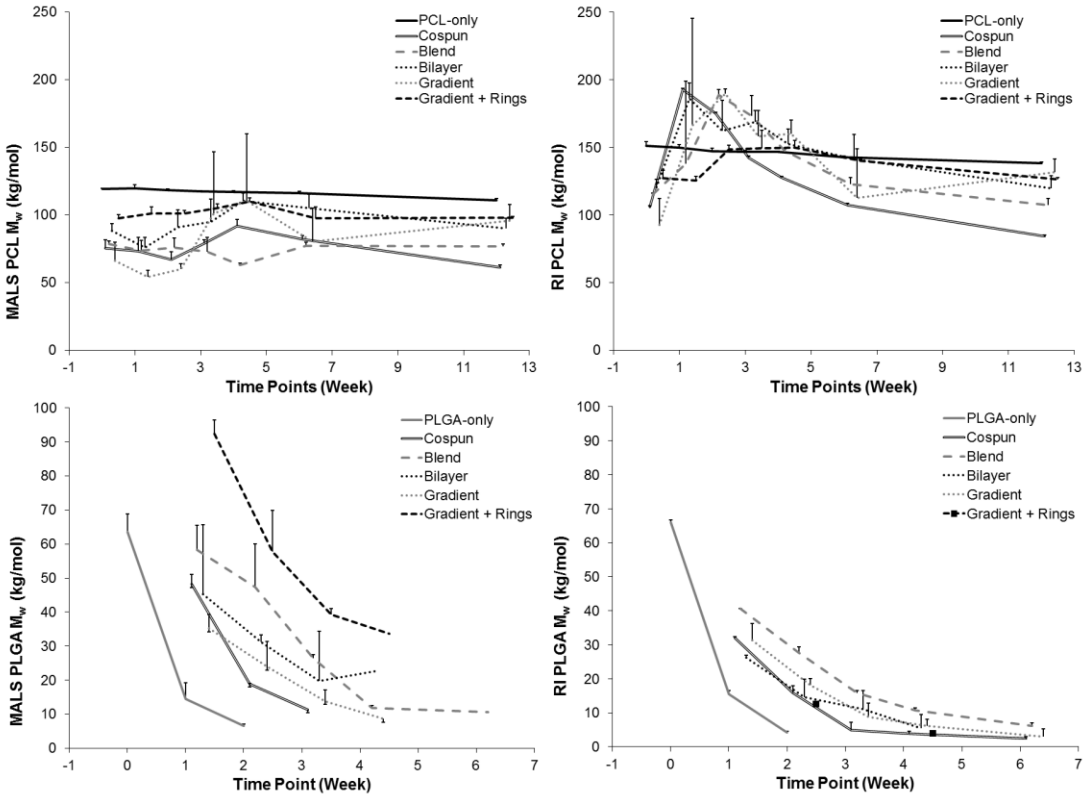

Figure 3.5: Weight-average molecular weight (Mw) for all retained scaffolds.

MALS and RI data followed similar trends, with a decrease in molecular weight of PLGA containing groups up to 6 weeks. PCL and PLGA chromatography peaks were differentiated by retention time, with slight overlap at 0 weeks. Data represents averages and error bars represent one standard deviation (n=3).

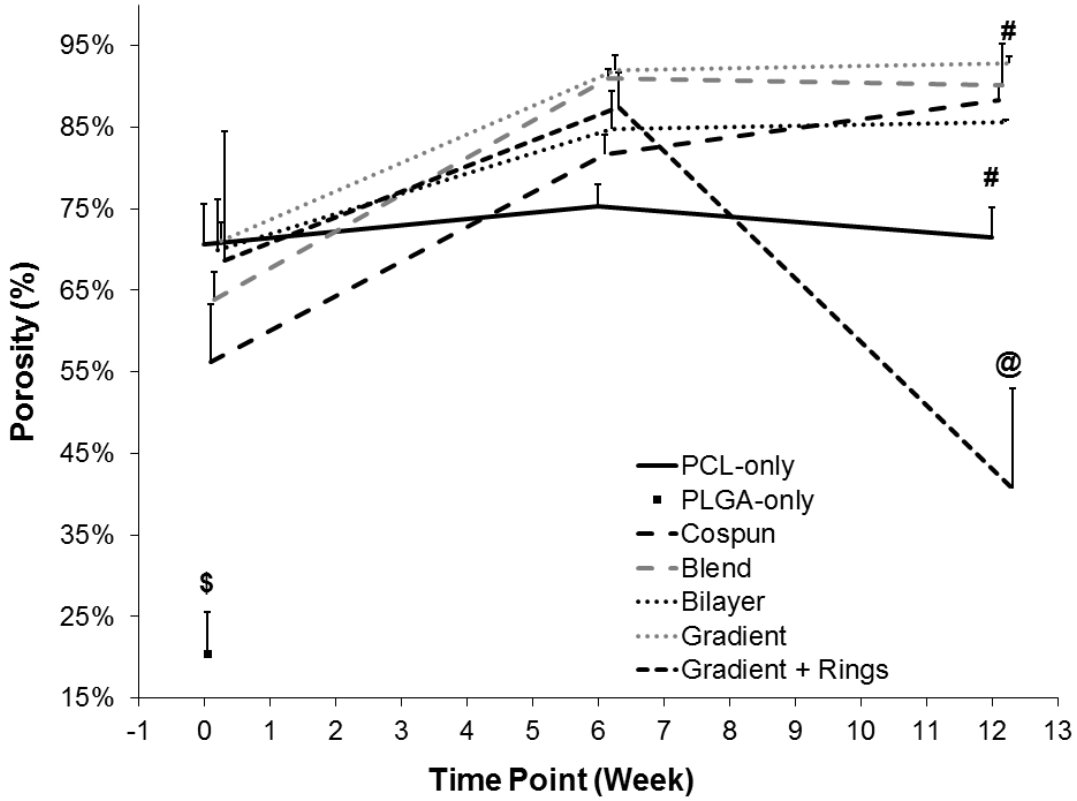

Figure 3.6: Porosity (%) of scaffolds.

Scaffolds increased in porosity over time, with the PLGA-only group being the least porous ($ denotes significantly smaller porosity than all other groups, $p<0.05$). The Gradient+Rings group decreased in porosity with time, due to the remaining PCL rings (@ denotes significant porosity decrease from all other groups, $p<0.05$). PCL-only scaffolds were less porous than the Gradient scaffolds at week 12 (denoted by #, $p<0.05$). Data represents averages and error bars represent one standard deviation (n=3).

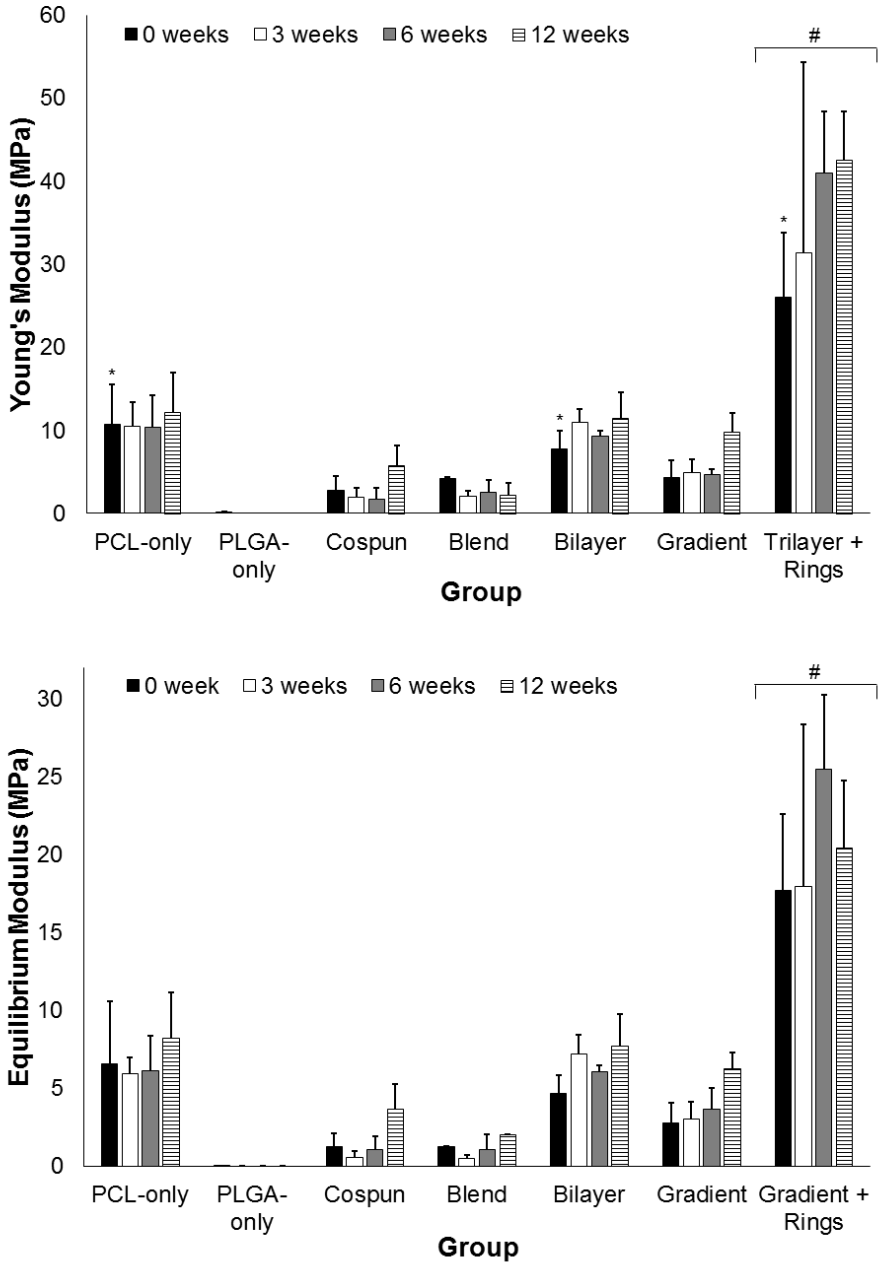

Figure 3.7: Tensile properties of aged scaffolds.

Gradient+Rings had superior Young's and equilibrium modulus as compared to all other groups (denoted by #, $p<0.05$). PCL and Bilayer scaffolds at week 0 performed similarly to the Gradient+Rings scaffolds at week 0 (denoted by *). Data represents

averages and error bars represent one standard deviation (n=3).

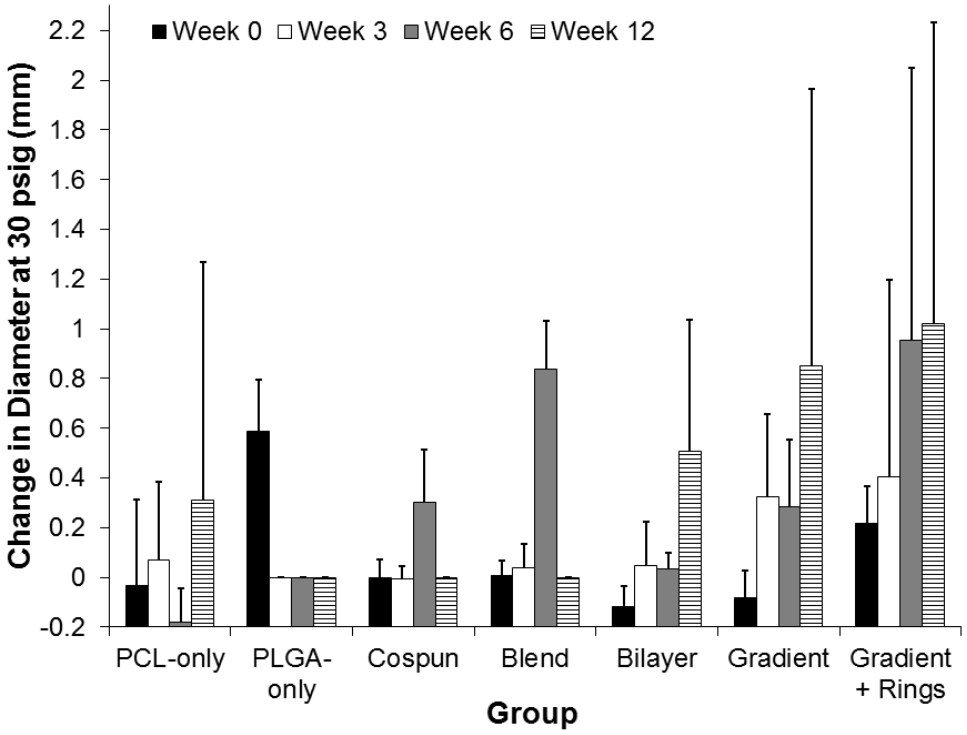

Figure 3.8: Diameter change during burst pressure testing.

As scaffold degraded, the diameters deformed (mm) more in response to the catheter balloon inflation. At week 0, scaffolds resisted deformation, except for PLGA-only. No statistically significant differences were present. Data represents averages and error bars represent one standard deviation (n=3).

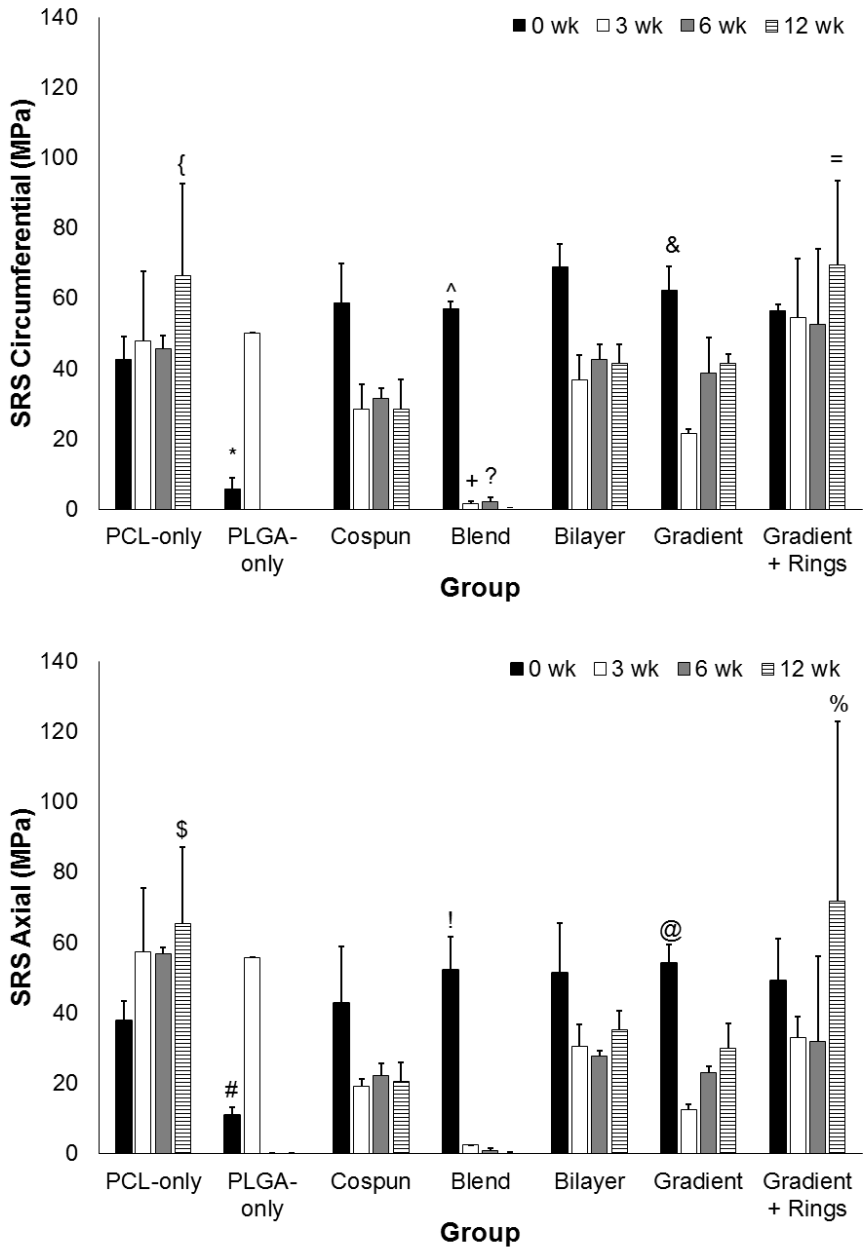

Figure 3.9: Suture Retention Strength (SRS) of scaffolds.

Data represents averages and error bars represent one standard deviation (n=5). Circumferential and axial testing simulated suture pull-out in the circumferential and axial directions when implanted in a trachea.

In the circumferential direction: SRS decreased from 0 to week 3, week 6, and week 12 (denoted by ^, $p<0.05$), Gradient SRS also had degradation dependent decline in SRS from week 0 to week 3 (denoted by ^, $p<0.05$), PCL Only, week 12 SRS were higher than Co-spun and Blend scaffolds at week 12 (denoted by $, $p<0.05$), PLGA Only, week 0 SRS were lower than all groups at week 0 (denoted by *, $p<0.05$), Blend, week 3 SRS were lower than PCL Only, Bilayer, and Gradient+Rings at week 3 (denoted by +, $p<0.05$), Blend, week 6 SRS were lower than PCL Only, Bilayer, Gradient, and Gradient+Rings at week 6 (denoted by ?, $p<0.05$), and Gradient+Rings, week 12 SRS were higher than Co-spun at week 12 (denoted by =, $p<0.05$).

In the axial direction: Blend and Gradient scaffolds were affected by degradation with the SRS decreasing over time (Blend, week 0-week 6 and week 0- week 12; Gradient, week 0-week 3) (denoted by ^, $p<0.05$), PCL Only and Gradient+Rings, week 12 had greater SRS than Co-spun and Blend at week 12 (denoted by $ and %, $p<0.05$), and PLGA Only, week 0 SRS were lower than Blend, Bilayer, and Gradient at week 0 (denoted by #, $p<0.05$).

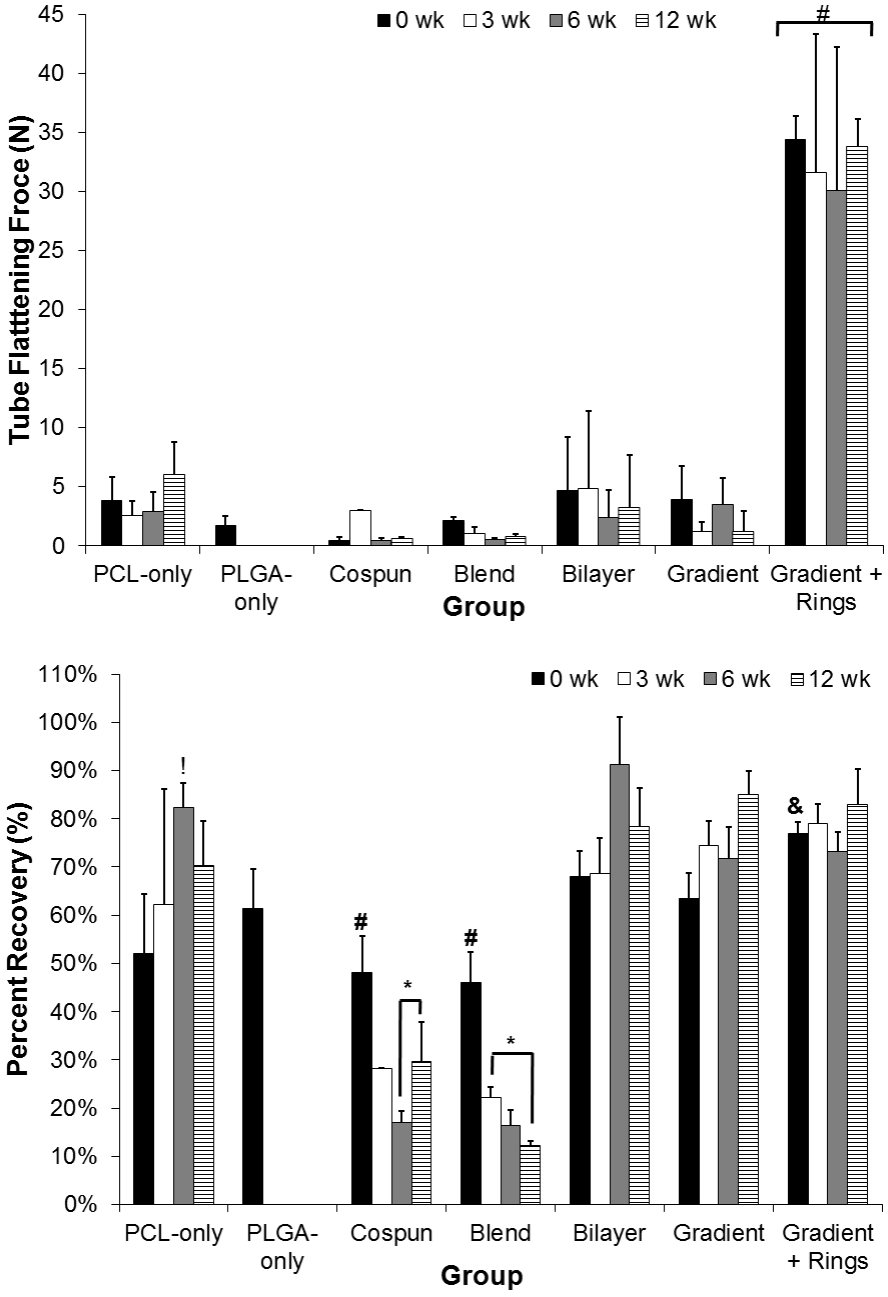

Figure 3.10: Tube flattening and recovery.

Data represents averages and error bars represent one standard deviation (n=5). The load required to flatten the scaffolds followed an overwhelming trend, where

Gradient+Rings scaffolds outperformed all other groups at corresponding time points (denoted by #, $p<0.05$). The recovery of scaffolds after flattening revealed that Co-spun and Blend scaffolds at 3, 6, and 12 weeks remained in a flatter state (or recovered less) than PCL Only, Bilayer, Gradient, and Gradient+Rings at the corresponding time points (denoted by *, $p<0.05$). Gradient+Rings scaffolds at week 0 recovered better than Co-spun and Blend at week 0 (denoted by = &, $p<0.05$). PCL Only, week 0 scaffolds recovered less than at week 6 (denoted by !, $p<0.05$). The reason for this may be due to measurement error or variability in scaffold properties or geometry. Co-spun, week 0 scaffolds recovered better than week 6 (denoted by #, $p<0.05$). Blend, week 0 scaffolds recovered better than week 6 and week 12 (denoted by #, $p<0.05$).

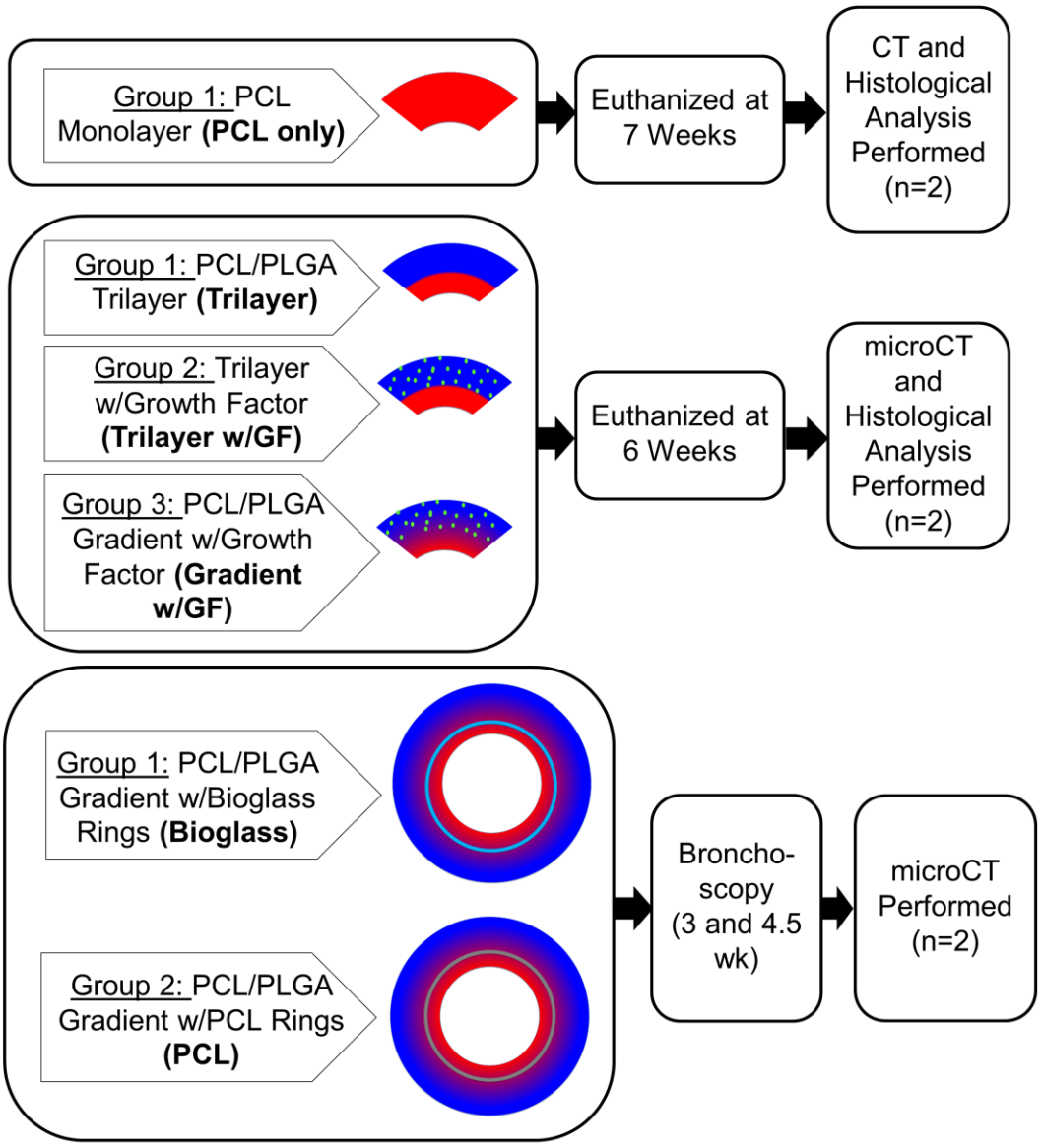

Figure 4.1: Pilot studies experimental design.

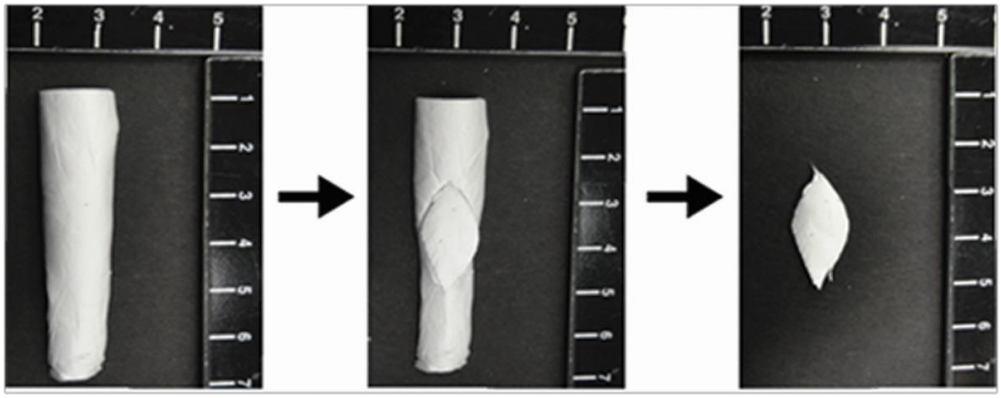

Figure 4.2: Creation of patch-type scaffold.

Demonstrating how the elliptical patch (1 cm by 2.5 cm) was cut from the cylindrical scaffold. A sheet of biomaterial is removed from the electrospinning collecting rod and a predefined elliptical shape was cut out with a scalpel.

Figure 4.3: Demonstrating that scaffolds are suturable.

Demonstrating that a suture can easily be run through the scaffold, which is important for practical ease of use for surgeons.

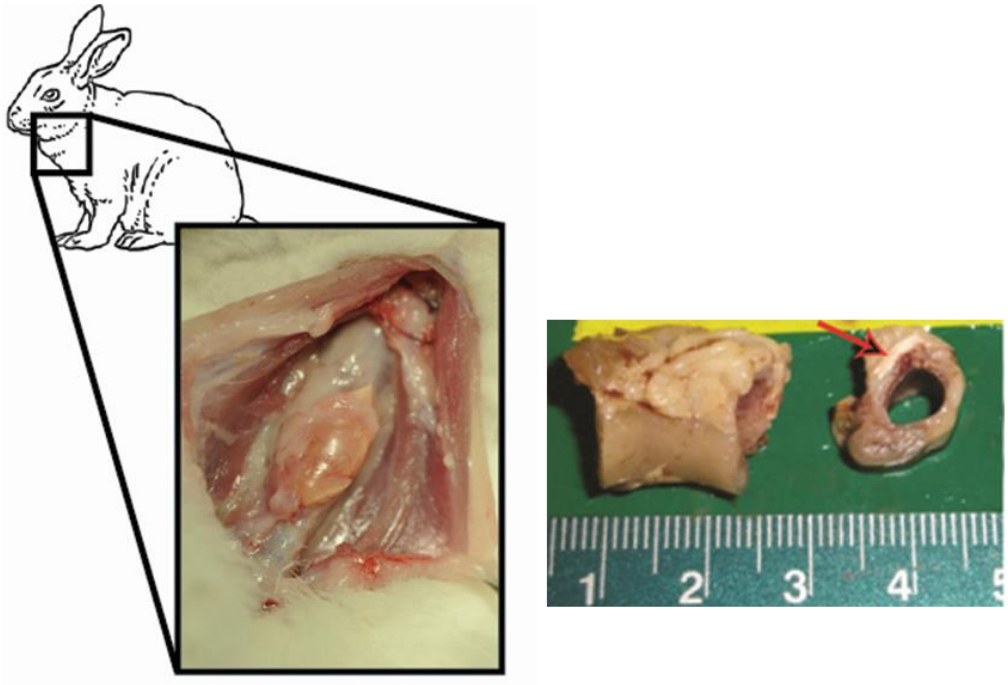

Figure 4.4: Gross morphological images of tracheas with scaffolds.

Gross appearance of the implant after 7 weeks, prior to excision of the trachea. Excised trachea after preliminary study (ruler = cm, arrow indicates PCL scaffold).

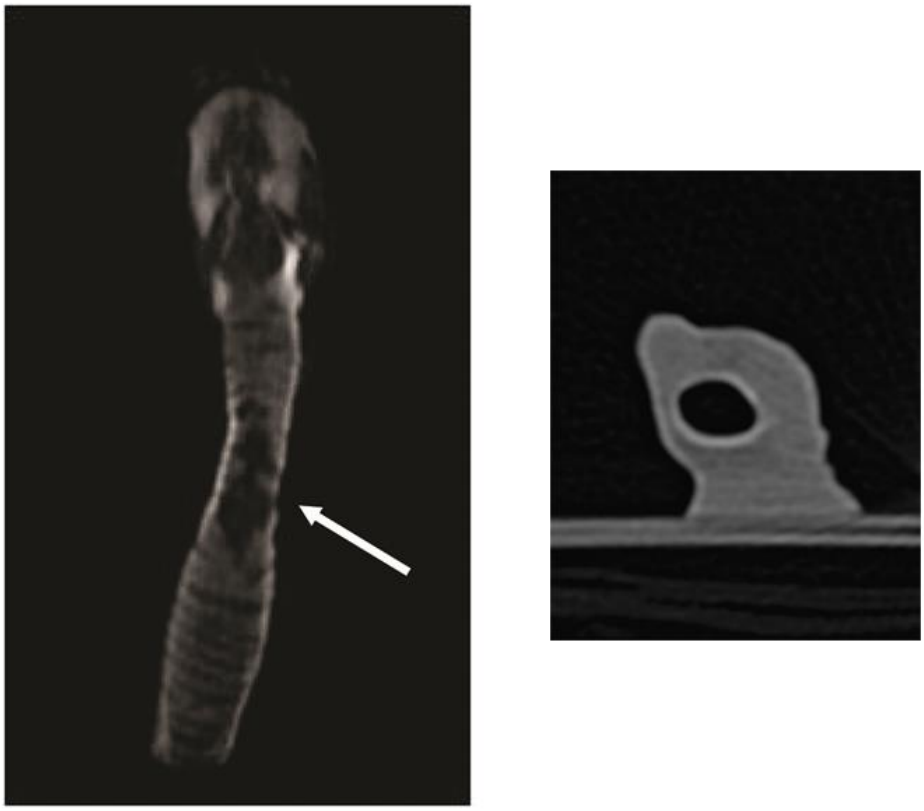

Figure 4.5: CT scans from the first pilot study.

Transverse plane of CT scan revealed that the airway was not blocked (image representative of both rabbits). The 3-D reconstruction suggests a change in tissue density in the region were the scaffold was implanted, suggesting a lack of cartilage arch formation (arrow indicates implant).

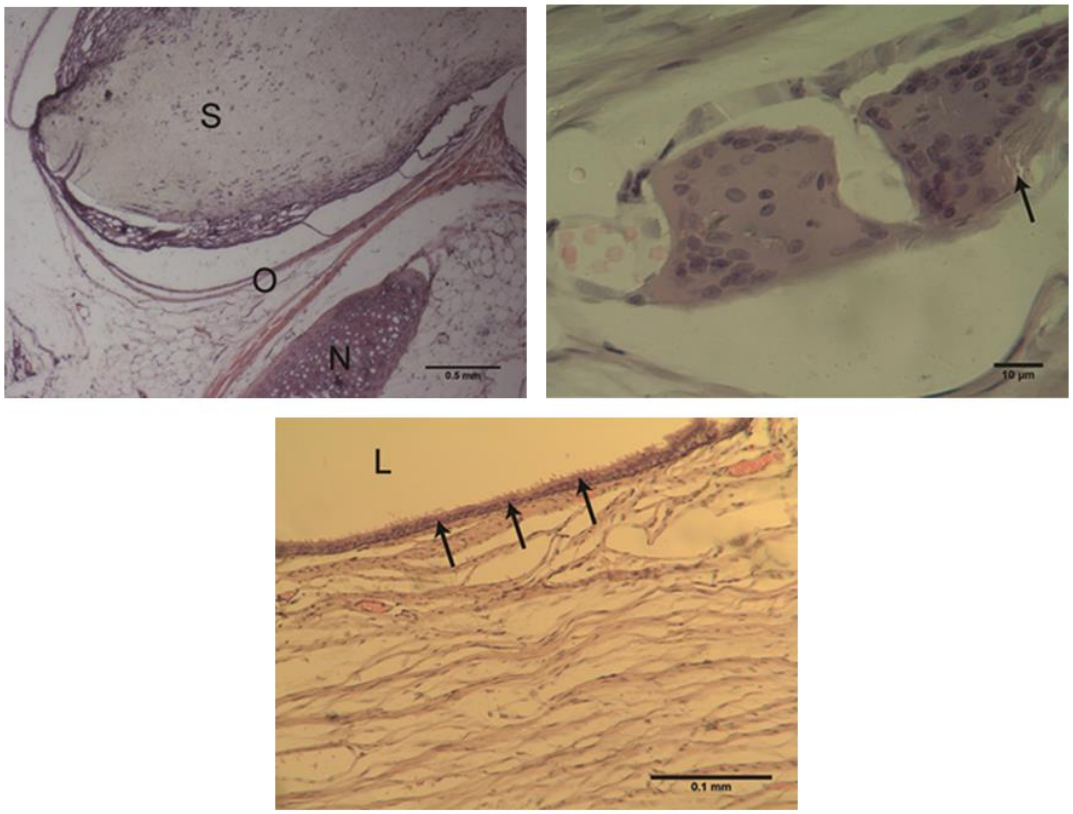

Figure 4.6: Histology images from first pilot study.

Figure 3.6: The lumen (L) was covered with a layer of normal ciliated respiratory epithelium (arrows) (H&E). Scale bar represents 0.1 mm. Multinucleated giant cell found in the scaffold with biomaterial fibers observed inside the cell mass (arrow) (H&E). Scale bar represents 10 µm. Overlap (O) of scaffold (S) over native cartilage (N); notice difference in staining intensity between native cartilage and scaffold (H&E). Scale bar represents 0.5 mm.

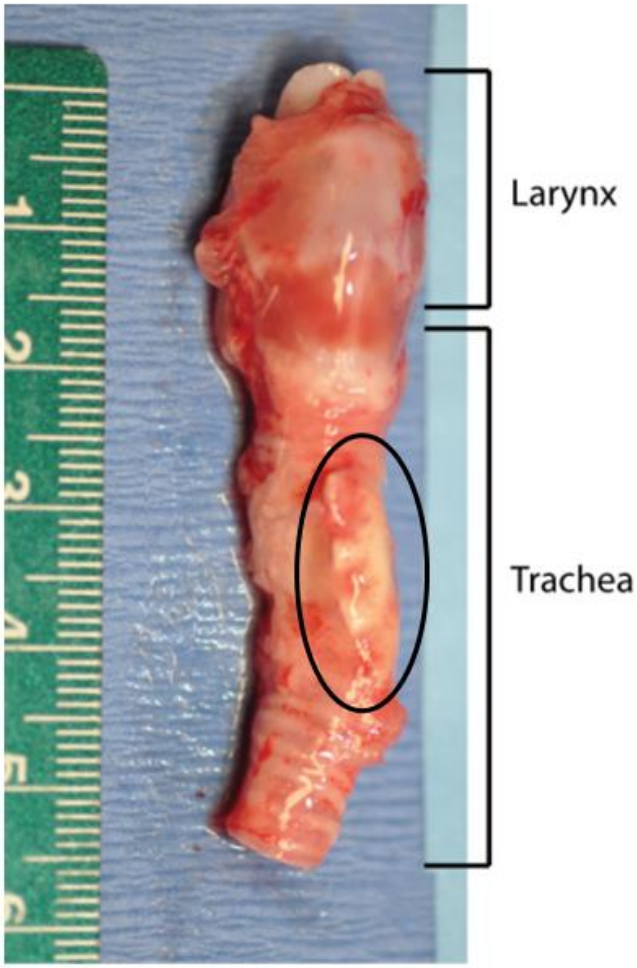

Figure 4.7: Gross morphology of excised trachea from the second pilot study.

The trachea was collected at 6 weeks. The circled region represents the scaffold, which is covered with tissue and residual polymer is visible.

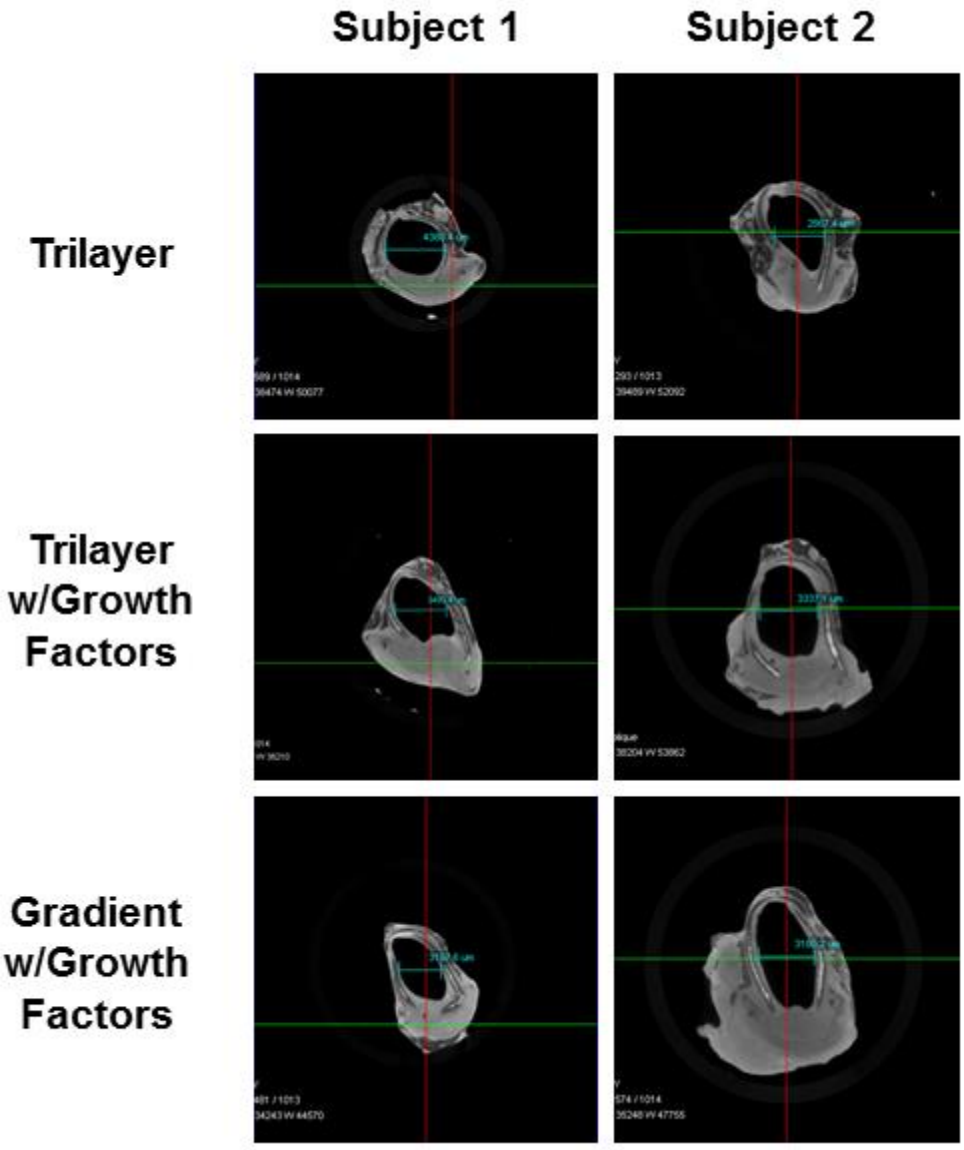

Figure 4.8: Transverse microCT slices from the second pilot study.

The scaffold is located at the 6 o'clock region of the trachea circumference. The lumen volume was measured and percent stenosis was calculated.

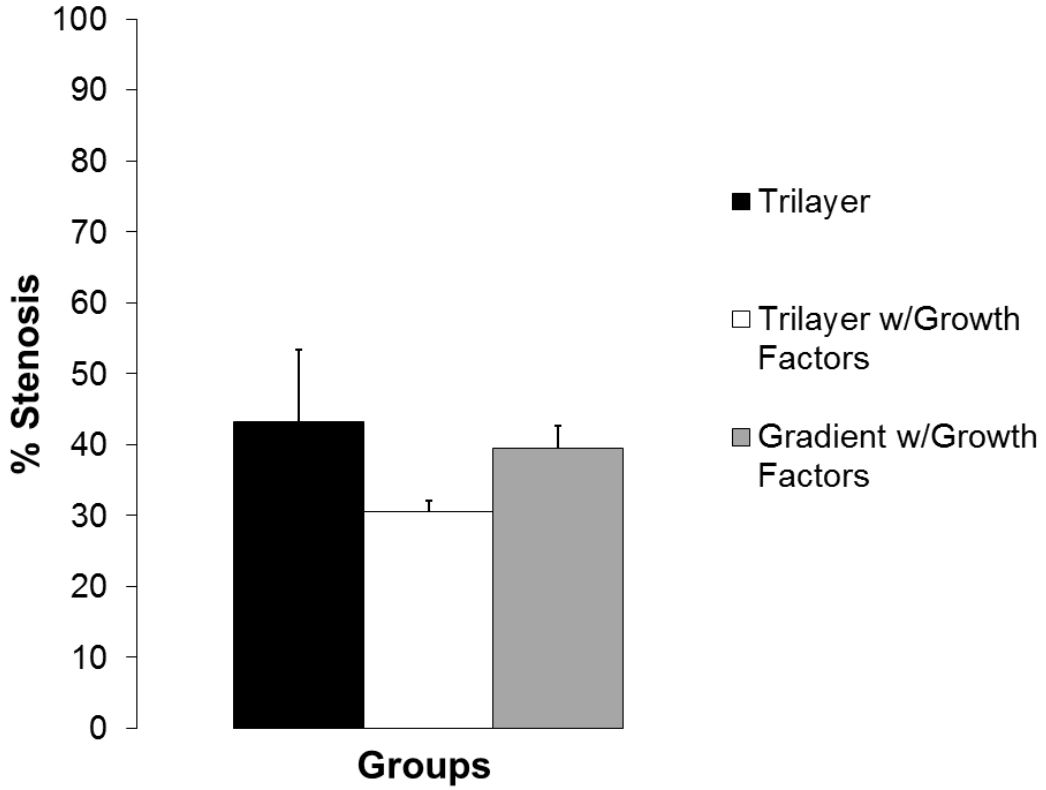

Figure 4.9: Tracheal stenosis (%) from the second pilot study.

Percent stenosis was calculated by obtaining diameter measurements form CT scans and comparing implanted tracheas to normal tracheas. Subjects exhibited a 30-45% stenosed airway. No statistically significant difference determined due to sample size. Data represents averages and error bars represent one standard deviation (n=2).

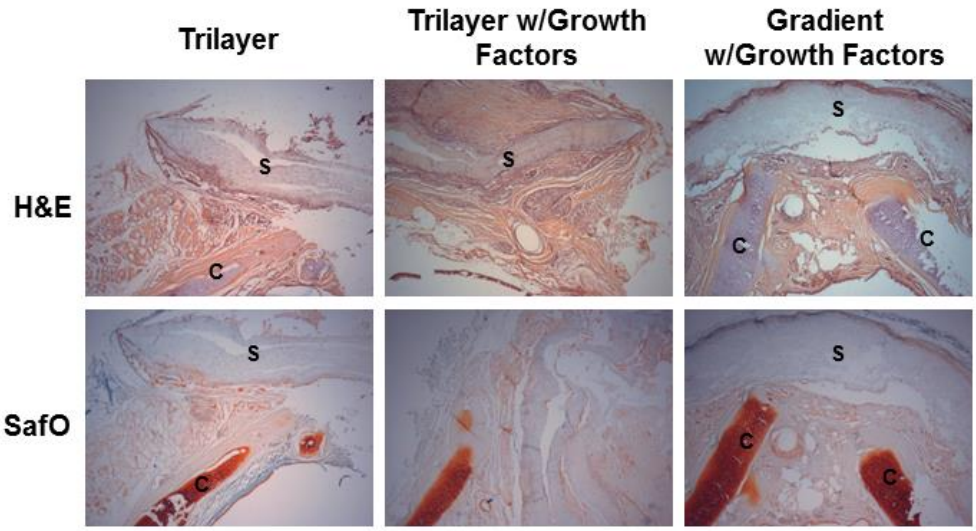

Figure 4.10: Histological images (H&E and Safranin O) of tracheas from the second pilot study.

Cells infiltrated into the scaffold (S) and areas of Safranin O staining around the outer surface of the Gradient w/Growth Factors scaffold were indicative of proteoglycans. Native cartilage (C) is represented in the images.

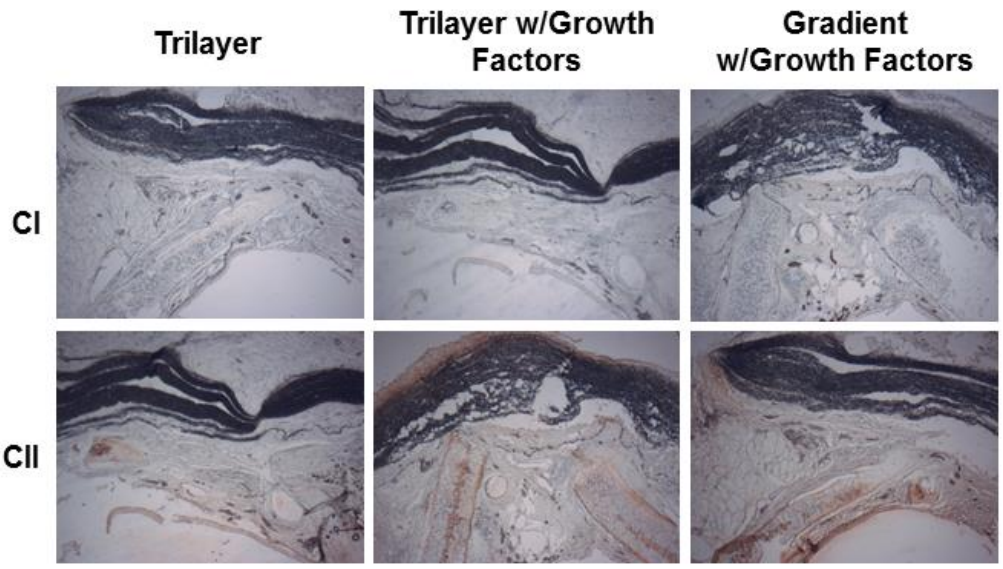

Figure 4.11: Immunohistochemistry images (CI and CII) of tracheas from the second pilot study.

Detection of collagen I (CI) or collagen II (CII) is represented in red. CI staining was negative and CII staining is presented in the native cartilage and in the outer region of the Trilayer w/Growth Factor scaffold.

Figure 4.12: Images of the rings and tubular scaffolds for the circumferential defect repair.

PCL rings, Bioglass rings, and rings encapsulated in the fibrous scaffold shown in the images (from top to bottom).

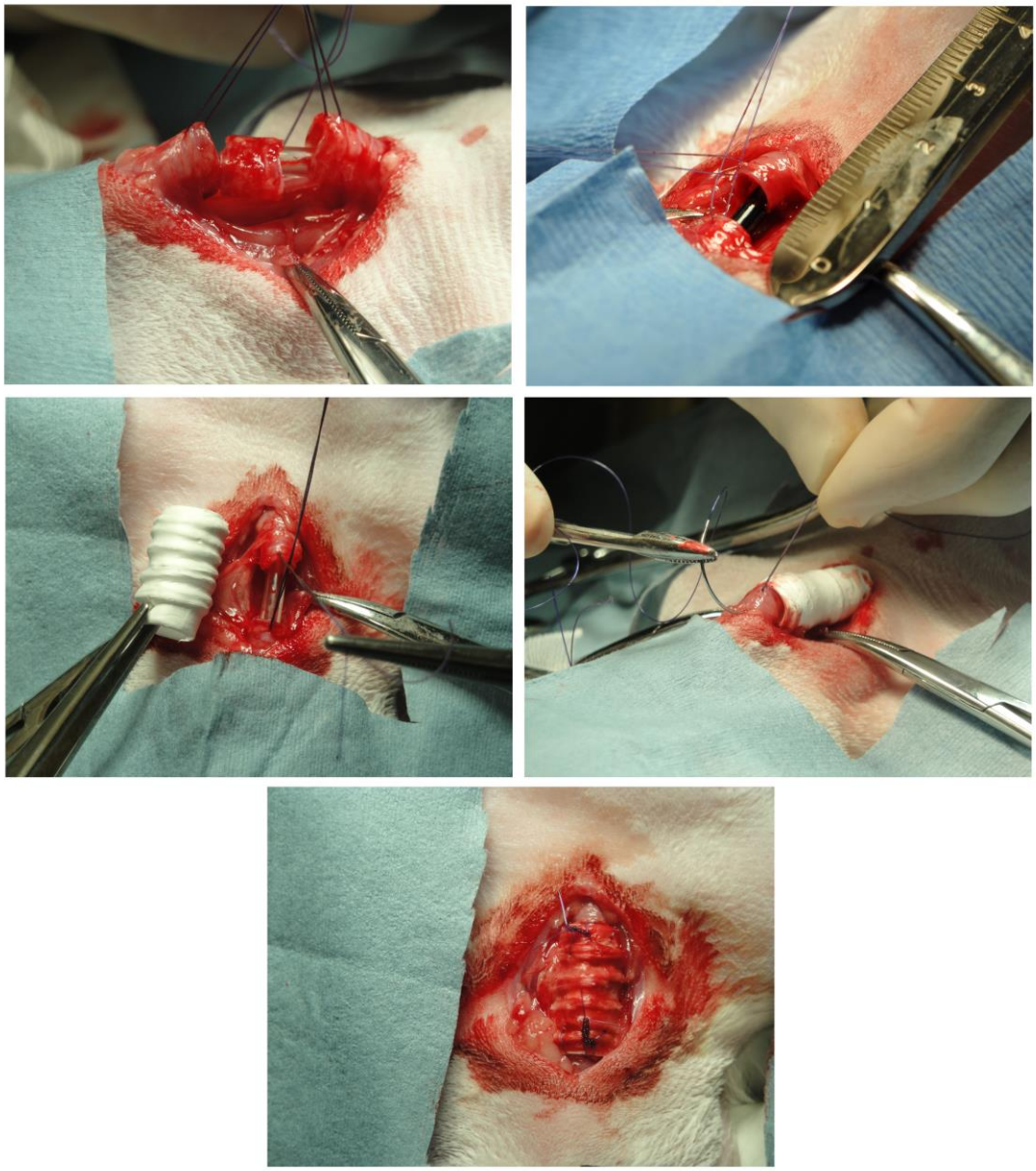

Figure 4.13: Surgical images from the circumferential defect study.

Images demonstrate the removal of a portion of trachea, anchoring free trachea ends with sutures, comparing the scaffold to the defect site, suturing the scaffold in place, and the final appearance of the scaffold in the trachea.

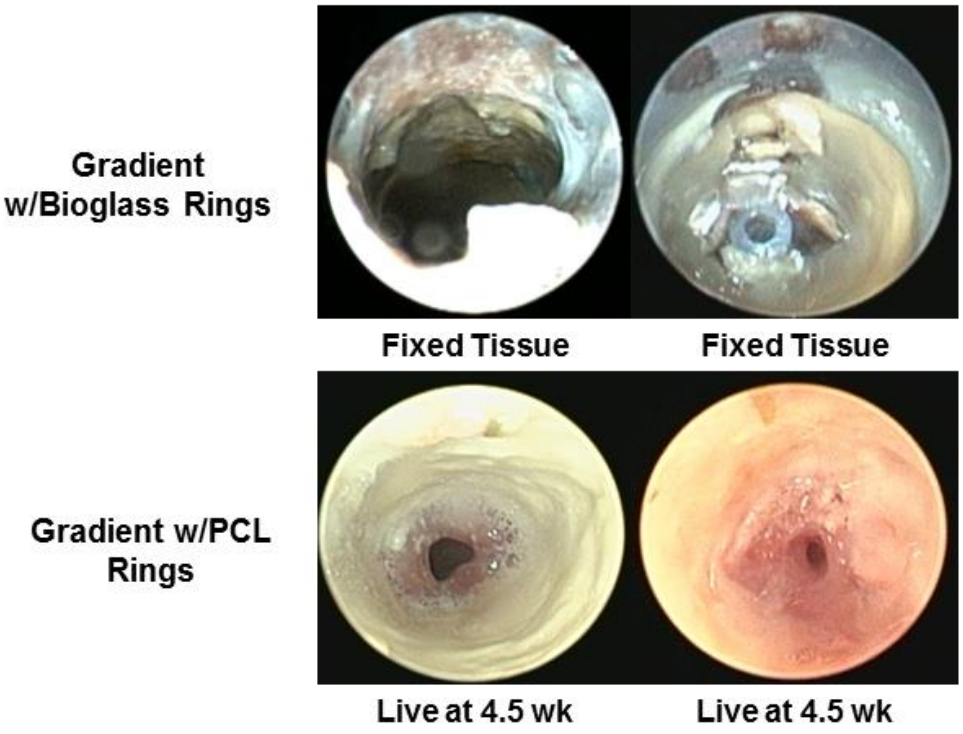

Figure 4.14: Bronchoscopy images from the circumferential defect study.

The top images were taken after tissue was excised and fixed and the bottom two were take in live animals. Stenosis was observed in all cases, except for subject 1 in the Gradient w/Bioglass Rings group.

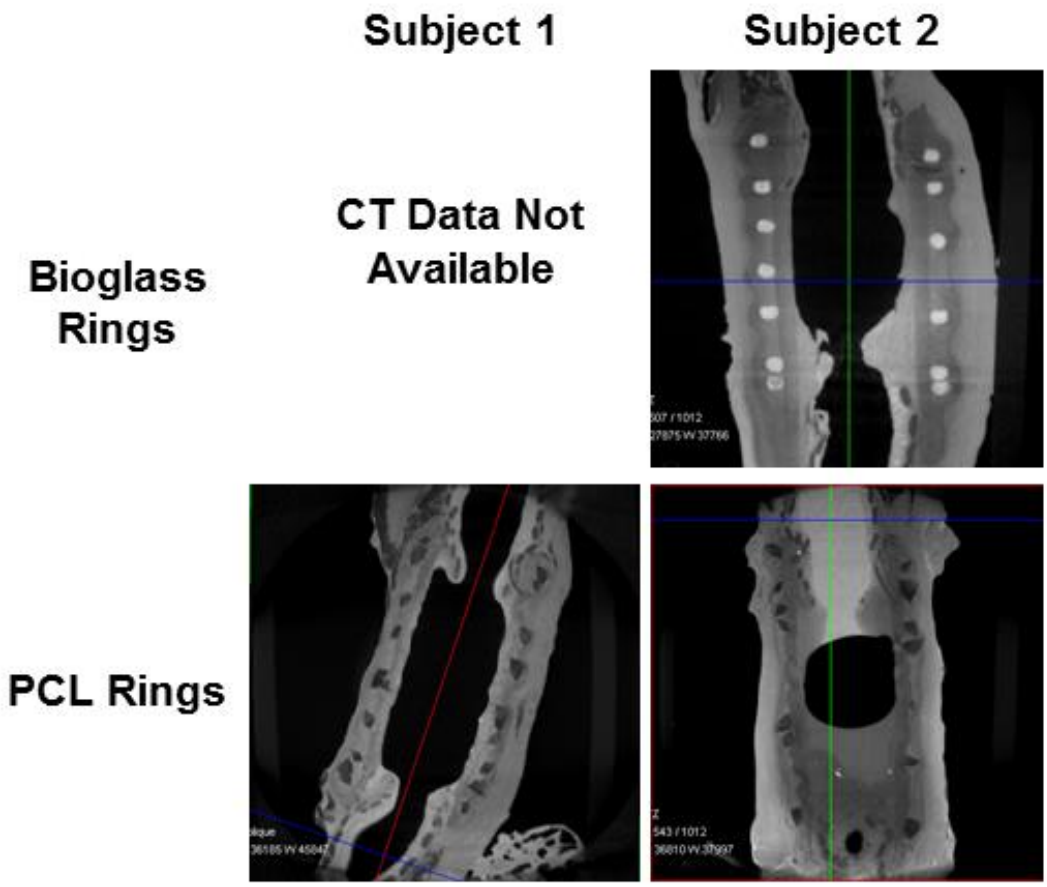

Figure 4.15: microCT images from the circumferentail defect study.

Regions of stenosis was observed at the proximal and distal ends of the scaffold (i.e. at the anastomosis sites). Different radiodensities of the ring components were due to the difference in material properties. The bioactive glass rings had a high mineral content (e.g., calcium) thus this material is more radiodense (or radiopaque). The PCL rings were polymeric materials with high carbon content thus this material is more radiolucent.

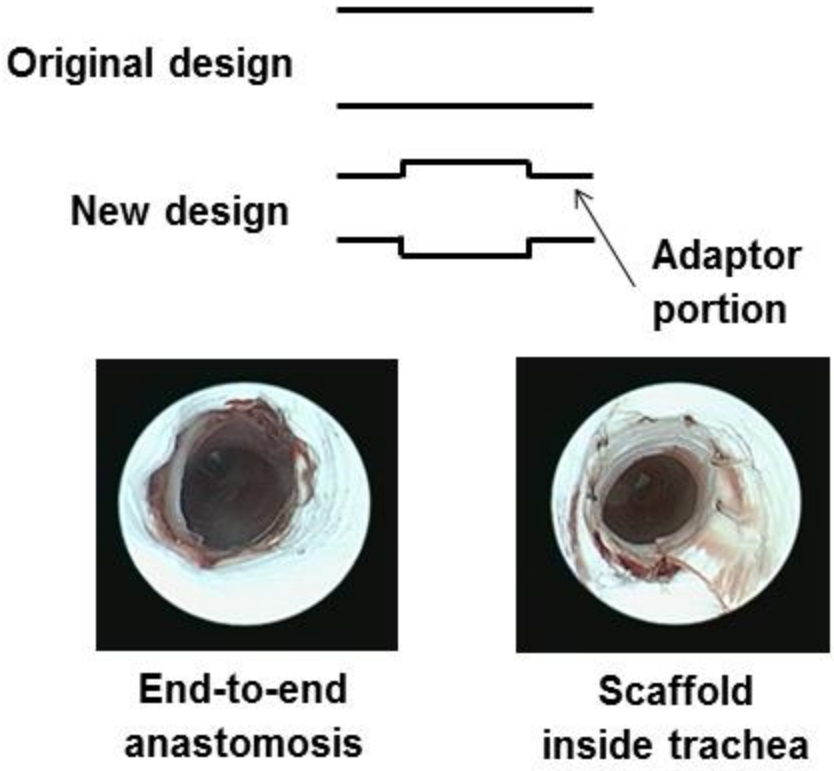

Figure 4.16: Schematic of tubular scaffolds redesign and bronchoscopy images of new surgical techniques on cadaver tracheas.

After circumferential defect pilot study, the scaffold design and surgical technique were reevaluated. It was determined that the scaffold should be inserted inside the trachea to for easier implantation and stenting of the airway at the anastomosis sites.

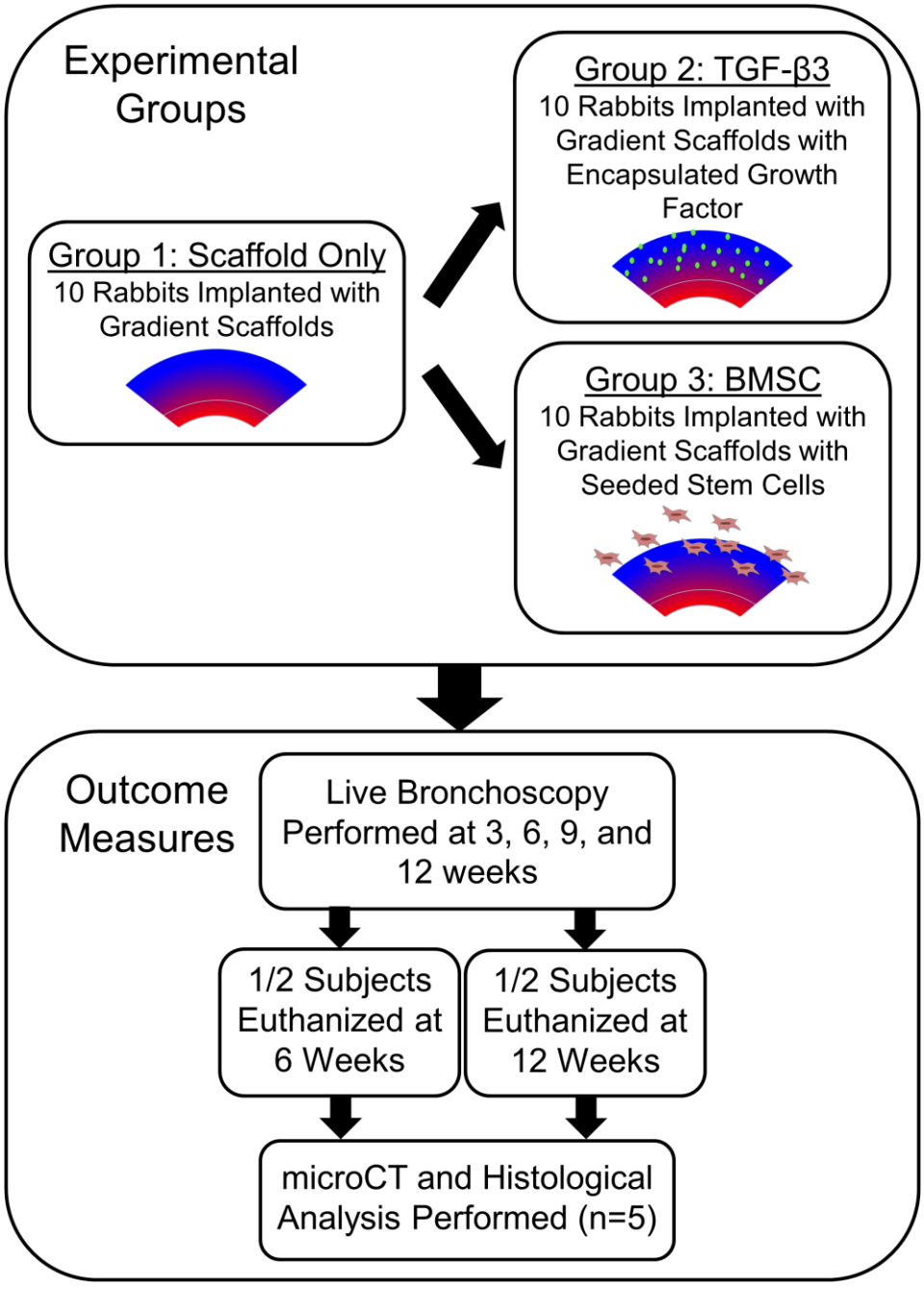

Figure 5.1: *In vivo* study design.

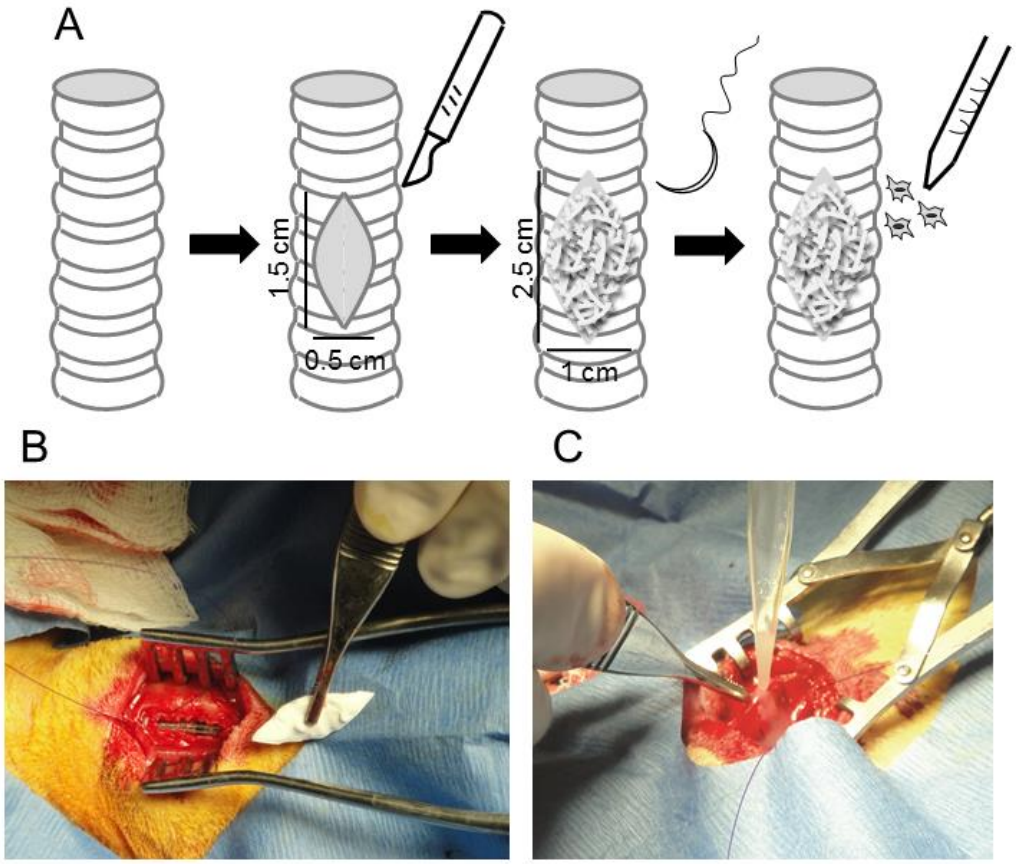

Figure 5.2: Surgical schematic and images.

Surgical schematic of defect creation and scaffold implantation (a). Photographs of the surgical procedure, showing induced tracheal defect and placement of scaffold (b) and intraoperative cell seeding (c).

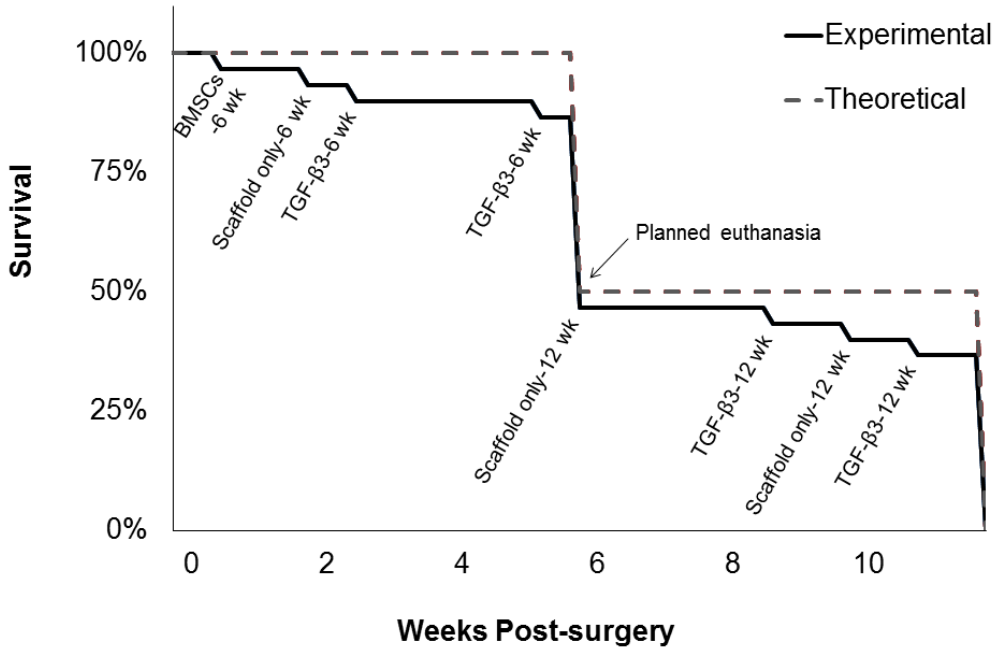

Figure 5.3: Survival rate post-surgery.

Chart mapping the survival rate of subjects over the course of 12 weeks.

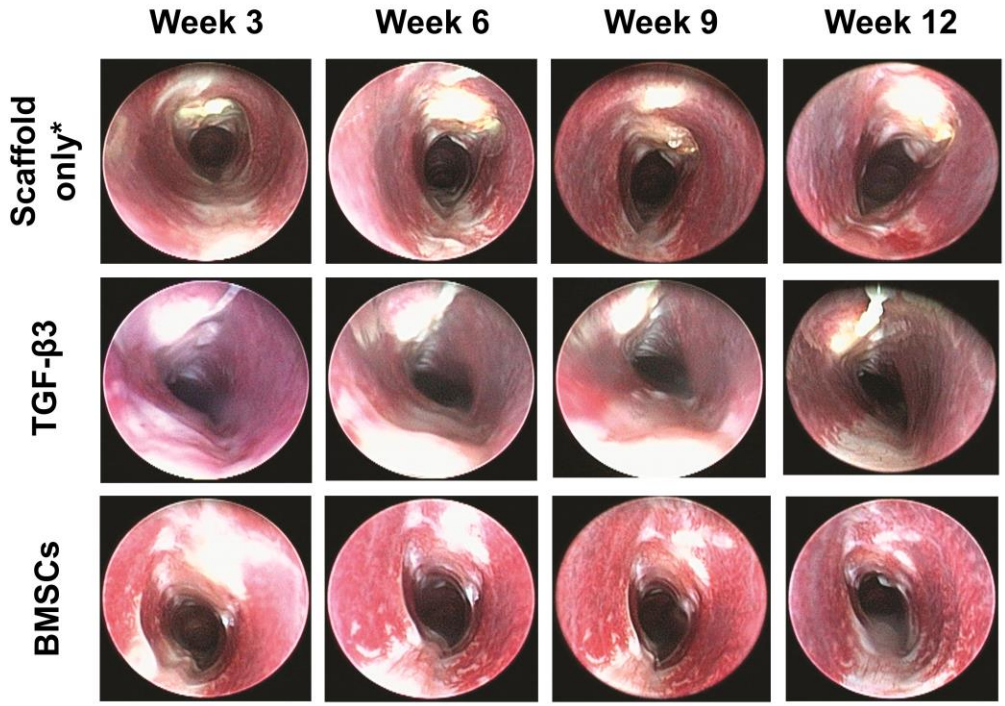

Figure 5.4: Bronchoscopy images.

Selected bronchoscopic images from each experimental group at the 4 bronchoscopic time points (3, 6, 9 and 12 weeks). *Scaffold only subjects were imaged at week 3, 7, 10, and 12. Images follow the progression of one subject from each group.

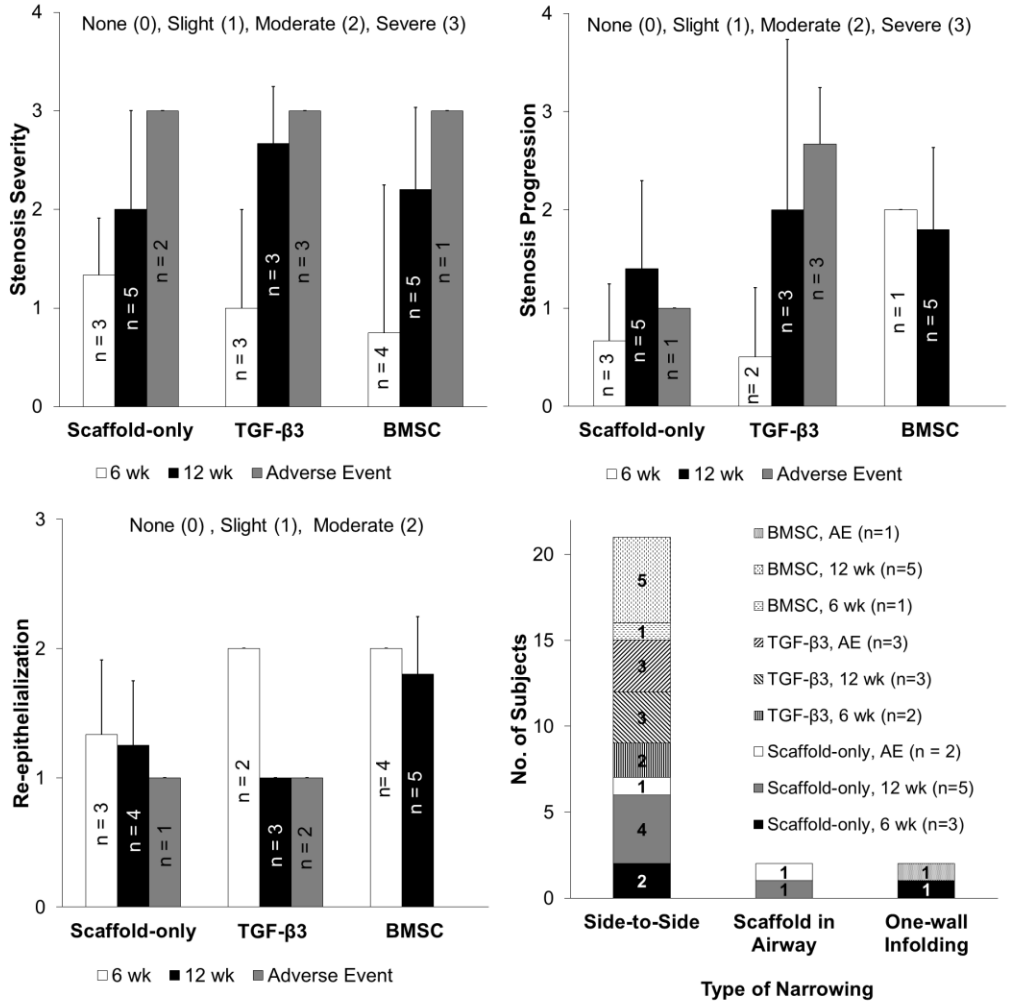

Figure 5.5: Bronchoscopy scoring.

Bronchoscopy image scoring based on stenosis severity, stenosis progression, type of stenosis, and re-epithelialization. The bronchoscopy scoring indicated that stenosis progressed over time, fatality is linked to stenosis, type of narrowing is side-to-side, and epithelium was present in all groups. For the stenosis severity, progression and re-epithelialization, data represents the averages and error bars represent one standard deviation. The type of narrowing chart illustrates the number of subjects with each type of stenosis of the subjects experiencing stenosis.

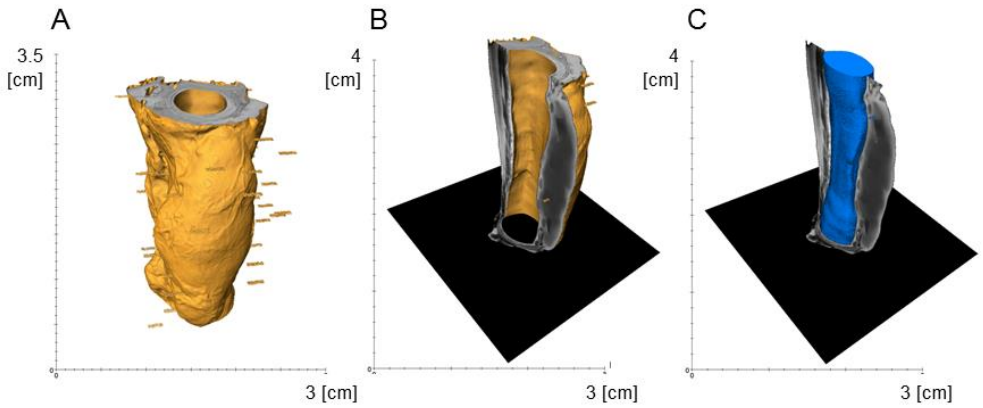

Figure 5.6: Illustration of the lumen quantification process in Avizo Fire.

The CT data was rendered into a 3D volume (trachea in yellow) (a). The lumen space was thresholded and reconstructed into a 3D volume and quantified (lumen in blue) (b-c).

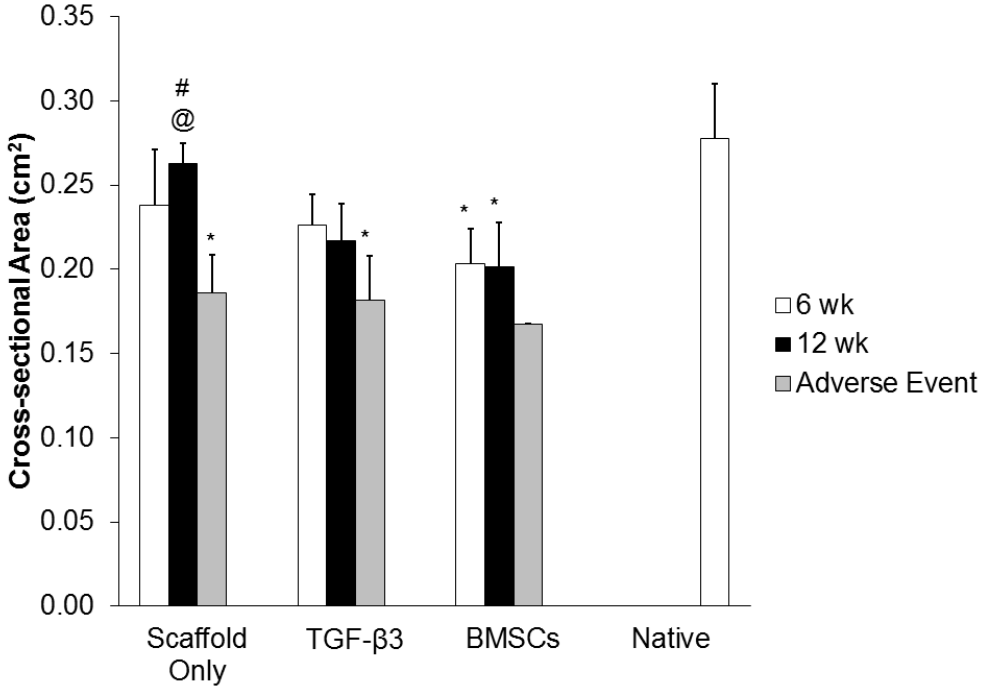

Figure 5.7: The area statistics from the Avizo Fire quantification.

The volume was normalized to the trachea length (volume divided by length) resulting in a cross-sectional area. The Scaffold Only and TGF-β3 group performed similarly to a native trachea. The sample size in each group and time point were the following: Scaffold-only 6 week (n=3), Scaffold-only 12 week (n=4), Scaffold-only AE (n=2); TGF-β3 6 week (n=3), TGF- β3 12 week (n=3), TGF- β3 AE (n=3); BMSC 6 week (n=4), BMSC 12 week (n=5), BMSC AE (n=1). [# significantly increased area when compared to the adverse events (AE) in the same group ($p<0.05$), @ significantly increased area when compared to the BMSC-group at week 12 ($p<0.05$), * significantly reduced area when compared to the native trachea ($p<0.05$)]

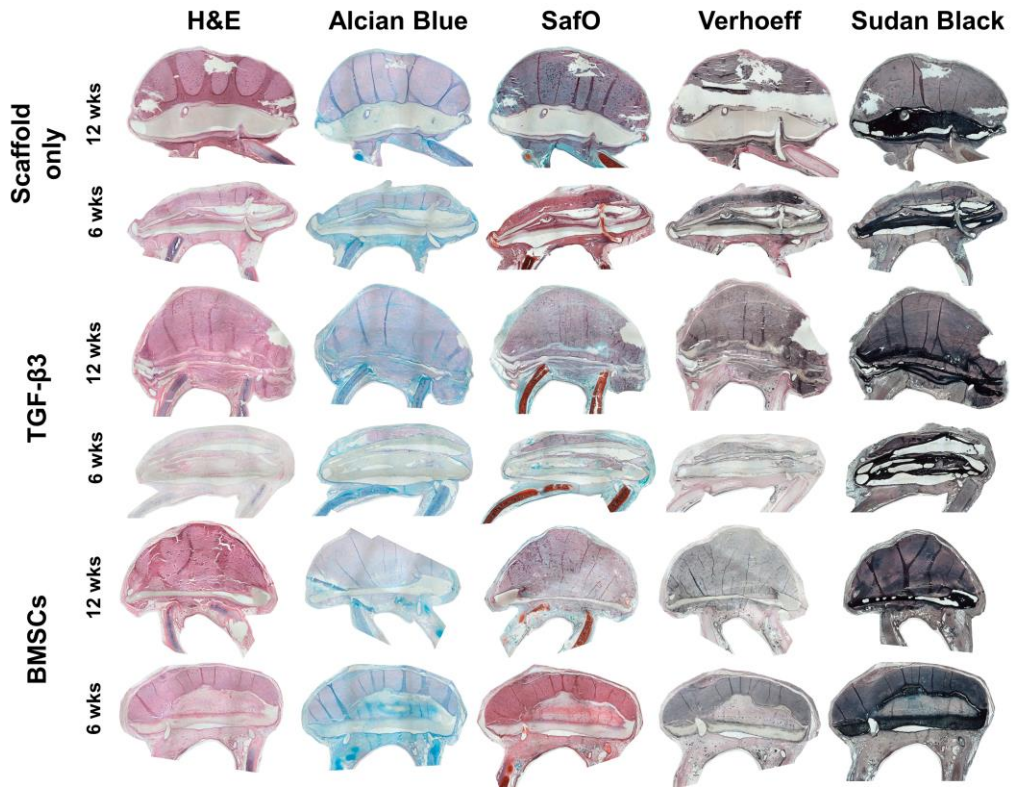

Figure 5.8: An overiew of histological images .

Images represent all three groups at the two time points. The scaffold is located at the top of the section and portions of the native trachea ring are at the bottom of the section. H&E stains for cell nuclei (purple) with a pink background stain. Alcian Blue stains glycosaminoglycans (GAGs) blue. Safranin O/Fast Green stains proteoglycans (red) with a background of green. Verhoeff Van-Gieson stains elastin (black), collagen (red), and background tissue (yellow). Sudan Black stains polymer (black).

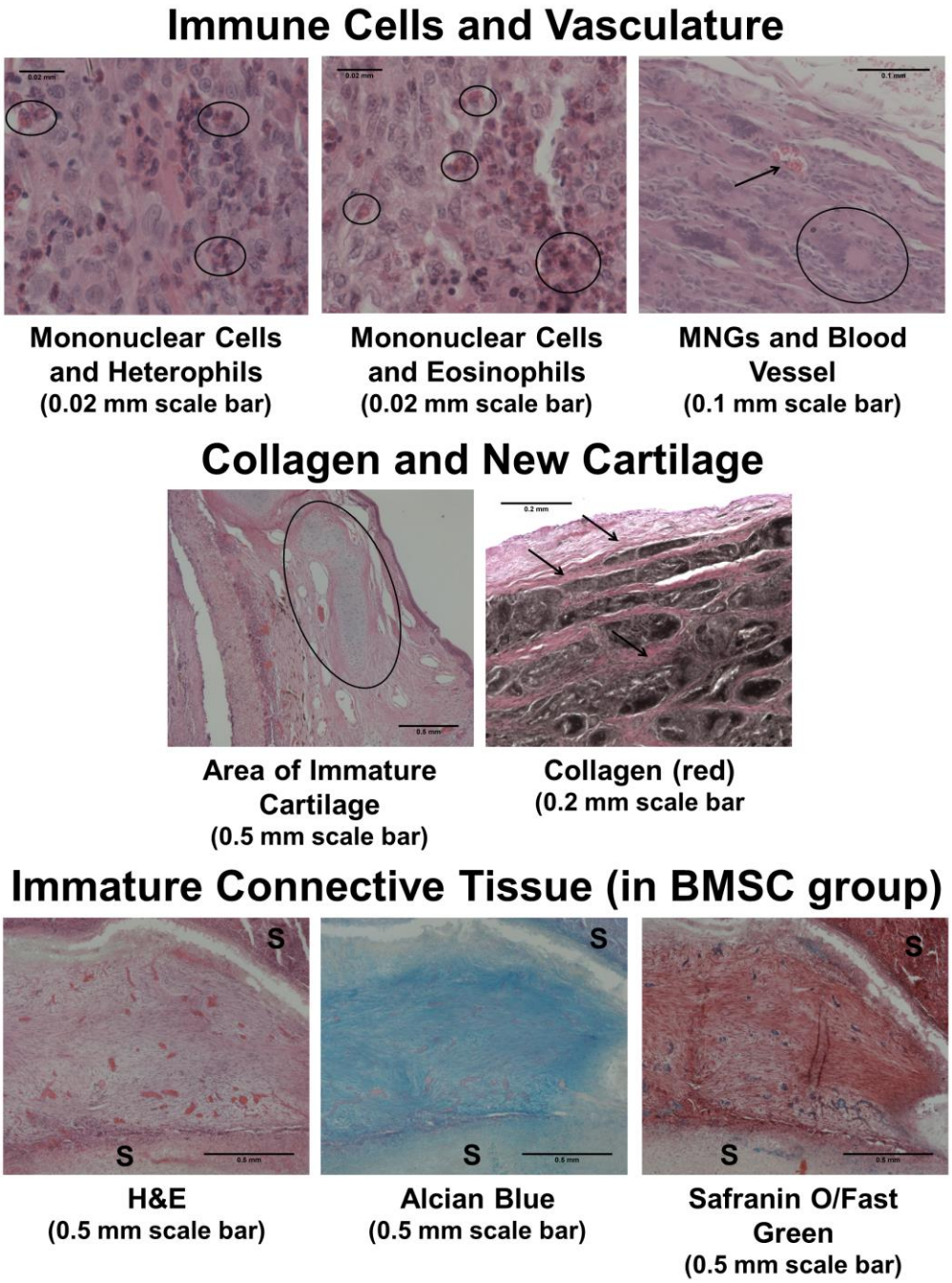

Figure 5.9: Magnified histological images representing scoring criteria.

The types of immune cells are illustrated in the top portion of the figure. The presence of new zones of cartilage and collagen are illustrated in the middle of the

figure. The region of unique connective tissue inside the BMSC scaffolds are illustrated at the bottom of the figure.

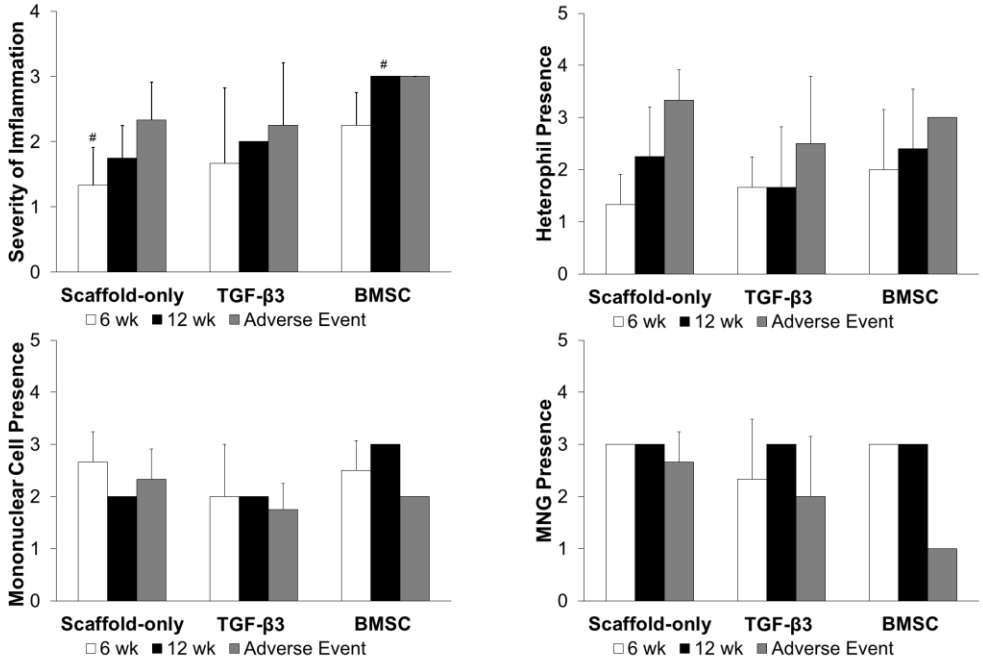

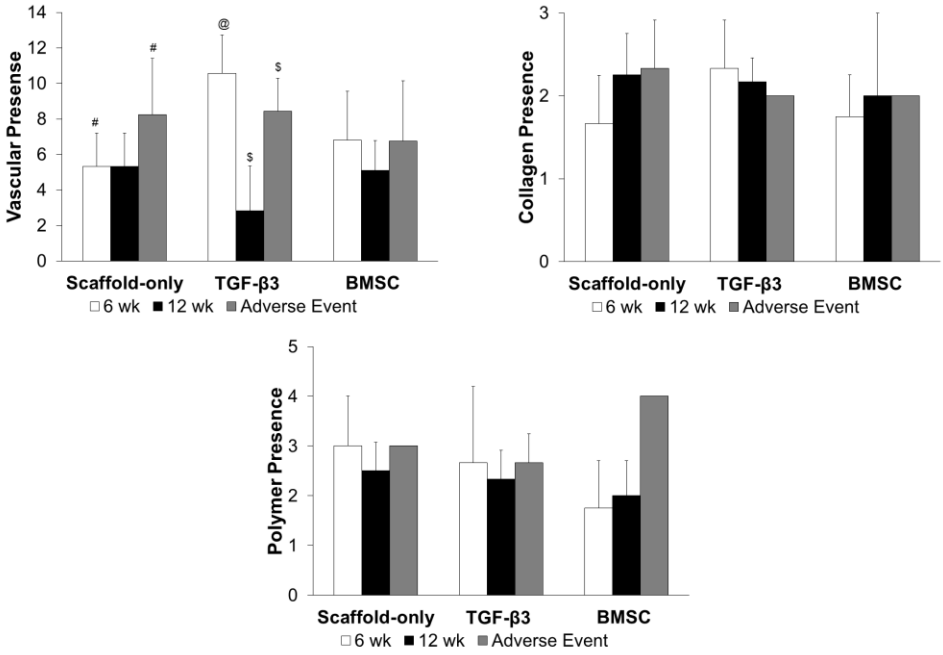

Figure 5.10: Histological scoring.

APPENDIX B: Tables

Chapter 2: Tables 2.1-2.5
Chapter 3: Table 3.1-3.2

Table 2.1: Requirements for tracheal replacement.

TABLE 1. Requirements for trachea replacement.
Characteristics for Prosthesis:(as seen in Neville et al. *paper)*
Airtight
Adequate strength to prevent airway collapse
Accepted by host
Minimal inflammatory reaction
Mold into various sizes and configurations
Incorporate into surrounding tissues
Impervious to fibroblastic and bacterial invasion into the lumen
Permit in-growth of respiratory epithelium
Additional Considerations for Tissue Engineered Trachea
Off-the-shelf accessibility (short fabrication time or ability to preserve for future use)
Neovascularization for nutrient transport
Ability to grow with patient
Relatively low cost
Little to no donor-site morbidity
Noncarcinogenic
Straightforward surgical procedure to implant
Accessible and available materials and cells for constructs

TABLE 2. Static *in vitro* culture studies

Author	Year	Material	Cell Type	Approach	Overall Findings
Goto *et al.*	1999	Human amnion	Epithelial cells and fibroblasts	Epithelial cells seeded on one side of amnion and fibroblasts seeded on the other; cultured in air-liquid interface	Increased frequency and improved morphology of epithelial cells indicate that fibroblast (mesenchymal) cells and epithelial cells interact
Risbud *et al.*	2001	Collagen-chitosan hydrogel	Epithelial cells	Cells seeded onto hydrogel and cultured for 7 days	Gel was not cytotoxic to macrophages; can support a mixed population of epithelial cells
Doolin *et al.*	2002	Chondrocytes: encapsulated in alginate gel or seeded on polypropylene mesh; Epithelial cells: collagen; To join constructs: Fibrin (TISSEEL) surgical adhesive	Epithelial cells, chondrocytes, fibroblasts (for conditioned medium)	Chondrocyte/polypropylene mesh cultured in rotating bioreactor, chondrocyte/alginate and epithelial cell/collagen cultured statically; Chondrocyte constructs and epithelial construct were joined together by fibrin surgical adhesive and cultured statically	Histology revealed that constructs remained viable after 5 days in culture, fibrin surgical adhesive can join two cell types without co-culture
Yang *et al.*	2003	Polyester urethane (DegraPol) strips	Chondrocytes	Agar-cultured chondrocytes seeded on DegraPol scaffold strip and cultured statically	Construct resembled native cartilage (SEM, histology), attachment rate was 80% compared to monolayer culture, heterogeneous cell distribution through scaffold with more cells on surface
Walles *et al.*	2004	Decellularized pig jejunum digested into liquid	Chondrocytes	Static culture of three different types of chondrocytes seeded in liquid collagen matrix	Liquid collagen matrix environment maintained phenotype of chondrocytes, three cell types had similar metabolic activity and viability scores
Walles *et al.*	2004	Pig decellularized jejunum with artery and vein pedicle	Chondrocytes, bone marrow-derived smooth muscle cells, bone marrow-derived endothelial cells, respiratory epithelium	Endothelial cells were perfused into the vascular pedicle, and then the other cell types were seeded onto the vascular scaffold separately	Possible to create a construct seeded with endothelial, smooth muscle cells, and epithelium cells, but the biomechanics were not evaluated

Table 2.2 cont.: Static *in vitro* culture studies.

Henderson *et al.*	2007	Hyaluronan-based scaffold	Chondrocytes	Three different types of chondrocytes seeded on hyaluronan scaffold individually and cultured in perfusion bioreactor	Auricular chondrocytes had higher GAG and collagen content, more consistent histological staining, and were capable of biomechanical testing, than compared to other chondrocytes
Moroni *et al.*	2007	CAD designed and prototyped PEOT/PBT in three geometries (cylindrical, toroidal, anatomical)	Chondrocytes	Constructs seeded in rotating bioreactor and then cultured statically	Chondrocytes produced more ECM and exhibited more differentiation (GAG/MTT ratio, SEM) in the anatomic construct as compared to the other geometries
Pfenninger *et al.*	2007	Chondrocyte pellet, cartilage chip, collagen membrane	Epithelial cells and chondrocytes	Three methods of co-culture were compared, chondrogenic cell pellet, cartilage explant, and both cell types grown on collagen membrane	Concluded that a basal lamina equivalent, fibroblast conditioned medium, and air-liquid interface are required for epithelial cell proliferation and differentiation
Tan *et al.*	2007	Polyester urethane (DegraPol) tube with epithelium coated ADM wrapped around it; DegraPol seeded with chondrocytes	Epithelial cells or chondrocytes	Epithelial cells were seeded statically and then cultured in intra-scaffold perfusion bioreactor; chondrocytes were seeded dynamically; VEGF was perfused through scaffold	SEM revealed an epithelial monolayer after 2 weeks, histology revealed improved proliferation and distribution of chondrocytes, CAM model revealed vessel formation in VEGF perfused group
Tan, El-Badry, *et al.*	2009	Epithelium–acellular dermal matrices on top of PEOT/PBT, Chondrocyte–polyesterurethane (DegraPol) tubes	Epithelial cells or chondrocytes	Both constructs were cultured with 0 and 10% Oxygent in medium; epithelial constructs cultured in intrascaffold perfusion bioreactor and chondrocyte statically	Oxygen carrier increased O_2 levels in epithelium, improved tracheal epithelial metabolism, did not impair CAM angiogenesis, however, O_2 carrier interfered with chondrocyte metabolism
Tan, Hillinger, *et al.*	2009	CAD designed and rapid prototyped poly(ethylene oxide terephthalate)-poly(butylene terephthalate) PEOT/PBT cubic scaffold	Chondrocytes	Semi-dynamic intra-scaffold seeding with bioreactor	Better chondrocyte incorporation with bioreactor compared with static (confirmed by histology, SEM, GAG)
Zhang *et al.*	2009	Cell sheet wrapped around PLGA internal support cylinder	Bone marrow derived chondrocytes	Cell sheet wrapped around PLGA, then cultured in bioreactor	Histology revealed lacunae in matrix, positive for Saf-O stain
Tani *et al.*	2010	Cell sheet wrapped around silicon tube	Chondrocyte	Cell sheets wrapped around silicon tube and cultured statically or dynamically in a rotating hybridization oven	No significant difference between bioreactor and static culture; GAG content in dynamic group was 3/4 of native tracheal cartilage; after removing silicon stent, good flexibility and rigidity (similar in static and bioreactor groups)

Abbreviations:
**PEOT/PBT: polyethylene oxide terephthalate (PEOT) and polybutylene terephthalate (PBT)
**ADM: cellular dermal matrix
**CAM: chorioallantoic membrane

Table 2.3: Orthotopic *in vitro* culture studies.

TABLE 3. Orthotopic *in vivo* culture studies

Author	Year	Material	Cell Type	Animal Model	Defect Type	Time Point	Survival Rate	Overall Findings
Okumura *et al.*	1994	Marlex mesh tube reinforced with polypropylene threads and covered with collagen sponge	None	Dog	Circumferential	26 months	100%	Tissue infiltration, varying degrees of epithelialization, exposure of mesh in lumen occurred in some cases
Osada *et al.*	1994	Silicon rubber coated on inside of knitted Dacron graft; fibrin-glue coated at end of stents to help anastomosis sites	Fibroblasts	Dog	Circumferential	11 months	33%	No epithelialization; unclear if fibroblasts help tissue ingrowth; experiment not completed so not sure how fibrin-glue affected anastomosis sites
Teramachi *et al.*	1997	Marlex mesh tube, reinforced with polypropylene spiral, coated with collagen sponge, silicon stent	Blood preclotting	Dog	Circumferential	24 months	80%	Construct was well integrated and epithelialized
Sekine *et al.*	1999	Marlex mesh formed into Y-shaped tube reinforced with polypropylene spiral and coated with collagen I and III, silicon stent also used for first 8 weeks	None	Dog	Bifurcation	7 months	30%	High mortality (mainly due to air leaks), successful implants were covered with tissue
Nakamura *et al.*	2000	Marlex mesh formed into Y-shaped tube reinforced with polypropylene spiral and coated with collagen I and III, silicon stent also used for first 8 weeks	None	Dog	Bifurcation	5 years	100%	Small sample size (1 dog), epithelization, no stenosis
Fuchs *et al.*	2002	PGA mesh treated with PLLA and collagen solution	Chondrocytes	Lamb	Patch	6-8 weeks (in vitro), 3 weeks--until birth (in utero)	85% in TE group, 90% in control (cartilage autograft)	Implanting grafts into fetal trachea is possible, TE construct was more structurally supportive than free graft
Lee *et al.*	2002	PLGA patch	Chondrocytes	Rabbit	Patch	6 weeks	100%	Growth factors adequate for chondrocyte culture, implanted construct maintained patency but no viable chondrocytes
Fuchs *et al.*	2003	Pretreated PGA mesh	Bone marrow progenitor cells OR chondrocytes	Rotating hybridization oven; Fetal lamb (in utero)	Partial	12 weeks (in vitro); 3 weeks--until birth (in utero)	100% in MSC group, 75% in chondrocyte group	Chondrocyte and MSCs-seeded constructs both displayed hyaline-like phenotype
Yamamoto *et al.*	2003	3 layer: BMP-2 loaded gelatin sponge, collagen sponge, silicone tube	None	Dog	Circumferential	8 months	20%	Silicon stent can be removed at 8 weeks without trachea collapse
Macchiarini *et al.*	2004	Decellularized porcine proximal jejunum segment	Fibroblasts and muscle cells	Bioreactor; human	Patch	24 month (human)	100%	Patient is functioning fine, endoscopy/IHC revealed that epithelial migrated onto lumen
Omori *et al.*	2004	Marlex mesh tube (polypropylene mesh), reinforced with polypropylene spiral ring, and coated with collagen	Blood preclotting	Dog	Patch	7 months	100%	Construct was asymtomatic, well integrated, epithelialized
Omori *et al.*	2005	Marlex mesh reinforced by polypropylene spiral coated with atelocollagen	Autologous blood	Human	Patch	2 years	100%	Construct was well integrated and completely reepithelialized after 20 months, no observed complications
Kunisaki *et al.*	2006	Nonwoven PGA mesh sprayed with PLLA and collagen, silicon tube as temporary stent	Mesenchymal amniocytes	Rotating bioreactor; Fetal lamb (in utero)	Partial or Circumferential	24 to 30 weeks (in vitro); 1 month--until birth (in utero) and 10 days after birth	71%	Some stenosis and stridor observed, epithelium and fibro-cartilage revealed in histology
Nomoto *et al.*	2006	Collagen sponge and collagen gel	Tracheal epithelial cells	Rat	Patch	30 days	81%	Epithelium was regenerated, the donor epithelial cells disappeared and were replaced with recipient epithelial cells
Yamashita *et al.*	2007	Polypropylene mesh reinforced with polypropylene strings and treated with atelocollagen	Peripheral blood	Dog	Patch	12 months	100%	Bloodclotting the scaffolds results in immature cartilage and epithelium formation
Gilbert *et al.*	2008	Pig acellular bladder, crosslinked bladder, trachea	None	Dog	Patch	6 months	80%	No cartilage formation in constructs, some epithelialization; hypthesized that lyophilized or vacuum-pressing the grafts causes poor tissue regeneration in material

Table 2.3 cont.: Orthotopic *in vitro* culture studies.

Igai *et al.*	2008	Gelatin sponge loaded with BMP-2	None	Dog	Native trachea ring removed and replaced with construct	12 months	100%	Histology revealed bone and cartilage formation in BMP-2 group
Komura *et al.*	2008	3-layers: Collagen sheet, PGA nonwoven mesh, L-lactide/E-caprolactone course mesh; outer surface coated with gelatin-based bFGF containing microspheres	Chondrocytes	Rabbit	Patch	3 months	80% control, 85% microsphere group	Histology revealed epithelium and some cartilage formation, more cartilage-formation on bFGF constructs
Macchiarini *et al.*	2008	Donor trachea with cells and MHC antigens removed	Epithelial cells and mesenchymal stem-cell-derived chondrocytes	Human	Circumferential defect	4 month followup	100%	Absence of anti-donor HLA antibodies; good integration; CT showed good patency; laser doppler revealed microvascular bed
Ni *et al.*	2008	Silk fibroin coated titanium mesh	None	Rabbit	Circumferential	12 weeks	100%	Silk fibronin is biocompatible, supporting fibroblast and vessel ingrowth
Nomoto *et al.*	2008	Polypropylene mesh with collagen sponge coating, and fibroblast loaded collagen gel layered on top	Fibroblasts	Rat	Patch	14 days	88% in fibroblast group	Collagen gel loaded with fibroblasts accelerated epithelial differentiation and proliferation
Omori, Nakamura, *et al.*	2008	Marlex mesh tube reinforced with polypropylene threads and covered with collagen sponge	Clotted with arterial blood	Dog	Patch	40 months	100%	Construct was well integrated, provided a rigid framework, and was epithelialized
Omori, Tada, *et al.*	2008	Polypropylene mesh (Marlex mesh) reinforced with polypropylene rings, covered with collagen	Autologous blood injected into construct	Human	Patch	8-34 month followup	100%	Construct was well integrated and epithelialized, no observed complications
Suzuki *et al.*	2008	Polypropylene mesh coated with collagen sponge and cell loaded collagen gel	Adipose-derived stem cell	Rat	Patch	14 days	95%	Histology revealed epithelium and immunofluorescent staining revealed neovascularization
Tada *et al.*	2008	Polypropylene mesh coated with collagen sponge and a vitrigel layer coated on lumen	None	Rat	Patch	28 days	100%	Vitragel possibly accelerated epithelialization
Zani *et al.*	2008	Denatured collagen matrices	Endothelial cells, epithelial cells	Rabbit	Brush injury	9 days	100%	Combination of epithelial and endothelial cells optimize vascularization and epithelialization
Lin *et al.*	2009	Cell loaded collagen placed in grooves of PCL mold to simulate trachea rings	Chondrocytes	Rotating bioreactor ; Rabbit	Circumferential	4-8 weeks (in vitro); 52 days (in vivo)	0%	Bioreactor stimulated chondrocyte proliferation; however, granulation tissue caused stenosis in animals
Nakamura *et al.*	2009	Polypropylene mesh tube reinforced with polypropylene spiral and atelocollagen layer	Peripheral blood, bone marrow aspirate, autologous multipotential bone marrow-derived cells		Circumferential	12 months	100%	Bone marrow derived cells and bone marrow aspirate enhance tissue regeneration in prosthesis
Seguin *et al.*	2009	Cryopreserved, decellularized, or glutaraldehyde treated sheep aortic grafts	None	Sheep	Circumferential	12 months	60%	Cryopreserved aorta graft can be used in the trachea
Tsukada *et al.*	2009	Titanium stent covered with (1) polyglactin mesh, (2) l-lactide and caprolactone sponge reinforced with polyglycoride fibers, or (3) l-lactide and caprolactone covered with knitted PLLA mesh; used omental flap	None	Dog	Circumferential	2 years	67% in group 1, 100% in other groups	Epithelium migrated, no cartilage formation, polyglactin was absorbed quickly and those constructs exhibited stenosis, P(CL/LA) PLLA graft was best–saw survival up to 2 yrs
Gilpin *et al.*	2010	Scaffold-free	Chondrocytes	Bioreactor ; Rabbit	Patch	8 weeks (in vitro); 12 weeks (in vivo)	100%	Good integration of graft; no foreign body reponse; graft slipped/folded so mechanical properties need to be reevaluated
Go *et al.*	2010	Pig decellularized trachea	Bone marrow stromal cell (BMSC) derived chondrocytes, epithelial cells	Pig	Circumferential	60 days	25% (only Group 4 alive)	BMSC-derived chondrocyte and epithelial cell seeded constructs performed the best, other constructs experienced contamination due to lack of epithelium
Kim *et al.*	2010	Fibrin/hyaluronic acid gel	Chondrocytes	Rabbit	Patch	4 months	100%	Epithelialization formed after 2 months, allograft cartilage partially preserved
Sato *et al.*	2010	Polypropylene mesh (Marlex mesh) reinforced with polypropylene rings, covered with collagen; and coated with L-C polymer on inside	None	Dog	Circumferential	18 months	80%	The L-C polymer remained for 14 days and protected the collagen layer to promote epithelization

Abbreviations:
**PLGA: poly(lactic-co-glycolic acid)
**PGA: Polyglycolic acid
**PLLA: Poly(lactic acid)
**L-C: poly(L-lactic acid-co-ε-caprolactone)
**P(CL/LA): copolymer of L-lactide and ε-caprolactone
**MSC: Marrow stromal cell
**PCL: Polycaprolactone
**TE: Tissue Engineered

Table 2.4: Heterotopic (subcutaneous) *in vivo* culture studies.

TABLE 4. Heterotopic (subcutaneous) *in vivo* culture studies

Author	Year	Material	Cell Type	Animal Model	Time Point	Survival Rate	Overall Findings
Sakata *et al.*	1994	Nonwoven PGA mesh wrapped around silastic tubes	Chondrocytes (in PGA) and tracheal epithelial cells (lumen)	Nude mouse	9 weeks	100%	Pus formation in half of the constructs, hyaline cartilage formation, epithelialization
Kojima *et al.*	2003	PGA non-woven mesh wrapped around silicon tube stent	Chondrocytes	Nude mouse	8 weeks	100%	Trachea and nasal chondrocytes have similar properties in a TE construct, mechanical properties of constructs were significantly reduced compared to native trachea
Kojima *et al.*	2003	PGA Mesh wrapped around silicon tube; tube removed and epithelial loaded Pluronic F-127 coated on lumen	Chondrocytes (in PGA) and epithelial cells (lumen in hydrogel)	Mouse	10 weeks	100%	Cartilage and pseudostratified columnar epithelium observed, quantitative measurement of TE construct ECM components were similar to native tissue
Kojima *et al.*	2004	PGA mesh placed in grooves of silicon tube mold, then coated with TGF-β2 loaded hydrogel microspheres	Bone marrow cells (in PGA)	Nude rat	6 weeks	100%	Cartilage formation was observed, and biochemical assays reveal that TE trachea is similar to native tissue
Ruszymah *et al.*	2005	Pluronic F 127, high-density polyethylene (HDP)	Chondrocytes (encapsulated in hydrogel, painted on HDP)	Mouse	8 weeks	100%	No inflammation, cartilage formation was observed on HDP
Matloub and Yu	2006	Polytetrafluoroethylene lined with fascial flap and skin graft, silicon rod used as stent	None	Rat	3 weeks	100%	Vascularization was observed with microradiograph injection and histology
Wu, Cheng, *et al.*	2007	Cell aggregate wrapped around silicon tube	Chondrocytes	Rabbit	8 weeks	100%	Constructs looked cartilage-like, but lack mechanical properties (which stent compensated for); epithelialization not addressed
Wu, Feng, *et al.*	2007	PLGA mesh enforced by collagen type I, shaped into C-rings	Chondrocytes	Mouse	8 weeks	100%	Good cartilage formation; less GAG's than native trachea (maybe due to short time point)
Komura *et al.*	2008	PGA mesh sheets	Chondrocytes	Athymic mouse	8 weeks	100%	Histology and GAG content reveal cartilage formation; human trachea cartilage is a source of chondrocytes for trachea replacement
Lin *et al.*	2008	PCL molded into tracheal ring shape with type II collagen sponge coating	Chondrocytes	Rat	8 weeks	100%	Cartilage-like tissue formed, mechanical modulus higher than native trachea
Weidenbecher *et al.*	2008	Silicon tube with skin flapped wrapped around it, then a muscle flap, then chondrocyte cell sheet	Chondrocytes	Rabbit	10 weeks	100%	Scaffold-free cartilage constructs can be implanted subcutaneously, however epithelium grafts produced hair and sebum
Jungebluth *et al.*	2009	Pig decellularized trachea	NA	Pig (allograft) or Mouse (xenograft model)	30 days	100%	Detergent-enzyme process has little effect on scaffold mechanics and reduces inflammatory response
Luo *et al.*	2009	PLA/PGA fibers wrapped around silicon tube	Chondrocytes	Static culture; Rabbit	2 weeks (in vitro); 4 weeks (in vivo)	100%	Preculture of the constructs before implantation reduces immune response and yields better ECM formation and mechanical properties that direct implantation

Abbreviations:
**PGA: Polyglycolic acid
**TE: Tissue Engineered
**PLGA: poly(lactic-co-glycolic acid)
**PLA/PGA: polylactic acid/polyglycolic acid

Table 2.5: Orthotopic and subcutaneous *in vivo* culture studies.

TABLE 5. Orthotropic and subcutaneous *in vivo* culture studies

Author	Year	Material	Cell Type	Approach	Survival Rate	Overall Findings
Vacanti *et al.*	1994	PGA nonwoven mesh wrapped around silastic tubes	Chondrocytes	Constructs placed in subcutaneously and in a circumferential defect	0% (in orthotopic group)	Histology revealed cylinders of hyaline cartilage; low survival rate; withstood negative pressure; implanted cells formed cartilage in grafts
Yanagi *et al.*	1994	Polyurethane sponge reinforced by MMA spiral ring coated with collagen, fibronectin, RGD, or apatite coating	Blood	Coated constructs were placed in a rat subcutaneously, and in a partial and circumferential defect in dogs	0% (in circumferential transplant group)	Circumferential repair--High mortality rate, limited tissue in-growth due to sputum absorption, no epithelialization
Kojima *et al.*	2002	Nonwoven PGA mesh, silastic tube	Chondrocytes and Fibroblasts	Chondrocyte-seeded matrix placed in grooves of silastic template, entire construct covered with fibroblast seeded matrix and placed in rats and sheep for 8 weeks	Rat-100%, Sheep - 0% (all died within 7 days)	Mature cartilage seen in both constructs, deaths due to stenosis and tracheamalacia due to low GAG content, possibly due to inflammatory response
Grimmer *et al.*	2004	RGD-linked alginate soaked into PGA mesh; PLLA 'finger trap' stent	Chondrocytes	Constructs were placed subcutaneously and in partial defects in trachea	20% in TE construct groups	High stenosis and death rates in all groups, except for the no-stent control group; mature cartilage formation seen in surviving animals, cartilage formation not enhanced by RGD
Kamil *et al.*	2004	Pluronic F-127	Chondrocytes	Cells incorporated in gel and injected subcutaneously, then excised, shaped, and implanted in trachea	100%	Auricular cartilage can be used in trachea TE, hydrogel produces excellent histological cartilage
Kanzaki *et al.*	2006	Dacron grafts with polypropylene reinforcement, lined with epithelial cell sheets	Epithelial cells	Dacron tube was implanted subcutaneous to prepare for epithelial sheet, once implanted into trachea the pedicle was still attached to construct	100%	Pseudostratified columnar epithelial seen on epithelial sheet constructs
Weidenbecher *et al.*	2007	Hyaluronic-acid based scaffold	Chondrocytes	Constructs placed in partial defect in trachea as well as paratracheally	100%	Construct initiated foreign body response, which degraded TE cartilage and replaced with fibrous tissue
Weidenbecher *et al.*	2009	Muscle flap wrapped around silicon tube, and cell sheet wrapped around muscle flap	Chondrocytes	Cell sheets formed in bioreactor, and then implanted paratracheal with muscle flap, then transferred to trachea	0%	High mortality rate caused stenosis due to scar tissue formation, the vascularized muscle flap facilitated vascularization and scaffold-free cartilage was formed
Kim *et al.*	2010	PLGA-gelatin scaffold with polypropylene/prolene support mesh, attached to omentum	Epithelial cells	Construct attached to omentum for 1 week, and then implanted circumferentially in trachea	Success Rate--53% after omentum attachment, 100% after trachea transplant	Omentum can improve performance of construct, but creating a omentum-construct for trachea reconstruction is challenging

Abbreviations:
**MMA: methyl methacrylate
**PGA: Polyglycolic acid
**PLLA: Poly(lactic acid)
**TE: Tissue Engineered
**PLGA: poly(lactic-co-glycolic acid)

Table 3.1: Average fiber diameters determined with SEM.

PCL fibers (PCL-only and Bilayer groups) were smaller than PLGA fibers (PLGA-only group) at week 0 (denoted by * and ^, p=0.05).

Average Fiber Diameter (μm)				
		0 wk	*6 wk*	*12 wk*
PCL Only		1.6 ± 1.4*	1.9 ± 1.2	1.5 ± 1.1
PLGA Only		6.3 ± 3.9*^	N/A	N/A
Cospun		2.9 ± 1.9	2.8 ± 1.9	2.5 ± 1.2
Blend		3.3 ± 1.3	3.8 ± 2.6	2.8 ± 1.8
Bilayer	*PCL*	1.52 ± 0.76^	2.9 ± 1.3	2.4 ± 1.0
	PLGA	3.1 ± 1.9	N/A	N/A
Trilayer	*PCL*	3.1 ± 1.0	4.9 ± 5.4	3.4 ± 2.2
	PLGA	4.4 ± 1.2	4.2 ± 3.8	2.3 ± 1.0
Trilayer + Rings	*PCL*	3.7 ± 1.3	3.0 ± 1.9	1.6 ± 1.5
	PLGA	3.1 ± 1.3	3.8 ± 4.3	3.8 ± 2.3

Table 3.2: Overview of scaffold types and their properties.

Scaffolds were compared to native tissue or physiological data as a benchmark for desired performance. The Gradient+Rings group has the best properties, although the fiber diameter and porosity should be refined.

Outcome Measure	Gross Morph.	SEM Diameter	Porosity	Young's Modulus	Equil. Modulus	Burst	SRS	Tube Flat	Tube Recovery
Desired outcome	Maintain structure for 12 wk	0.25-2 µm	70-90%	0.35 +/- 0.11 MPa (rabbit)	13.6 +/- 1.5 MPa (human)	2.13 - 3.48 psi (porcine)	No native tissue data	10 N (porcine)	80-100%
PCL Only	+	+	+	+	-	+	+	-	+
PLGA Only	-	-	-	-	-	+	-	-	-
Cospun	+	-	+	+	-	+	+	-	-
Blend	+	-	+	+	-	+	-	-	-
Bilayer	+	-	+	+	-	+	+	-	+
Trilayer	+	-	+	+	-	+	+	-	+
Trilayer + Rings	+	-	-	+	+	+	+	+	+